Synthesis and Characterization of TiO_2 polymeric nanocomposites with tunable optical properties

by

Annalisa Colombo

Ph. D Tutor: Dott. Roberto Simonutti
Ph. D Director: Prof. Gianfranco Pacchioni

XXIV Cycle
School in Nanostructures and Nanotechnologies
Department of Materials Science

The creativity takes courage…

(Paul Gauguin)

Abstract

The objective of my Ph. D thesis was to realize and characterize polymer-TiO_2 hybrid nanocomposites. When dispersed at the nanoscale level, TiO_2 can tune the optical properties of the polymeric matrix, such as UV filter and the increase of refractive index, preserving the transparency and the flexibility of the polymer in the visible.

The first part of this work involved the study of different types of TiO_2 used as optical diffusers. Aeroxide P25® (Degussa), Rutile (Aldrich) and anatase synthesized by non-aqueous route, were tested and modified on the surface, in order to stabilize them in methylmethacrylate (MMA). Some phosphonic acids (phenyl phosphonic acid and octylphosphonic acid) were used as modifying agents. The degree of surface coverage was examined by thermogravimetric analysis (TGA) and phosphorous elemental analysis, while the binding modes between the functionalizing agent and titanium dioxide were investigated with FTIR and Solid-State NMR. ^{31}P MAS NMR showed that phosphonic acids adsorb on the surface through different geometries depending on the defects of the titanium dioxide surface, the acidity of the modifying agent and the synthesis conditions., The formation of bulk phosphonate structures was also investigated under high temperature condition; from this point of view, rutile was the most sensitive.

Rutile nanoparticles were also modified on the surface with some amines (hexylamine and octylamine) and carboxylic acids (propionic acid and octanoic acid). Amines interact with Lewis and Brønsted acid sites present on the rutile surface according to FTIR and ^{13}C CP MAS NMR measurements, while carboxylic acids bind through a chelate coordination and a bidentate one. Nanopaticles modified on the surface were dispersed in MMA and polymerized in bulk, in order to obtain optically transparent TiO_2/Poly-methylmethacrylate (PMMA) sheets. The application of these objects was in the solid-state lighting field, where the nanoparticles play the role of light diffusers. In order to obtain transparent objects characterized by controlled diffusing properties, nanoparticles aggregates of about 100 nm in MMA were required. Best results were obtained with P25 and anatase modified with octylphosphonic acid, and rutile modified with hexylamine. The nanoparticles size was investigated with Dynamic Light Scattering. Nanocomposite sheets filled of rutile modified with hexylamine in concentrations from 0.005% to 0.02% in weight in the polymeric matrix were prepared. The fabrication procedure of the nanocomposites did not induce further agglomeration of the aggregates according to Transmission Electronic Microscopy (TEM) images. Moreover, UV-visible spectroscopy measurements revealed that the nanocomposite sheets diffused the light according to Rayleigh Scattering: from this point of view, the diffusion properties could be tuned modifying the concentration of nanoparticles in the polymeric matrix.

The second part of the project involved the preparation of nanocomposite films based on poly 2-ethyl-2-oxazoline (PEOX) and TiO_2 nanoparticles with concentrations up to 44 % in weight. Films were prepared by casting from water solutions. Anatase particles synthesised by non-aqueous route were used. Transmission electron microscope images (TEM) of the films showed that the nanoparticles are clustered into small aggregates of the order of 40 nm, and that these clusters are homogenously distributed in the polymeric matrix. Atomic Force Microscopy (AFM) images of the films showed that the clusters partially protrude out of the composite surface providing a nanometric roughness. Water contact angle measurements highlighted a hydrophobic behaviour of the nanocomposites compared to the hydrophilic one of the pristine polymer, confirming that the organic coated nanoparticles stand outside the polymer surface. Nanocomposites films remained highly transparent in the visible range, and the refractive indices of the films raised from about 1.52 to 1.65 with increasing TiO_2 concentration. While Specular Gloss measurements showed an increase of the root-mean-square surface roughness with TiO_2 content, Distinctness-Of-Image Gloss measurements showed that it does not negatively affect the image information carried by the underlying layer. The good physical properties of these materials and their solubility in water could allow their application in the paint and coating industry and in the field of conservation of cultural heritage as consolidant or varnish of polychrome paintings.

The role played by TiO_2 in the films' optical properties was studied comparing them with lower refractive nanocomposite films prepared with SiO_2 nanoparticles dispersed in the PEOX matrix. The light stability of these films was also checked by artificial degradation in a weather-ometer equipped with arc-xenon lamp.

Acknowledgements

First of all, I would like to acknowledge my Ph. D. tutor, Dr. Roberto Simonutti, for his support in my academic work, all members of the research group: Alberto (known as Brodo), Luca, Lucio, Michele, Tommaso, and the students that helped me in these three years: Francesco, Chiara, Riccardo, Silvio and Marzia.

Many thanks are extended to Francesco Tassone, Alfredo Gambirasio, Prof. Leo Miglio and Domenico Salerno, for their helps and enjoyable discussions during my research work.

I would like to acknowledge Prof. Markus Niederberger for his reviewing of my thesis and his patience.

I would like to acknowledge René de la Rie, John Delaney and the other members of the National Gallery of Art Conservation Department at Washington DC for their support and useful discussion during my research experience at the Gallery.

Many thanks are extended to the conservation studio Carlotta Beccaria & Co., and – in particular – the corservators Carlotta Beccaria and Valentina Mombrini for the preparation of the painting models and interesting opinion on my research work.

Moreover many thanks for their useful support to Maurizio Crippa, Massimiliano D'Arienzo and Cristiana Sburlino.

I could not complete this thesis without the plentiful support from my family: my parents, my sister and my brother; and my boyfriend Emanuele. Their support and love were fundamental and helped me to better survive every single challenge in these last years.

Special thanks for their teachings and love to my American family: Tim and Page, Farah and Ruth, Espedito and his family. They helped me to pass a wonderful time in the U.S.A; I felt like at home!

Moreover, special appreciation is given to my friends for their friendship and helping me to be always positive. Many thanks to all!!!

Contents

Chapter 1
Introduction

In this chapter the state of art of the application fields of my research and, as consequence, the motivations that induced my Ph. D. studies are explained.

1.1 A new devise based on transparent TiO_2/PMMA nanocomposite sheets for lighting application

Because of the strong limitation of the fossil resources, the efficient conversion of the solar radiation to electricity is subject of intense global research. In fact, solar energy will be available indefinitely, as long as humanity exists, and it is free. At the same time, also the reverse conversion - from electricity to light – points out much interest in the last years. What the transistor meant to the development of electronics, the light-emitting diode (LED) does to the field of photonics. In fact, this core device has the potential to revolutionize how we use the light. These uses include illumination, communication, sensing, and imaging.

Figure 1.1 shows the luminous efficacy of conventional lighting (incandescent light bulb and fluorescent lamp) compared to the light-emitting diode technology. The

important difference is that the luminous efficacy of conventional lighting is limited by fundamental factors that cannot be overcome, while the efficiency of solid-state sources is limited only by human creativity and imagination. From this point of view, the theoretical limit of the conversion for white light generated by three LEDs has been shown to be 320 lm/W [1]. This theoretical limit will be difficult to reach, but it is reasonable to presume that up to 2/3 of the theoretical value could be achieved on large-scale.

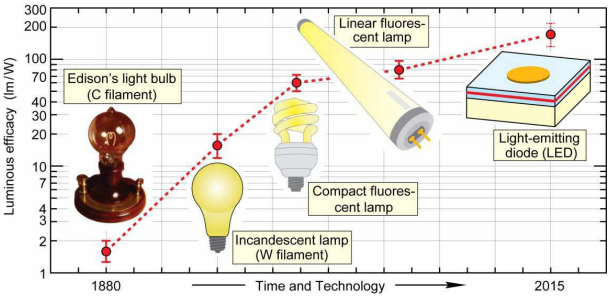

Figure 1.1. Comparison of the luminous efficacy (source efficacy) of conventional lighting technologies with the potential of light-emitting diode technology [2]. The luminous efficacy measures the capacity to convert the electrical power to luminous flux of white light. The unit of measurement is lumen (lm) per watt (W), where "lumen" is the unit of luminous flux (optical power as perceived by a human).

The high efficiency of solid-state sources already provides energy savings and environmental benefits, such as the reduced energy consumption, emission of green-house gases (CO_2), emission of acid rain–causing SO_2, and mercury pollution [3]. In future, it is presumed that the solid-state lighting could cut

the electricity used for lighting (private and commercial), currently at 22%, in half. Several promising strategies to create white light with the use of inorganic sources, organic sources, and phosphors has been developed [4]. The aim is the achievement of an equilibrium between the luminous efficacy and the color rendering, that is the ability of a light to show the "true color" of an object. Apart from the realization of efficient and color-stable LEDs, other challenges are relative to the devise design, paying attention to the cost-processing, and the integration of devise in luminaries.

In this work, we thought about a device characterized by a blue LED chips array as light source, that is the most efficient LED available up to now (emission wavelength about 465 nm). The light source is placed at the edge of a highly transparent polymer sheet (several tens of centimeters long and wide) that is the lamp, filled with phosphors as light converter (the output light should be a warm white). Since the light produced by LED chips is highly directional, the polymeric sheet is filled with TiO_2, whose role is to spread out the light. In order to have the major efficacy in the light diffusion preserving the sheet transparency, TiO_2 particles should be about 100 nm. The amount of scattered light for such small particles can be tuned by the Rayleigh's equation considering all the basic characteristics of the diffuser (volume fraction of the nanoparticles, optical path of the light inside the diffuser, refractive indices of the components) and the spectral distribution of the light source. In order to obtain these objects, poly-methylmethacrylate (PMMA) was chosen as polymeric

matrix thanks to its chemical stability, mechanical properties and high transparency. Titanium dioxide was used as optical diffuser as it is transparent in the visible, it absorbs in the ultraviolet (UV) region protecting the organic matrix from the UV radiation, and it is characterized by a high refractive index, compared to the polymer one, favoring the light scattering.
After the background informations on the polymeric nanocomposites reported in chapter 2, chapter 3 and 4 describe the experimental methods used to modify TiO_2 surface and the techniques employed to analyze the modification. The second part of chapter 4 reports the in-situ polymerization of a PMMA/TiO_2 nanocomposites set and the optical characterization.

1.2 Transparent TiO_2/PEOX nanocomposite films as coating of Matte Painted Surfaces

Until the middle of XIX century artists had the custom to apply a final transparent layer to the surface of paintings, whose binder was generally oil. The aim of this layer, called *varnish*, was to modify the paintings appearance; in particular colour saturation and gloss (see Figure 1.2).

Figure 1.2. Govaert Flinck, *Portrait of a Man*, 1641. The unvarnished side on the left is compared with the varnished side on the right. The left side appears more saturated that the right one.

From this point of view, varnish is as important as the painted layers since it contributes to the right vision of the work of art. On the other hand, the varnish is the most vulnerable part of the painting. It is the layer exposed directly to the environment and it is prone to the deterioration induced by the light (in particular UV radiation), pollutants and dust. Traditional varnishes were based on triterpenes and sesquiterpenes and degraded rapidly: crackings and yellowing occurred obscuring the images beneath them. So, varnishes were removed regularly during restoration interviews and replaced by new ones. From this point of view, although - in the conservation field - materials should respect the first requirement of

durability, removability is the most important one for varnishes. In fact, the cleaning procedure should not compromise the painting layers. These are all reasons why varnishes have been so widely studied in literature [5-8]. From 1930s acrylic, methacrylic and vinylic resins began to be used as varnishes because of their stability on time; on the other hand, the optical result is less gloss and effective than the natural resins. This optical difference was attributed to the different molecular weight (few hundreds of Daltons for natural resins versus some dozens of thousands of Daltons for the synthetic resins) that induces the formation of surfaces characterized by different roughness and, as consequence, different surface scattering [9]. This problem was got over in the Nineties years with the introduction in the conservation field of the low molecular weight resins: the so-called aliphatic, aldehydic and ketonic resins. In fact, these varnishes permit to have the same optical effects of the natural resins with a major stability on time. Moreover, studies were done to investigate the possibility of inhibiting autoxidative degradation of natural resins and other varnishes with stabilizing additives, such as ultraviolet absorbers and hindered amine light stabilizers (HALS) [10].

With the beginning of twentieth century the use of varnish by the artists came to decline. The invention of new materials linked to the Industrial Revolution leaded to new artistic manners where the materials play an important role on the work of art meaning. The restoration procedure has to pay attention not to change the optical appearance of this type of

works of art, that in general appear matte for the absence of the varnish. As to this, the choice of consolidants and adhesives used for their treatments is very important. These particular regards are required not only for the conservation of modern and contemporary works of art, but also for pictures on paper and wall, paintings made of tempera and watercolours.

Into this question we thought about changing the optical properties of a material already used in the conservation field as adhesive and consolidant, the poly 2-ethyl-2-oxazoline (Aquazol 200®), by the addiction of TiO_2 nanoparticles in the polymeric matrix. The introduction of the nanoparticles in the polymer leaded to films characterized by a raising roughness and bulk scattering with the increasing of nanoparticles concentration in the polymeric matrix, even if they preserved high optical transparency. The surface and optical properties of these nanocomposite films compared to the pristine polymer are described in chapter 5. Chapter 6 reports the application of these films on painted models realized according to the modern manner of painting. In order to understand the role played by the bulk scattering, nanocomposite films filled with SiO_2, characterized by a low refractive index, were fabricated and compared to those ones charged with TiO_2. Chapter 7 describes a small studio involved on these films in order to verify their stability on time and the mechanism of degradation of the material, paying attention to the fact that a system that depolymerise, becoming weaker, is better than a system that cross-links, becoming stronger. The artificial aging of these films were leaded in a weather-ometer equipped with an arc

xenon lamp in collaboration with the National Gallery of Art at Washington DC.

1.3 References

[1] Chhajed S, Xi Y, Li Y-L, Gessmann T and Schubert E F 2005 *J. Appl. Phys.* **97** 054506
[2] Kim J K and Schubert E F 2008 *Opt. Exp.* 21836
[3] Bergh A, Craford G, Duggal A and Haitz R 2001 *Phys. Today* **54** 42
[4] Schubert E F and Kim J K 2005 *Science* **308** 1274
[5] R H Lafontaine 1979 *Studies in Conservation* **24** 14
[6] Feller R L, Stolow N and Jones E H 1985 *On Picture Varnishes and their Solvents*, National Gallery of Art, Washington, DC, USA
[7] E R de la Rie 1987 *Studies in Conservation* **32** 1
[8] E R de la Rie 1989 *Analytical Chemistry* **61** 1228A
[9] de la Rie E R, Delaney J K, Morales K M, C A Maines and Sung L-P 2010 *Stud. Conserv.* **55** 134
[10] E R de la Rie and C W McGlinchey 1990 "The Effect of a Hindered Amine Light Stabilizer on the Aging of Dammar and Mastic Varnish in an Environment Free of Ultraviolet Light," in *Cleaning, Retouching and Coatings*, eds. J. S. Mills and P. Smith, International Institute for Conservation of Historic and Artistic Works, London 160

Chapter 2
Literature Review

This review is written with purpose to obtain general understanding of the preparation and properties of polymeric nanocomposites. We start with an overview of nanocomposites recent manufacturing approaches, followed by a glimpse on nanoparticles properties. General comprehension of the surface chemistry, modification of TiO_2 and its applications is to be summarized in the third section. Finally, properties of TiO_2-polymer nanocomposites are discussed.

2.1 Nanocomposites Synthesis

Generally, three ways have been applied to disperse nanopowders in polymers. The first is direct mixing or blending of the polymer and the nanopowder as discrete phases (known as melt mixing). The second is the mixture of the nanoparticles dispersion with the polymer in solution (known as solvent casting). The third is the dispersion of the nanopowder in the monomer followed by in situ polymerization of the polymeric nanocomposite. All these manufacturing approaches are summarized in Figure 2.1.

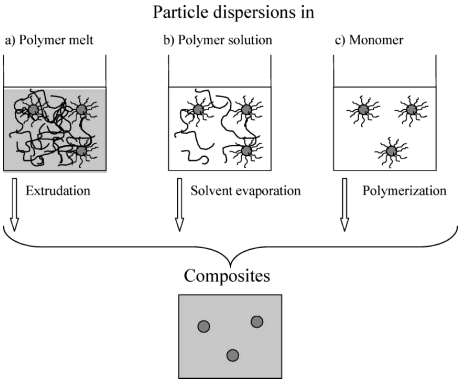

Figure 2.1. Schematic image of the three approaches for the fabrication of nanocomposites [1].

2.1.1 Melt Compounding

Melt mixing is the fastest method for introducing new nanocomposites from thermoplastic polymer to market since it can take full advantage of well-built polymer processing equipments including extruders or injectors. For example, nanoscale silica or $CaCO_3$ filled Nylon composites have successfully been produced by using high velocity oxy-fuel (HVOF) combustion spray process [2].

Hong and coworkers also reported that nano-ZnO and low-density polyethylene (PE) were melt compound in a high-shear mixer to prepare nanocomposites with an increase in the resistance to thermal degradation [3], while Zhao et al. [4] prepared by extrusion polypropylene (PP) composites in which ZnO nanoparticles modified with an organo- silane agent were good dispersed.

Although being successful in many cases, melt mixing method has several drawbacks. First, this process only builds up relatively weak interaction force between the polymer and the nanopowder. Nanopowders have a very strong tendency to aggregate and even if the surface modification is applied, breaking aggregates during melt processing is often difficult. Second, for some polymers, this processing method may be limited due to rapid increase of the viscosity with the addition of a few volume fractions of nanopowder.

2.1.2 Film Casting

Another approach for the preparation of nanocomposites is the dispersion of nanoparticles in the polymer solution. The mixture may be cast in containers, or coated on substrates. Films or sheets are obtained by evaporation of the solvent.

The major requirement in order to get homogeneous materials is the good solubility of polymer and dispersability of the nanoparticles in the solvent. It is possible to use different solvent to disperse nanoparticles and dissolve the polymer, but they have to be compatible. Due to its simplicity the film casting method is widely used mainly for the preparation of films of about 1-100 μm in thickness. They are prepared by spin coating or casting through a blade.

Since the polymer synthesis can be separated from nanoparticles synthesis and the nanocomposite fabrication, from simpler to more complex polymer architectures can be used. For example, Sooklal used this approach for the manufacturing of CdS/dendrimer nanocomposites [5] and we

obtained well dispersed TiO_2/poly 2-ethyl-2-oxazoline nanocomposites.

2.1.3 In situ polymerization

Another method is the graft polymerization, where nanopowders are dispersed in the monomer, and the resulting mixture is polymerized by standard polymerization methods.
Since the viscosity of monomer is quite low and the polymerization process can last some days, while the nanoparticles sedimentation can proceed quite quickly, the main challenge of this approach is to obtain stable dispersions of nanoparticles in the monomer. In order to get over this drawback, nanoparticles surface has to be modified in order to reduce the interfacial tension between the nanoparticles and the monomer, that would induce the formation of aggregates.
Three types of modification are reported in literature.
The first approach (called *ad-polymerization*) consist in the absorption of amphiphilic molecules, such as long chains acids, alcohols or amines, on the particles surface. The surfactant molecules interact with the surface by ionic attractions, hydrogen or coordinative bonding building a sort of hydrophobic shell that avoid the nanoparticles aggregation. The surfactant molecules do not participate directly on the polymerization but permit a good dispersion of the nanoparticles in the monomer and, in a second step, in the polymer. Avella et al. have used $CaCO_3$ particles covered by stearic acid for in situ polymerization of the PMMA nanocomposite [6].

This is the approach used in our project in the fabrication of TiO_2-PMMA sheets, in which nanoparticles were functionalized with some amphiphilic molecules in order to disperse them in MMA. The dispersion stability was verified for a month because the bulk polymerization of the material lasts several days.
Figure 2.2 shows schematically the principle of this approach.

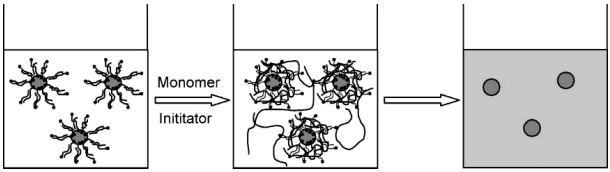

Figure 2.2. *Ad-polymerization* at the surface of inorganic nanoparticles by surfactant adsorption [1].

The other two approaches are relative to the graft polymerization. One approach is "*grafting to*", in which polymer chains modified with anchoring groups are used to bind to the particle surface. As result, the polymer is grafted to the inorganic surface.
The third approach is called "*grafting from*", which involves the grafting of an initiator or a monomeric group onto the nanopowder surface to form polymer chains from the surface. Different type of the grafting agents can lead to different types of polymerization: anionic, cationic or free radicals polymerization. Moreover, in the last decades, in order to achieve most appropriate polymer grafting density, polydispersity, composition and microstructure, new strategies

of free living radical polymerization has been developed. Figure 2.3 summarized the two “grafting” approaches.

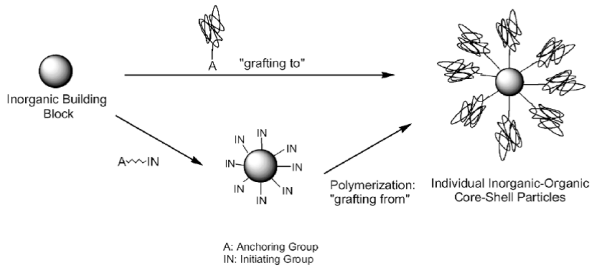

Figure 2.3. Two approaches of graft polymerization [7]

2.1.4 In situ particle generation

In the approaches described until now, nanoparticles are an isolated system to re-disperse in a second step in a solvent or monomer. Nevertheless, novel methods allow the one-step synthesis of nanocomposite materials in which the nanoparticles are *in situ generated* in presence of the polymer or the monomer. We talk about the so-called “reverse microemulsions”-

Reverse microemulsions consist of nanometric aqueous droplets dispersed in an oil phase by the presence of surfactant molecules. The formation of nanoparticles is achieved in two ways.

In the single-microemulsion approach, one microemulsion is prepared and subsequently a precursor or reactant is added diffusing through the phase oil to the micelles containing a reactant [8]. Fernández-García et al., by addition of titanium(IV) isopropoxide to an inverse emulsion containing an

aqueous phase (50 mL) dispersed in *n*-heptane (85/10 v/v versus H_2O), using Triton X-100 as surfactant and 1-hexanol (105/100 v/v versus surfactant) as cosurfactant, obtained anatase nanocrystals [9].

The second route is the multi-microemulsion that consists of the mixing of two or more separately prepared microemulsions characterized by the same water/surfactant/oil ratio. After the mixing, the particle formation occurs by intermicellar exchange of reactants. Microemulsions characterized by the use of the monomer as oil phase were also prepared. In this case the direct polymerization of the system can be perform, as Figure 2.4 shows [10].

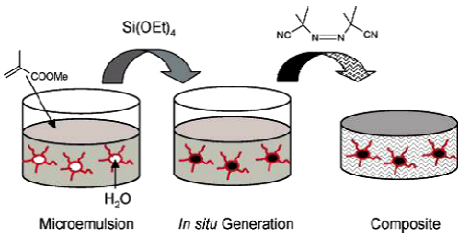

Figure 2.4. *In-situ generation* of SiO_2 nanoparticles in reverse microemulsion for the manufacture of PMMA nanocomposites.

Other possibilities are the use of amphiphilic block copolymer as nano-templates for the controlled synthesis of inorganic nanoparticles thanks to their ability to shape spherical or rod-like micelles [11], and the sol–gel hydrolysis and condensation of a precursor such as tetraethyloxysilane (TEOS), tetrabutyl titanate, aluminum iso-propoxide starting from a preformed functional organic polymer such as polyvinyl alcohol [12],

polymethylmethacrylate [13], polyamides [14] and several other polymers.

2.2 Nanopowder Properties

Nanopowders are the three dimensional relatively uni-axial nanosized objects at a level intermediate between atom/molecule and bulk. Although nanopowders involving metals (Au, Pt, Pd, Cu, etc.), semiconductors (ZnS, CdS, CdSe, etc.), metal oxides (SiO_2, Al_2O_3, TiO_2, ZrO_2, Fe_2O_3, etc.) are everywhere in nature, they grow into micro-powders or macroscopic materials instantaneously and then lose their specific features. Therefore, how to produce a nanopowder with controlled size and degree of aggregation is a key issue which attracts many efforts. Recently, significant progress in the diversity of preparative methods has been made. Good reviews in this area have been presented elsewhere in the literature, which involve gas-phase synthesis of nanopowders (flame hydrolysis, gas condensation, chemical vapor condensation, pyrolysis, laser ablation, etc.) given by Kammler et al [15], Kruis et al. [16], Hahn [17], and Swihart [18]; liquid-phase synthesis (co-precipitation, sol-gel processing, micro-emulsion, hydrothermal and solvothermal processing, templated synthesis, non-aqueous route, etc.) by Grieve et al. [19], Trindade et al. [20], Murray et al. [21], Cushing et al. [22], Niederberger et al. [23]; and grinding methods [24].

In general, when grinding processes are employed, appreciable agglomeration and contamination by material abraded from the grinding body must be expected. Very small particles (diameter

<50 nm) are usually only obtainable to a limited degree. For technical processes, grinding methods are extremely important, as they allow even large quantities of substance to be obtained inexpensively. Gas-phase methods are typically employed as continuous processes that provide crystalline nanoparticles with largely uncoated surfaces. However, owing to the high temperature synthesis (above 500 °C), such approaches may result in the formation of hard aggregates that are difficult to separate into primary particles. Since gas-phase reactions are usually subject to thermodynamic control, the production of compounds that are metastable under synthesis conditions is only possible to a limited degree. In liquid-phase syntheses, particle size and agglomeration behavior can usually be controlled effectively. The reactive surfaces can be saturated and functionalized with organic molecules as stabilizers immediately after nucleation. With the aid of such stabilizers, it is possible to control the shape of nanoparticles, permitting a wide variety ranging from simple spheres through lenticular and rod shape forms to nanoparticle tetrahedra, octahedra, cubes, or stellate shapes. However, the use of high-molecular weight organic stabilizers can be a disadvantage if they have undesired effects on the properties and functions of the nanoparticles after completion of the synthesis. For example, the quantum yield of luminescent nanoparticles or the catalytic activity of nanoparticles can be reduced considerably by unsuitable surface functionalization. It is possible to burn out organic stabilizers, but this requires temperatures above 500°C and usually results in the formation of agglomerates, which

either may still be separable into primary particles if appropriate force is applied, or may not be physically separable at all.

The primary driver for this growing synthetic interest is the effect of powder size on properties. For example, the optical absorption spectrum of gold (Au) changes with the size of the Au nanoparticles. The electroluminescence of semiconductors is also size-dependent. Generally, nanopowders do not exhibit classical bulk properties, while on the other hand they also differ from the molecules or atoms. In this section we discuss some typical physicochemical characteristics of nanopowders, with emphasis on size-dependent phenomena.

2.2.1 High Surface-to-Volume (S/V) Ratio

One of the main characteristic of nanoparticles is the high surface area. Goesmann et al. [25] illustrated simply this concept using a sugar cube with edges 1 cm in length. If you divide the cube, step by step, into cubes with edges 1 nm in length, the sum of the volumes remains the same, while their total area surfaces increases dramatically. Figure 2.5. shows this example:

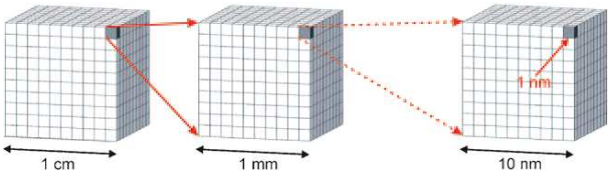

Edge length of cubes	Number of cubes	Volume of cubes	Surface area of cubes
1 cm	1	1 cm^3	0.0006 m^2
1 mm	10^3	1 cm^3	0.006 m^2
1 µm	10^{12}	1 cm^3	6 m^2
1 nm	10^{21}	1 cm^3	6000 m^2

Figure 2.5. Surface area of NPs: a simple model

Compared to a three-dimensional solid ("bulk"), the physicochemical properties are strongly influenced by the surface. In addition, the surface atoms are chemically more active compared to the bulk atoms because they usually have fewer adjacent coordinate atoms and unsaturated sites or more dangling bonds [26]. The increasing number of weakly bound surface atoms is directly reflected in changes in the physicochemical properties, such as the melting point depression.

2.2.2 Depressed Melting Temperature (T_m)

Melting is one important type of phase transformations widely studied in thermodynamics. In quite a large quantity of materials ranging from metals to semiconductors to insulators, a decrease in T*m* has been observed with decreasing nanopowder size. First observations were made for tin by Takagi and Wronski in the 1950s and 1960s [27-28]. A sample

of the magnitude of the effect was presented by Goldstein et al. for experiments performed on CdS nanopowders. Figure 2.6 shows a melting point lowering of over 50% for sufficiently small sized CdS nanopowders [29]

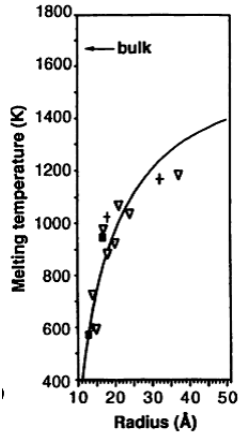

Figure 2.6. Melting temperature vs size for CdS nanopowder [reproduction of Figure 2.2 in the ref. [29]

Apart from the lowering of melting point, the imperfection of the particle surface induces additional electronic states in the band gap, which act as electron or hole trap centers. At high densities of surface defects, a decrease in the observed transition energy and a red-shifted emission band can be observed due to defect band formation. As the size of the materials decreases, the surface to-volume ratio increases and the surface effects become more apparent and thereby easier to explore. These are surface-dependent properties, but there are

also properties size-dependent, as the modification of the materials' electronic structure ("quantum effects").

2.2.3 Discrete Electronic Structure

For small powders, the electronic energy levels are not continuous as in bulk materials but are discrete, due to the confinement of the electron wavefunction because of the physical dimensions of the powders. As a result, electronic, magnetic, optical properties of a nanopowder become size dependent. In electric conductivity, an important gain result from wide investigations of metallic nanopowders of various sizes by photoelectron spectroscopic measurement is that as the metal particle size decreases, the core-level bonding energy of metals such as Ag, Hg, Au, Ni, Cu increases dramatically [30]. This increase is a manifestation of the size induced conductive-nonconductive transition phenomena in nano-metals.

Rademann et al. showed that Hg, the same element, behaves as either a metal or a nonmetal, depending on its particle size [31]. Among several techniques of investigating size-dependent optical properties, optical absorption spectra generally exhibit peak at the threshold which is assigned to the creation of the excitons. The position and shape strongly dependent on the particle size have been observed in many nanopowder systems. Figure 2.7 shows the absorption spectra for a series of CdSe nanoparticles of different sizes [32].

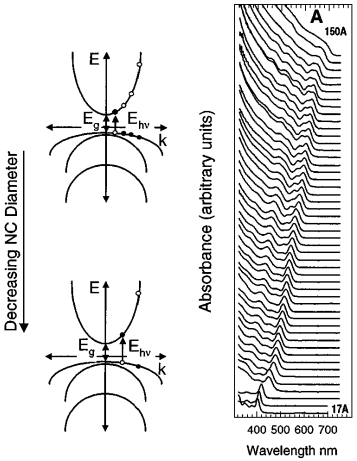

Figure 2.7. The bulk conduction and valence bands for semiconductors are assumed to be parabolic in the simple effective mass approximation. Energy diagrams (E versus k) show the complexity of the valence band for the example of CdSe, important in assigning NC electronic states. The finite size of the NC quantizes the allowed k values. Decreasing the NC diameter shifts the first state to larger values of k and increases the separation between states. (*a*) This is seen spectroscopically as a blue shift in the absorption edge and a larger separation between electronic transitions for a homologous size series of CdSe NC dispersions, collected at RT.

Magnetic properties of nanopowders of transition metals such as Ni, Co and metal oxides such as Fe_2O_3 also show remarkable changes with size. We know that in the nanometric domain, the coercivity (H_c) of the particles tends to zero. Hence, the nanopowder behaves as superparamagnets with no associated H_c. The blocking temperature that marks the onset of this superparamagnetism also rises with the nanopowder size. Moreover, the magnetic moment per atom is seen to increase with the decreasing size of a powder [33].

2.2.4 High Reactivity

Due to a large fraction of surface atoms and a higher surface area, a nanopowder would be expected to be more active. Furthermore, the qualitative change in the electronic structure arising due to quantum confinement in tiny nanopowders also bestow unusual catalytic properties on these powders, totally different from those of the bulk. The ability of supported or non-supported metal nanopowders such as Ni, Cu, Pt, Au, Pd as catalysts and metal oxides such as SiO_2, TiO_2 and Al_2O_3 as catalyst supports has been investigated. Rao et al revealed that the significant dependence of the reaction of elemental O_2 with Ag was on the particle size of Ag. The smaller Ag powders were more capable to dissociate O_2 molecules to atomic oxygen O, unlike oxygen ion predominantly adsorbed on the bulk Ag. They also reported that unlike bulk Ni, small nanopowders exhibit less dependence in their catalytic activity on ambient temperature as they interacted with H_2S and different sizes of nanopowders show different temperature profiles [34].

One study of Valden et al. showed another significant example that Au nanopowders supported on a TiO_2 surface have a marked size effect on their catalytic ability for CO oxidation reaction; Au nanopowders in the range of 3.5nm exhibit the maximum chemical reactivity [35].

2.3 Titanium-dioxide

2.3.1 General Remarks

Titanium dioxide adopts at least 8 structures. Besides its four polymorphs found in nature (i.e. rutile, anatase, brookite, TiO_2 (B)), additional high-pressure forms have been synthesized: TiO_2 (II) with the α-PbO_2 structure, TiO_2 (H) with hollandite, baddelleyite with ZrO_2, Cotunnite with $PdCl_2$ [Banfield, 2001]. Among them, rutile and anatase are mostly manufactured in chemical industry as microcrystalline materials. The two polymorphs are based on interconnected TiO_6 octahedra, but their linkages and degree of edge and face sharing differ (Figure 2.8). Anatase can be regarded to be built-up from octahedrals that are connected by their vertices; in rutile, the edges are connected [36].

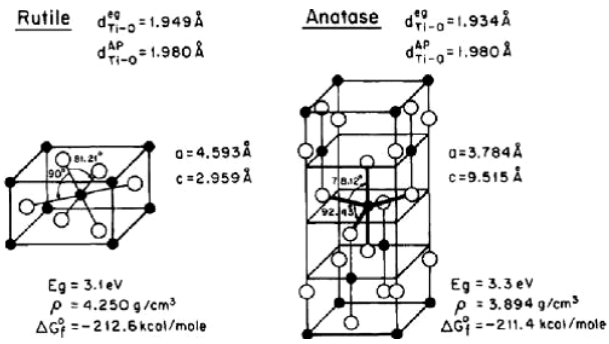

Figure 2.8. Lattice structure of rutile and anatase TiO_2. Reproduction of ref. [36].

Thermodynamic calculations show that rutile is the most stable phase at all temperatures and pressures below 60 kbar, when

TiO_2 (II) becomes the favorable phase. Reverse phase stability is described by particle size experiments due to size effect on surface energy. Anatase is most stable at sizes less than 11 nm, brookite at sizes 11-35 nm, rutile at sizes greater than 35 nm [37].

2.3.2 Applications of TiO_2

Titanium dioxide was first industrially introduced to replace toxic lead oxides as a white paint pigment in 1900's. Nowadays, the annual world consumption of TiO_2 exceeds 4.4 million tons [38]. It is used in as a white pigment in paints, plastics, paper and cosmetic products which represent the major end-use sectors of TiO_2. The consumption of TiO_2 increased in the last few years in a number of minor end-use sectors such as a photocatalyst, photovoltaics, sensing, and electrochromics as well as photochromics.

2.3.2.1 White Pigment

TiO_2 has recently become the most used white pigment thanks to its stability, its relatively low and uniform absorption of visible light and its UV absorption. Half of all TiO_2 pigment produced is consumed in decorative and architectural paints widely serving to house buildings, wood or furniture, industrial coating, and automobile finishes. TiO_2 is non-toxic, safe, and corrosion protective and can be dispersed easily. Moreover it filters the UV radiation protecting the paint from direct photochemical degradation of organic binder and making it

ideally suited for the paint industry [39]. In the paper industry, TiO_2 is used in conjunction with clay, $CaCO_3$, and other pigments to impart lightness at the paper pulp and as additive of white ink correction fluid. In cosmetics TiO_2 is used as sun-screener and in the toothpaste.

2.3.2.2 Photocatalysis

TiO_2 photocatalysis has its origins in early research effort into photoelectrochemical systems for solar to chemical energy conversion. A major landmark in the study of Fujishima and Honda in 1972 found that TiO_2 could be used as catalytic electrode in photoelectrolysis cell to decompose water into H_2 and O_2, without the application of an external voltage [40]. After a few years that it was realized, Fujishima-Honda micro-cells, consisting TiO_2 particles with deposit of Pt on them, was also able to work as photocatalysis for splitting H_2O.
Since that moment, much attention was paid to the use of TiO_2 for photo-assisted degradation of organic compounds and oxidation/reduction of inorganic compound.
TiO_2 nanomaterials have electronic band gaps larger than 3.0 eV and by the adsorption of energies equal or higher than 3.0 eV, electrons are excited from the valence band to the conduction band. So some excited electrons are in the conduction band and some positive holes are in the valence band. These charges can recombine radioactively or non-radioactively, or they can get trapped and react with electrons donors and acceptors adsorbed on the surface. The result is the complete or selective decomposition of organic species or the

transformation of inorganic molecules into their oxidized and/or reduced states. Szczepankiewicz et al. reported the following mechanism [41]:

$$TiO_2 + h\nu \rightarrow e^- + h^+ \quad (1)$$

$$e^- + Ti(IV) - OH \rightarrow Ti(III) - OH^-(X) \quad (2)$$

$$h^+ + Ti(IV) - OH \rightarrow Ti(IV) - O^{\bullet}H^+(Y) \quad (3)$$

$$h^+ + \frac{1}{2}O^{2-}{}_{lattice} \rightarrow \frac{1}{4}O_2(g) + vacancy \quad (4)$$

$$e^- + O_{2,s} \rightarrow O_{2,s}{}^- \quad (5)$$

$$H^+ + O_{2,s}{}^- \leftrightarrow HO_{2,s} \quad (6)$$

$$h^+ + Ti(III) - OH^- \rightarrow Ti(IV) - OH \quad (7)$$

$$e^- + Ti(IV) - O^{\bullet}H^+ \rightarrow Ti(IV) - OH \quad (8)$$

$$O_{2,s}{}^- + Ti(IV) - O^{\bullet}H^+(Y) \rightarrow Ti(IV) - OH + O_{2,s} \quad (9)$$

Reaction 1 is the photons absorption and the photogeneration of a couple e^--h^+ that diffuse on the surface. Reactions 2-3-4 are the redox pathways: the reduction of Ti(IV) in Ti(III) by interaction with the electron, and the formation of bound OH• radicals and O vacancies by oxidation of the lattice oxygen leaded by the holes. Reactions 7-8-9 represent recombination channels. The reverse of reaction 4 generates O adatom intermediates upon exposing defective surfaces to O^{2-}. Electron paramagnetic resonance (EPR) measurements confirmed that electrons are trapped as two Ti(III) centers, while the holes are trapped as oxygen-centered radicals covalently linked to surface titanium atoms (Figure 2.9).

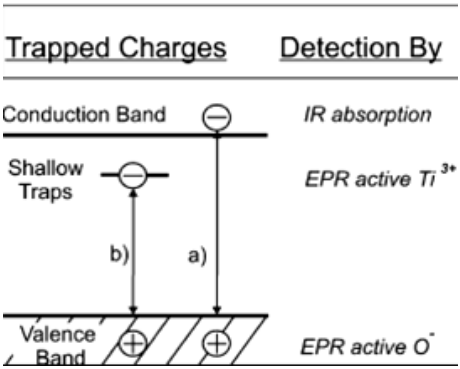

Figure 2.9. Scheme of UV-induced charge separation in TiO_2. Electrons from the valence band can either be trapped (a) by defect states, which are located close to the conduction band (shallow traps), or (b) in the conduction band, where they produce absorption in the IR region. Electron paramagnetic resonance spectroscopy detects both electrons in shallow traps, Ti^{3+}, and hole centers, O^{-} [42].

The species X and Y are chemically active and react with adsorbed organic molecules, inducing their complete or selective decomposition, or transforming inorganic molecules into their oxidized and/or reduced states.

From this point of view, the photocatalytic activity is largely controlled by (i) the light absorption properties, e.g., light absorption spectrum and coefficient, (ii) reduction and oxidation rates on the surface by the electron and hole, (iii) and the electron-hole recombination rate. A large surface area with a constant surface density of adsorbents leads to faster surface photocatalytic reaction rates. In this sense, the larger the specific surface area, the higher the photocatalytic activity is. On the other hand, the surface is a defective site; therefore, the

larger the surface area, the faster the recombination. The higher the crystallinity, the fewer the bulk defects, and the higher the photocatalytic activity is. High temperature treatment usually improves the crystallinity of TiO_2 nanomaterials, but can induce the aggregation of small nanoparticles and decrease the surface area. As conclusion, the relation between the physical properties and the photocatalytic activities is complicated. Optimal conditions are sought by taking these considerations into account and may vary from case to case.

Some applications are:

i) Selective organic synthesis, for example, the selectivity of the epoxidation of 1-decene is improved by using rutile [43]; selective oxidation of alcohol catalyzed by light-activated TiO_2 yields very high carbonyl compounds such as ketones ad aldehydes [44].

ii) Non-selective destruction of organic and inorganic waste materials under normal temperature and pressure, such as waste water purification [45], pollutant air cleaning [46].

iii) Photokilling of pathogenic organisms (viruses, bacteria, algae, protozoa and cancer cells), for instance, antitumoral activity in the experiment of subcutaneous injection of a TiO_2 in rats under near- UV illumination [47].

iv) Use of self-cleaning or antifogging materials, ranging from self-cleaning facades (e.g. the preservation of ancient marble Greek status against environmental damage [48]) to antifogging films on car windshields [49]. In this field, Feng et al. found that reversible superhydrophilicity and superhydrophobicity could be switched back and forth for TiO_2

nanorod films. When the TiO_2 nanorod films were irradiated with UV light, the photogenerated hole reacted with lattice oxygen to form surface oxygen vacancies. Water molecules kinetically coordinated to these oxygen vacancies, and the spherical water droplet filled the grooves along the nanorods and spread out on the film with a contact angle of about 0°, resulting in superhydrophilic TiO_2 films. After the hydroxy group adsorption, the surface transformed into an energetically metastable state. When the films were placed in the dark, the adsorbed hydroxy groups were gradually replaced by atmospheric oxygen, and the surface evolved back to its original state. The surface wettability converted from superhydrophilic to superhydrophobic [50].

2.3.2.3 Gas Sensor

TiO_2 nanomaterials have also been used as sensors for various gases and humidity due to the electrical or optical properties which change upon adsorption. So far, TiO_2 is commonly used as an oxygen gas sensor, e.g. to evaluate the combustion process of fuel in car engines for controlling fuel consumption and environmental pollution [51].

2.3.2.4 Other application by TiO_2 bulk modification

Many applications of TiO_2 nanomaterials are closely related to its optical properties. However, the highly efficient use of TiO_2 nanomaterials is sometimes prevented by its wide band gap. The band gap of bulk TiO_2 lies in the UV regime (3.0 eV for

the rutile phase and 3.2 eV for the anatase phase), which is only a small fraction of the sun's energy (<10%). Thus, one of the goals for improvement of the performance of TiO_2 nanomaterials is to increase their optical activity by the onset of the response from the UV to the visible region. There are several ways to achieve this goal.

First, doping TiO_2 nanomaterials with other elements can narrow the electronic properties and, thus, alter the optical properties of TiO_2 nanomaterials. Second, sensitizing TiO_2 with other colorful inorganic or organic compounds can improve its optical activity in the visible light region. Third, coupling collective oscillations of the electrons in the conduction band of metal nanoparticle surfaces to those in the conduction band of TiO_2 nanomaterials in metal-TiO_2 nanocomposites can improve the performance. In addition, the modification of the TiO_2 nanomaterials surface with other semiconductors can alter the charge-transfer properties between TiO_2 and the surrounding environment, thus improving the performance of TiO_2 nanomaterials-based devices.

One of the most important research areas for future clean energy applications is to look for efficient materials for the production of electricity and/or hydrogen. When sensitized with organic dyes or inorganic narrow band gap semiconductors, TiO_2 can absorb light into the visible light region and convert solar energy into electrical energy for solar cell applications. For example, an overall solar to current conversion efficiency of 10.6% has been reached by the group

led by Grätzel with DSSC technology [52]. Another application of TiO_2 nanomaterials when sensitized with dyes or metal nanoparticles is to build photochromic devices [53]. In fact a blue coloration of the material caused by the reduction of Ti(IV) to Ti(III) has been observed in literature [54].
The role of TiO_2 as support of many metals or metal oxides in heterogeneous catalysis have also been studied. One famous example of these systems is that V_2O_5 supported on TiO_2 in which the catalytic properties of many hydrocarbons or selective catalytic reduction of nitric oxides are highly superior than those of unsupported V_2O_5 [55].

2.4 TiO_2-Polymer Nanocomposites

Titanium dioxide is a widely applied filler to many polymers, such as – for example - polyvinylchloride (PVC), polystyrene (PS), polyolefines. The successful of TiO_2-composites is due to the possibility to improve the physical and mechanical properties of the material induced by the presence of the inorganic phase, without loss of ease processing, light weight, and often ductile nature of the pristine polymer. Traditionally, the polymeric composites were reinforced with micron-sized TiO_2. Recently, processing techniques have been developed to allow the introduction of nano-size TiO_2 nanoparticles. Experiments have shown that it contributes to the fabrication of renewed materials with improved thermo-mechanical, morphologic, electrical and optical properties, and correspondingly extended applications. In this section several studies are reported.

2.4.1 Thermo-mechanical Properties

TiO_2 has relatively high elasticity modulus, which can be exploited to obtain the mechanical gain of the polymeric nanocomposites. Chiang et al., for example, performed a series of tests on the mechanical properties (elastic modulus, elongation, strength, yield stress, thermal stability, and glass temperature T_g) of TiO_2-polyimide (PI) nanocomposites with various contents of inorganic phase and three different PI systems. They found that the TiO_2 nanoparticles enhanced mechanical properties of the PI matrix. For all three series of systems the elastic modulus increased with the TiO_2 content. The reverse effect was found to elongation coefficient. Also the transition glass temperature (T_g) increased with the TiO_2 content, obtaining stiffer materials than the pristine polymers. There was also a marked lowering of the coefficient of thermal expansion (CTE) in hybrids with small amount of titania because TiO_2 not only had lower CTE values but also served as cross-link points resulting in a decrease in the segmental mobility of the PI chain [56]. From this point of view, the large surface area of the nanoparticles can significantly affect morphology of polymer in the nanocomposites, by the enhancement or restriction of chain mobility near the particle surface.

2.4.2 Electrical Properties

With a high dielectric constant in bulk and size-dependent discrete electric properties, TiO_2 nanoparticles can be

introduced into a polymer matrix to prepare nanocomposites for electrical applications. Chiang et al. pointed out that the surface and volume resistivity of TiO_2-PI hybrids decreased with the titania content. This electrical property can be tailored to other non-conductive or low-conductivity polymers and applied in the coating industry [56].

Liu et al. studied that TiO_2-polyethylene oxide (PEO) nanocomposites increased the ionic conductivity of Li^+ in the lithium-ion battery. A maximum value of ionic conductivity was obtained at 10% of TiO_2 nanoparticles leading to a conductivity of 7×10^{-7} S/cm, which was over an order of magnitude higher than that of the electrolytes without TiO_2, also higher than that of microsized-TiO_2 filled electrolytes [57].

2.4.3 Optical Properties

Since TiO_2 absorb UV light up to the proximity of the visible wavelengths and is transparent in the region of the visible range can be use to obtain transparent UV filters, including transparent coatings for UV-sensitive materials.

In fact, for many applications, a decisive advantage of nano-size particles is their markedly reduced light loss by scattering, which varies with the particle diameter (and other parameters). In order to estimate the intensity loss of light passing through a nanocomposite by scattering, Rayleigh equation is used [58]:

$$\frac{I}{I_0}(\lambda) = e^{-\left[32\pi^4 f_v L \frac{r^3}{\lambda^4}\left(\frac{\varepsilon_p - \varepsilon_m}{\varepsilon_p + 2\varepsilon_m}\right)^2\right]}$$

which is valid for spherical particles with radius r and where, ε_p and ε_m are the relative electric permeability of the nanoparticles and the polymer, I is the intensity of the transmitted light and I_0 of the incident light, f_v the volume fraction of the particles, λ the wavelength of light, and L the optical path length. As an example, the transmittance as a function of the particle radius calculated by the Rayleigh equation is shown in Figure 2.10 for L=100 μm (typical thickness of freestanding nanocomposite films), f_v=0.1, λ=500 nm, n_m=1.5 (typical refractive index of polymers), and n_p=2.7 (refractive index of rutile).

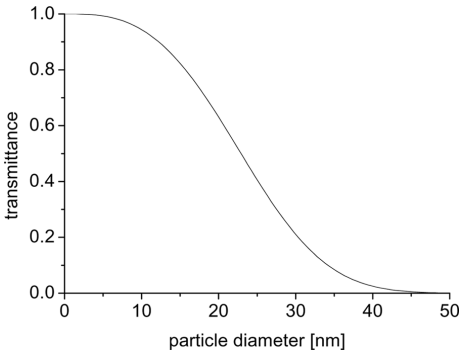

Figure 2.10. Transmittance of composites of 100 μm thickness, volume fraction of the particles of 0.1, refractive index of the matrix of 1.5 and of the particles of 2.7 at a wavelength of 500 nm, calculated with Rayleigh equation [59].

This example shows that even substantially filled nanocomposites with large refractive index differences between polymer and particles can be virtually fully transparent if the particles are very small, in the above example of approximately 5 nm diameter (r = 2.5 nm) or less, while composites with larger particles appear opaque. On the other hand, if n_m and n_p are equal, the equation indicates that the composites are completely transparent regardless of the particle diameters.

Nussbaumer et al. prepared transparent TiO_2-poly(vinyl alcohol) (PVAL) films of thicknesses between 40 and 80 mm and TiO_2 contents between 2 and 35% w/w [60]. TEM images revealed that the TiO_2 particles of radius about 2.5 nm were randomly dispersed in the polymer matrix. UV-visible absorption spectra disclosed that the samples absorbed light in the UV region, while absorption in the visible wavelength region was pronounced only above about 25% w/w of TiO_2.

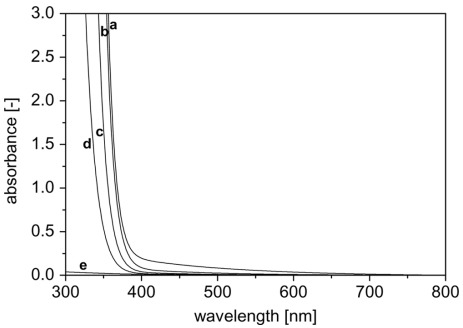

Figure 2.11. Optical absorption spectra of poly(vinyl alcohol)-TiO2 nanocomposites with the following TiO_2 contents (in % w/w): (a) 30.8, (b) 23.0, (c) 11.0, (d) 6.9, and (e) 0.0 (pristine polymer).

Another properties of titanium dioxide is the high refractive index (about 2.61 for rutile and 2.49 for anatase). In fact, the possibility to tune the refractive index of organic polymers by incorporation of inorganic nanoparticles is important, for example, in the area of lenses, wave guides, gloss, iridescence, holographic memories, and reflectors or antireflection layers. Chang et al., for example, by filling a PI polymer with TiO_2 from approximately 8% to 36% v/v, increased the material refractive index from 1.69 to 1.82 [61].

Finally, titanium dioxide nanoparticles show reversible photochromism linked to the oxidation state of titanium ions. In fact Ti(III) ions absorb in the visible leading a bluish color of the material. As consequence, if the irradiation of a TiO_2 nanocomposite with artificial light sources induces the reduction of Ti(IV) in Ti(III), the material become blue until oxidizing agents (in general atmospheric oxygen), oxide again Ti(III) to Ti(IV). From this point of view, the reversibility rate of this phenomenon is linked to the oxygen permeability of the polymer. Nussbaumer et al. showed, for example, that the blue color of nanocomposite TiO_2-poly(vinyl alcohol) (PVAL), irradiated by UV light for 12 hours, persisted for weeks under environmental conditions; i.e., PVAL obviously stabilized the Ti(III) centers [62]. It appears, therefore, that the PVAL retarded or even prevented the contact of atmospheric oxidizing agents with the TiO_2 particles, perhaps as a result of the limited permeability of oxygen in the polymer [63].

2.5 References

[1] Althues H, Henle J and Kaskel S 2007 *Chem. Soc. Rev.* **36** 1454
[2] Petrovicova E, Knight R and Twardowski T E 2000 *J. Appl. Polym. Sci.* **77** 1684
[3] Hong J I, Cho K S and Siegel R W 2002 *J. Mater. Res.* **17** 940
[4] Zhao H and Li R K Y 2006 *Polymer* **47** 3207
[5] Sooklal K, Hanus L H and Ploehn H J 1998 *Adv. Mater.* **10** 1083
[6] Avella M, Errico M E and Martuscelli E 2001 *Nano Lett.* **1** 213
[7] Kichelbick G 2003 *Prog. Polym. Sci.* **28** 83
[8] Uskokovic V and Drofenik M 2005 *Surf. Rev. Lett.* **12** 239
[9] Fernández-García M, Wang X, Belver C, Hanson J C and Rodriguez J A 2007 *J. Phys. Chem. C* **111** 674
[10] Palkovits R, Althues H, Rumplecker A, Tesche B, Dreier A, Holle U, Fink G, Cheng C H, Shantz D F and Kaskel S 2005 *Langmuir* **21** 6048
[11] Mayer A B R 1998 *Mater. Sci. Eng. C* **6** 155
[12] Suzuki S, Onishi H, Sasaki T and Iwasawa Y 2001 *Stud. Surf. Sci. Catal.* **132** 753
[13] Silveira K F, Yoshida I V P and Nunes S P 1995 *Polymer* **36** 1425
[14] Sengupta R, Bandyopadhyay A and Bhowmick A K 2005 *Polymer* **46** 3343
[15] Kammler H K, Madler L and Pratsinis S E 2001 *Chem. Eng. Technol.* **24** 583

[16] Kruis, F. E.; Fissan, H.; Peled, A.; *J. Aerosol. Sci.*, 1998, 29, 511
[17] Hahn H 1997 *Nanostruct. Mater.* **9** 3
[18] Swihart M T 2003 *Cur. Opin. Colloid Interf. Sci.* **8** 127
[19] Grieve K, Mulvaney P and Grieser F 2000 *Cur. Opin. Colloid Interf. Sci.* **5** 168
[20] Trindade T, O'Brien P and Pickett N L 2001 *Chem. Mater.* **13** 3843
[21] Murray C B, Kagan C R and Bawendi M G 2000 *Annual Rev. Mater. Sci.* **30** 545
[22] Cushing B L, Kolesnichenko V L and O'Connor C J 2004 *Chem.Rev.* **104** 3893
[23] Pinna N and Niederberger M 2008 *Angew. Chem.* **120** 5372
[24] Newbery A P, Han B Q, Lavernia E J, Suryanarayana C and Christodoulou J A 2007 *Mater. Process. Handb.* **13** 1
[25] Goesmann H and Feldmann C 2010 *Chem. Int. Ed.* **49** 2
[26] Burda C, Chen X and El-Sayed M A 2005 *Chem. Rev.* **105** 1025
[27] Takagi M 1954 *J. Phys. Soc. Jpn.* **9** 551
[28] Wronski C R M 1967 *Br. J. Appl. Phys.* **18** 1731
[29] Goldstein A N, Echer C M and Alivisatos A P 1992 *Science* **256** 5062
[30] Johnson D C, Benfield R E and Vargas M D 1985 *Nature* **314** 231
[31] Rademann K, Even U and Hensel F 1992 *Phys. Rev. Lett.* **69** 3208

[32] Yu, W.W.; Qu, L.; Peng, X.; *Chem. Mater.*, 2003, 15, 2854
[33] Schmid G 2004 *Nanoparticle: From Theory to Application,* Wiley VCH, Weinheim
[34] Rao C N R, Santra A K and Prins M W J 1992 *Angew. Chem. Int .Ed. Engl.* **31** 1062
[35] Valden M, Lai X and Goodman D W 1998 *Science* **281** 1647
[36] Linsebigler A L, Lu G, Yates J T 1995 *J. Chem. Re*v. **95** 735
[37] Zhang H and Banfield J F 2000 *J. Phys. Chem. B* **104** 3481
[38] Adams R 2005 *Focus on Pigm*. **1** 1
[39] Preuss H P 1974 *Pigments in Paint*, Noyes Data Corp., Park Ridge, N. J.
[40] Fujishima A and Honda K 1972 *Nature* **238** 37
[41] Szczepankiewicz S H, Colussi A J and Hoffmann M R 2000 *J. Phys.Chem. B* **104** 9842
[42] Berger T, Sterrer M, Diwald O, Knoezinger E, Panayotov D, Thompson T L and Yates J T 2005 *J. Phys. Chem. B* **109** 6061
[43] Ohno T, Masaki Y and Matsumura M 2001 *J. Catal.* **204** 163
[44] Pillai U R and Sahle-Demessie E 2002 *J. Catal.* **211** 434
[45] Mills A, Davies R H and Worsley D 1993 *Chem. Soc. Rev.* **22** 417
[46] Peral J, Domenech X and Ollis D F 1997 *Biotechnology* **70** 117

[47] Cai R, Hashimoto K and Fujishima A 1991 *Bull. Chem. Soc. JPN* **64** 1268
[48] Poulios I, Spathis P and Tsoumparis P 1999 *J. Envir. Sci. Health A* **34** 1455
[49] Paz Y, Luo Z, Rabenbery L and Heller A 1995 *J. Mater. Chem.* **10** 2848
[50] Feng X, Zhai J and Jiang L 2005 *Angew. Chem., Int. Ed* **44** 5115
[51] Xu Y, Yao K and Cao Q 1993 *Sens. Actuators B* **13–14** 492
[52] Grätzel M. 2004 *J. Photochem. Photobiol. A* **164** 3
[53] Kawahara K, Suzuki K, Ohko Y and Tatsuma T 2005 *Phys. Chem. Chem. Phys.* **7** 3851
[54] Nussbaumer R J, Caseri W R and Smith P 2006 *J. Nanosci. Nanotechnol.* **6** 459
[55] Martin C, Rives V, Sanchez-Escribano V, Busca G, Lorenzelli V and Ramis G 1991 *Surf. Sci.* **251/252** 825
[56] Chiang P C, Whang W T, Tsai M H and Wu S C 2004 *Thin solid film* **447-448** 359
[57] Liu Y and Lee J Y 2003B *J. Appl. Polym. Sci.* **89** 2815
[58] Nussbaumer R J 2004 Synthese und Charakterisierung von Rutilnanopartikeln und deren Einbau in transparente Polymer-Nanoverbundwerkstoffe, Ph.D. diss., Eidgenössische Technische Hochschule Zürich.
[59] Caseri W 2009 *Chem. Eng. Comm.* **196** 549
[60] Nussbaumer R J, Caseri W R, Tervoort T and Smith P 2003 *Macromol. Mater. Eng.* **288** 44

[61] Chang C M, Chang C L and Chang C C 2006 *Macromol. Mater. Eng.* **291** 1521
[62] Nussbaumer R J, Caseri W R and Smith P 2006. *J. Nanosci. Nanotechnol.* **6** 459
[63] Ohtani B, Adzuma S, Nishimoto S-I and Kagiya T 1987 *J. Polym. Sci. C* **25** 383

Chapter 3

Surface Modification of Titanium Dioxide by Phosphonic Acid derivates

3.1 Introduction

The development of polymer loaded with opportune nanoparticles in order to obtain materials with renewed optical properties such as tailored absorption/emission properties, high/room refractive index, non-linear optical behavior has received great interest from the scientific world for the expected potentialities of these materials. In particular, it was point out that these materials had to be characterized by high transparency in the visible range for applications in the optoelectronic and in the industry of coating [1, 2]. One of the most excellent host is the poly-methylmethacrylate (PMMA) for the high optical clarity and know physical and chemical properties [3 - 5], while several metal oxides (ZnO, ZrO, TiO_2, CdS, etc.) are good candidates in order to tune the polymer optical properties without changing its appearance [6].

Titanium dioxide is a well-known multi-functional metal oxide characterized by a strong UV absorption and high refractive index. These two features represent interesting properties in order to obtain highly refractive materials characterized by an inner UV filter. On the other hand, some drawbacks emerged. The first one is the titanium dioxide photo-catalytic activity

induced by the absorption of the UV light in oxygen's presence [7, 8]. The second drawback is linked to the mismatch of refractive indices between the titanium dioxide (from 2.49 to 2.61 according to the crystalline phase) and the polymeric matrix, whose refractive index is generally around 1.5. This mismatch is tolerable when the particle size is much smaller than the wavelength of the incident light ($2r < \lambda/10$), then the material became haze for the scattering of the visible light. In fact, also a small percentage of aggregates larger than 100 nm can cause the material loss of transparency, due to the fact that the light scattering intensity is proportional to r^3. Other factors such as the material thickness and the concentration of fillers in the polymeric matrix play also an important role in the amount of the scattered light but the dependence is linear [9]. On the other hand, the formation of aggregates or clusters of crystallites is very likely to occur because of nanoparticles high surface energy. This is the reason because a lot of attention was pointed out on the TiO_2 surface modification in order to reduce its photo-activity, to alter its hydrophilic character and improve its dispersibility in organic media. There have been many patents and papers issued for TiO_2 modifying methods, which can be divided into four groups. i) Modification by chemi-sorption of small molecules in which coordination, hydrogen bond formation, or proton transfer occurs. ii) Modification by coupling agents involving covalent bond formation between the adsorbed species and hydroxyl groups present on TiO_2 surface. iii) Modification by the adsorption of polymers, called also *grafting to* technique. iv) Modification by

functionalization of the inorganic surface with initiating group, such as the monomers, called also *grafting from* technique.

Not only the method, but also the selection of the proper surfactant and the way in which it is anchored on the metal oxide surface are very important for the nanoparticles stabilization in the media. For example, thiols are excellent stabilizer for gold and silver [10]; amines are good capping agent for Pd and Pt [11]; metal oxides have been modified successfully with silanes and acidic surfactants: carboxylic acids and phosphonic acids (PAs) are the most used [12, 13].

In this work we report the surface modification of three different types of titanium dioxide: a commercial rutile from Aldrich, an anatase synthesized by non-aqueous route, and a commercial mixture of anatase and rutile (Aeroxide P25® from Degussa), with two types of phosphonic acids, characterized by an aliphatic and aromatic tail. The aim was to understand the role played by the different titania surfaces [14] and the PAs tails on the binding modes of phosphonic acids to the substrate. The temperature of the synthesis was also considered. We chose the phosphonic acids because of the recognized capacity to form a monolayer on the metal oxides surface [15-16], compared to the silanes that tend to be cross-linked on the surface via condensation of the terminals hydroxyl groups, forming uncontrolled multilayers. Furthermore, phosphonic acids are known to bind to metal oxide surfaces more strongly than carboxilic acids [17]. The type of anchoring was studied by FTIR and ^{31}P Solid State NMR, while the degree of coverage was calculate using thermogravimetry (TGA) and

phosphorous elemental analysis. The stability of the modified titanium dioxide nanoparticles in an organic media, in this case the monomer methylmethacrylate (MMA), was verified by Dynamic Light Scattering (DLS) measurements.

3.2 Experimental

3.2.1 Materials

Three different type of titanium dioxide nanoparticles were modified on the surface: TiO_2 rutile (Aldrich), characterized by a declared surface area of 130-190 m^2/g, Aeroxide® TiO_2 P25 (Evonik), mixture of rutile and anatase with a surface area of 50 m^2/g and anatase, synthesized according to the Niederberger et al. [18] recipe. Rutile and P25 were purchased by the relative suppliers and used without other treatments, while a description of the anatase synthesis is reported in the chapter 4. Phenylphosphonic Acid (98% Aldrich) and 1-Octylphosphonic Acid (99%, Alfa Aesar) were chosen as modifying agents and used without further purification. Solvents and other chemical reagents are also obtained as analytical grade and used without other treatments.

3.2.2 TiO_2 surface modification

3.2.2.1 High Temperature Synthesis (HT).

A dispersion of 200 mg of TiO_2 in 20 ml of deionized H_2O was treated in ultrasonic conditions for 15 min (350 W power) with a Sonics Vibracell (Sonics Materials). The colloidal dispersion

was added dropwise to 100 ml of 1:3 water:ethanol solution containing 2.5 fold excess of phosphonic acid relative to the moles for a full surface coverage of the metal oxide. The reaction mixture was then heated to 373 K for 72 h under magnetic stirring. The titania nanoparticles were collected by centrifugation and washed 3 times with ethanol. Finally the powder was dried at 313 K under vacuum overnight.

3.2.2.2 Room Temperature Synthesis (RT).

A dispersion of 200 mg of TiO_2 in 20 ml of water was treated in ultrasonic conditions for 15 min (350 W power) and added dropwise to 100 ml of 3:1 methanol:water mixture containing 2.5 fold excess of phosphonic acid relative to the moles for a full surface coverage of the metal oxide and left to react for 72 h at room temperature under magnetic stirring. The titania nanoparticles were collected by centrifugation and washed 3 times with ethanol. Finally the powder was dried at 313 K under vacuum overnight.

3.2.3 Characterization Techniques

Nitrogen adsorption-desorption isotherms were measured at liquid nitrogen temperature using an ASAP 2010 analyzer (Micrometrics). The titanium dioxide powders were outgassed for 12 h at 473 K. Nanoparticles surface areas were calculated using the Brunauer, Emmet, and Teller model (BET model) [19]. Pore-size distributions were evaluated folrooming the

method developed by Barret, Joyner, and Halenda (BJH model) [20].

The TiO_2 powders XRD patterns were checked using a D8 Advance powder diffractometer (Bruker), with CuKα1 radiation (λ=1.5418Å) and secondary-beam monochromator, while their morphologies and sizes were verified by Transmission Electron Microscopy (TEM). TEM images were recorded on a Jem 1011 microscope (JEOL) operating at 100 kV. TEM samples were prepared by leaving 1-2 drops of the nanoparticles dispersions in water onto lacey carbon copper grid.

Attenuated Total Reflection (ATR) Fourier Transform Infrared (FTIR) spectra of nanoparticles powders were recorded at room temperature from 4000 e 600 cm^{-1} with a spectral resolution of 4 cm^{-1} on a FTIR Spectrum 100 spectrometer (Perkin Elmer, USA). Each spectrum was averaged on 32 scans with 0.2 cm/s speed.

Thermogravimetry was carried out with TA Q500 analyzer (TA Instruments) by heating the samples powders from room temperature to 1073 K at 10 K/min in air.

The sizes of the nanoparticles clusters in Methylmethacrylate (MMA) and water were determined by Dynamic Light Scattering (DLS) using a 90Plus instrument (Brookhaven Instrumental Company) at 298 K equipped with a monochromatic light source working at 659 nm with a CCD detector at 90°. Samples were prepared by dispersion of 10 mg of nanoparticles in 10 ml of solvent. Before the measurements,

ultra-sonication for 3 min (350 W power) of the colloidal solutions was performed.
^{31}P solid-state NMR spectra were obtained with an Avance 300 spectrometer (Bruker), using magic angle spinning (MAS) (spinning rate 8 kHz), $\pi/3$ excitation pulse and 15 s of recycling delay (single pulse technique). Chemical shifts are referenced against H_3PO_4 (85% in water). The peaks deconvolutions were performed by MestReC software.

3.3 Results and Discussion

3.3.1 Characterization of pristine TiO_2 nanoparticles

In Figure 3.1 the powders XRD patterns and the corresponding TEM images are reported.

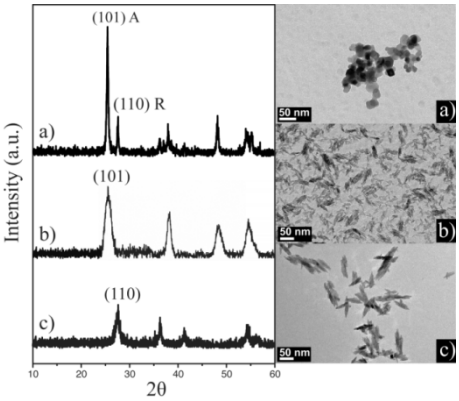

Figure 3.1. XRD images of titanium dioxide nanoparticles: a) P25, a mixture of anatase and rutile crystalline phase; b) anatase; c) rutile. On the right the corresponding TEM images are reported.

Powders XRD patterns confirm the data published in literature for the anatase synthesized by non-aqueous route [18], and in the technical datasheets for the commercial products.
Particles sizes were calculated with the Scherrer formula from the (101) peak for anatase (peak "A" in Figure 3.1a) and (110) peak for rutile (peak "R" in Figure 3.1a) in powder XRD patterns. In table 1 these data are reported with the BET results and, only for anatase and P25, with the crystalline sizes calculated by BET measurements. Particles sizes by BET were calculated using the folrooming formula: Surface Area (BET) = 6000/[ρ (in g/m^3) D (in nm)], where ρ and D are the nanoparticles density and the diameter. Given to the fact this equation works only for the spherical nanoparticles, it is not used for rutile particles that are lengthen, as TEM image shows (Figure 3.1c). The hydrodynamic diameters of nanoparticles in water are also reported. DLS results show that all types of titanium dioxide aggregates in water in strange shapes, but while anatase and rutile clustes are quite small, P25 precipitates in water within few days. These information are in good agreement with the particles aggregates observed by TEM. In Table 3.1 a summary of these information is reported.
From these results, anatase and rutile were chosen as good candidates to load the polymeric matrix in order to obtain transparent nanocomposites because of the small size of the nanoparticles (see table 1), P25 was investigated as comparison with other powders because it has been well characterized in literature, although in general for its photocatalytic activity [21].

Table 3.1. Surface areas and particulate sizes calculated by BET and XRD data for the different types of TiO_2 nanoparticles. The diameter of the TiO_2 clusters in water as measured by DLS is also reported.

Products	BET		XRD Particles size[b] (nm)	DLS Hydrodynamic diameter (nm)
	Surface Area (m^2/g)	Particles size (nm)[a]		
P25 (Degussa)	50	34	24 (A) - 31 (R)	n.m.[c]
Anatase	250	6.2	5.6	40 [20][d]
Rutile (Aldrich)	210	-	12	115 [40][d]

[a] Particles size measured by BET data.

[b] Particle size calculated with the Scherrer formula from the (101) peak for anatase and (110) peak for rutile by the powder XRD patterns.

[c] "n.m." means "not measured" by DLS because the particles precipitates in few minutes.

[d] The numbers in the square brackets represent the standard deviation.

In Figure 3.2, the IR spectra of the titanium dioxide nanoparticles are reported.

The rutile IR spectrum reveals signals relative to Si-O species at around 1035 cm^{-1} and 929 cm^{-1}, indicating that the surface is partially coated with silicon dioxide. This process is used by titanium dioxide suppliers in order to reduce the particles' catalytic activity.

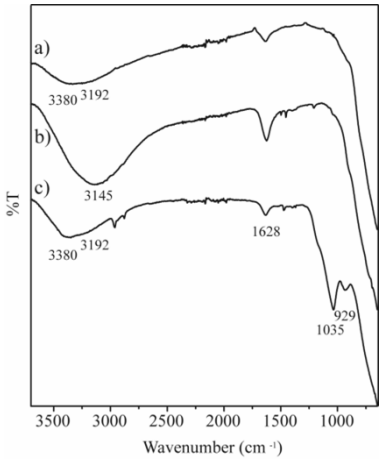

Figure 3.2. FT-IR spectra of a) P25 titanium dioxide nanoparticles; b) anatase obtained by non-aqueous route; c) rutile (Aldrich).

Then, in the region relative to the stretching and bending modes of the C-H species (3000-2850 cm^{-1} and 1480-1350 cm^{-1} respectively) are visible some peaks that are linked to aliphatic organic residuals on the particles surface. Peaks relative to the other type of organic species on the TiO_2 surface are also visible in the IR anatase spectrum. They are less intense than those ones of the rutile spectra probably because of the intense band relative to the O-H moiety, but they are probably linked to some residuals of the anatase synthesis. In fact, literature reports that the nanoparticles obtained by non-aqueous route are characterized by an important amount of organic residuals on the nanoparticles surface, probably benzyl alcohol (see signal at 1500 cm^{-1} linked to the aromatic C-H

moiety), while P25 IR spectrum does not show any organic species.

Stretching and bending modes of the O-H group (at about 3380 cm^{-1} and 1628 cm^{-1} respectively) present in all spectra are attributed to the water physically absorbed on the titanium dioxide surface by inter-molecular interections. Only anatase spectrum shows a more intense band at around 3145 cm^{-1}, probably linked to acid O-H moiety bonded covalently on the surface.

TGA measurements of untreated particulates reveal several weight losses for rutile and anatase powders, while P25 weight loss is unimportant (about 1.6 %), as Figure 3.3 shows. The weight loss within 393 K is due to physically absorbed moisture [22]; this is the reason because the calculation of the total weight loss is performed from 393 K. Between 393 K and 873 K we observe four weight losses at 459 K, 506 K, 577 K, and 648 K for rutile particulate with a total weight loss of about 6% due to the chemically bounded water (surface OH groups) and organic residuals. Anatase TGA curve shows other weight losses at 428 K, 533 K and 693 K with a total weight loss of about 15% due to the expulsion of the organic residuals of the nanoparticles synthesis (for example benzyl alcohol) and the condensation of the O-H groups on the surface confirming IR spectrum (see Figure 3.3c) and the information reported in literature [18].

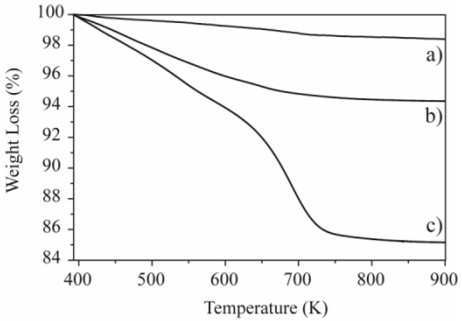

Figure 3.3. TGA curves of a) P25 TiO_2 nanoparticles; b) rutile (Aldrich); c) anatase obtained by non-aqueous route.

3.3.2 Characterization of Titanium Dioxide Surface Modification with Phosphonic Acids

Titanium dioxide has been functionalized with two phosphonic acids characterized by a quite long aliphatic chain and an aromatic ring in order to study the role played by the substituent in the surface coverage and, as consequence, in the stability of the nanoparticles dispersions in organic media, such as the monomer MMA. Functionalizing agents used are 1-octylphosphonic acid (OPA) and phenyl phosphonic acid (PPA). The choice of the PAs family as modifying agents is due to the good anchorage of the H_2PO_3 group to the surface of titania with the possibility of setting up three types of covalent bonds and the formation of a monolayer. IR and solid state ^{31}P NMR assess the type of surface grafting obtained in terms of monodentate, bidentate and tridentate coordination [23-25]. Several different methods of surface modification are reported for titania, however it is possible to define two main

approaches: high temperature [26] and room temperature treatment in hydroalcoholic mixtures [27].

3.3.2.1 FT-IR Results.

In Figure 3.4 the spectra of the different types of titanium dioxide nanoparticles modified by the alkyl phosphonic acid (OPA@rutile, OPA@anatase and OPA@P25) together with the spectrum of the free acid are depicted.
The presence of stretching and bending modes of C-H moiety, respectively in the region between 2960-2850 cm^{-1} and 1500-1400 cm^{-1}, shows the integrity of the aliphatic chain in all the samples. The disappearance of the peaks related to P-O-H vibrations of free phosphonic acids (between 2700-2300 cm^{-1} and around 950 cm^{-1}) and of the P=O group (~1258 cm^{-1}) in the spectra of functionalized TiO_2 particles is an indication of a strong interaction between the head of phosphonic acids and the metal oxides surfaces. In particular, according to the literature [28], the complete absence of P=O vibrational mode and the appearance of a broad band at around 1030 cm^{-1} [29] is a strong hint that the bond between phosphonic acid and the titania surface is tridentate. This is evident in the OPA@anatase and OPA@P25 spectra in which it is possible to see the total disappearance of the P=O mode at 1258 cm^{-1} and the appearance of a broad band at 1042 and 1063 cm^{-1} respectively. On the other hand, OPA@rutile spectrum show a weak band in the P=O region, while the absorption bands of SiO_2 at about 1036 cm^{-1} hides additional evidence for the

chemical bonding between the phosphonic group and the rutile surface.
No differences appears between the IR spectra of the samples synthesized at room and high temperature.

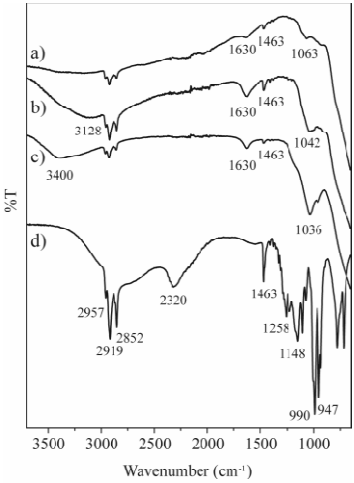

Figure 3.4. FTIR spectra of: a) OPA@P25, b) OPA@anatase, c) OPA@rutile, d) OPA. They are the spectra of the samples synthesized in condition of room temperature. No evident differences appear between the IR spectra obtained in different condition of temperature.

In the spectrum of modified titanium dioxide with phenylphosphonic acid (see Figure 3.5), the disappearance of the peaks related to P-O-H vibrations of free phosphonic acid at 2658-2131 cm^{-1} and around 935 cm^{-1} and of the P=O group points to the coordination of all the phosphoryl oxygens. The samples PPA@anatase and PPA@P25 show a new broad band at about 1010 cm^{-1} and 1063 cm^{-1} respectively, as already observed in the spectra of the particulates modified with the

aliphatic acid, attributed in literature to a tridentate coordination in the case of alumina and zirconia surfaces. Also in this case, the sample PPA@rutile spectrum shows the persistence of a very weak signal for the P=O group points to the partially coordination of the phosphoryl oxygens. The presence of the peak at 1142 cm^{-1} related to P-$C_{aromatic}$ moiety and C-H vibrational modes of the aromatic ring around 1500 cm^{-1} indicate that the tail of the organic molecule is preserved in all cases [30]. Also in this case, there are not important differences between the spectra of the samples obtained in condition of high and room temperature. From this point of view, ^{31}P Solid State NMR is more sensitive for studying the modes in which the phosphonic acids interact with the titanium dioxides surfaces.

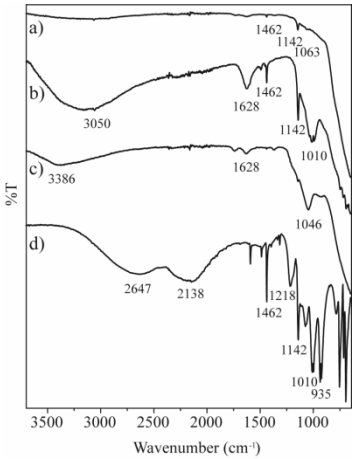

Figure 3.5. FTIR spectra of: a) PPA@P25, b) PPA@anatase, c) PPA@rutile, d) PPA. They are the spectra of the samples synthesized in

condition of room temperature. No evident differences appear between the IR spectra obtained in different condition of temperature.

3.3.2.2 Surface coverage.

The comparison between the weight losses of functionalized and pristine TiO_2 particles, measured by TGA, alrooms to determine roughly the amount of modifying agent attached to the surface and the degree of surface coverage. According to the literature, the weight loss observed up to 393 K is due to the water (or any solvent) physically absorbed on the nanoparticles surface, while losses from 393 K to 873 K are effectively due to the detaching of chemically bounded species to the surface and the condensation of hydroxyl group present on the surface (sintering). Assuming that all phosphonic acids are chemisorbed as a single layer on the titanium dioxide surfaces the amount of chemisorbed species per nm^2 has been calculated subtracting the weight loss of the pristine TiO_2 from the weight loss of the treated samples over 393 K. This computation of the percentage of surface coverage has been performed by the folrooming assumptions: 1) whole molecule detaches from the surface during the heating; 2) the surface area occupied by every phosphonic acid is 0.24 nm^2 [3, 23]. Because of a lot of assumptions, this calculation is very rough, but the comparison with the results of the phosphorous elemental analysis permits to make some previsions on the anchorage strength of the phosphonic acids head on the titanium dioxide surface. All data are summarized in table 3.2.

Table 3.2. Mass loss calculated as difference between the weight losses of functionalized nanoparticles and the pristine nanoparticles, measured by TGA. Phosphorous in percentage measured by elemental analysis. In each case, the calculation of the surface coverage in percentage is revealed.

Sample		TGA		Elemental analysis	
		Mass Loss (%)	Coverage (%)	%P	Coverage (%)
OPA@P25	RT	1.6	25	0.45	43
	HT	1.3	20	0.28	27
OPA@anatase	RT	3.6	9	3.16	74
	HT	0.3	4	2.39	53
OPA@rutile	RT	2.0	8	0.15	3
	HT	3.8	15	1.04	25
PPA@P25	RT	0,8	16	0.26	25
	HT	0.3	7	0.27	26
PPA@anatase	RT	2.3	11	3.31	75
	HT	0.4	2	2.22	47
PPA@rutile	RT	1.4	7	0.14	3
	HT	5.4	27	0.86	20

The most relevant information is obtained in the case of anatase nanoparticles. While the surface coverage percentages calculated starting by TGA are very small for all samples (up to about 11%), the same information obtained by phosphorous elemental analysis show that over about 47% of anatase surface is covered by phophonic acid molecula. This discrepancy can be attributed to the substitution of the organic residuals present on the anatase nanoparticles surface (see the thermogravimetry trace in Figure 3.3) with the functionalizing agents. Less important differences between the data calculated starting from

TGA and elemental analysis are emerged instead in the cases of rutile and P25 nanoparticles. On the other part, the amount of organic residuals on their surfaces is less important than in the case of anatase. Different result is that relative to P25 nanoparticles. In fact, in this case, TGA measurements and phosphorous elemental analysis can be compared considering that only the phosphonic acids tails detach from the P25 surface during the TGA thermal program. More unpredictable is the rutile behavior, probably linked also to the fact that the surface is partially coated by silicon dioxide. In fact, according to Mutin et al. [31], phosphonic acids do not bind to SiO_2 in aqueous conditions. This behavior has been ascribed to the sensitivity of the Si-O-P bonds to hydrolysis. From this point of view, the assumption that the whole rutile surface area is available for the bonding is very rough and the calculated surface coverage is underestimated.

3.3.2.3 ^{31}P Magic Angle Spinning NMR.

^{31}P chemical shift is quite sensitive to the variety and number of chemical bonds occurring on the phosphonic group and permits to elucidate the nature of bonding between the phosphonic acids and the titania surface. Figure 3.3.5 shows the comparison between the spectra of the bulk phosphonic acids: OPA and PPA, and the surface bound PAs (OPA@P25 and PPA@P25). In this case the spectra of the commercial titania P25 modified at room temperature are reported. OPA and PPA are two crystalline solids characterized by a sharp signal at 37.1 and 22.3 respectively (see Figure 3.6a and 3.6c).

The spectra of the oxide modified with PAs (Figure 3.6b and 3.6d) appear quite broadened and signals are shifted as compared to those of unbounded acids. The enlargement of the line width and chemical shifts arise from a distribution of binding sites and modes of the phosphonic acid groups on the TiO_2 surface. Even if the peaks attribution is still much debated, the signals are linked to the different bonding modes (monodentate, bidentate, tridentate) of phosphonic acids to the particles surface.

In particular ^{31}P MAS spectrum of OPA@P25 shows a quite sharp signal centered at 28.9 ppm and very broad and weak signals at around 33.6 and 36.8 ppm. The main resonance is ascribed to bidentate specie. This attribution is validated by the fact that ^{1}H-^{13}P HETCOR NMR spectrum of the same commercial titanium dioxide modified with a long chain alkylphosphonic acid showed the presence of protons P-OH [32]. Also the ^{13}P MAS NMR spectrum of PPA@P25 is characterized by more signals: one more intense at around 13.6 ppm and one weaker at around 19.4 ppm. The main peak at 13.6 ppm is attributed by the literature to the tridentate mode. In fact, ^{17}O MAS NMR research on a PPA-titania hybrid revealed a majority of the bond P-O-Ti with few residual of P=O and P-OH oxygens [33]. The different behavior between the alkyl phosphonic acid and the phenylphosphonic acid might be related to the higher acidity of the second one. The other low field resonances arise from phosphonate species with different binding modes or in a distorted geometry.

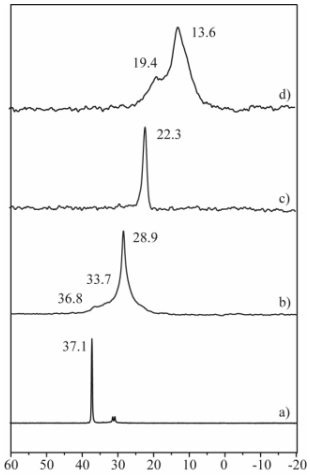

Figure 3.6. ^{31}P MAS NMR spectra of P25 modified with octylphosphonic acid and phenylphosphonic acid at room temperature a) free OPA, b) OPA@P25, c) free PPA and d) PPA@P25.

In Figure 3.7 a schematic representation of the bidentate (on the left) and tridentate (on the right) binding modes by coordination and condensation of a PA on the metal oxide surface is depicted.

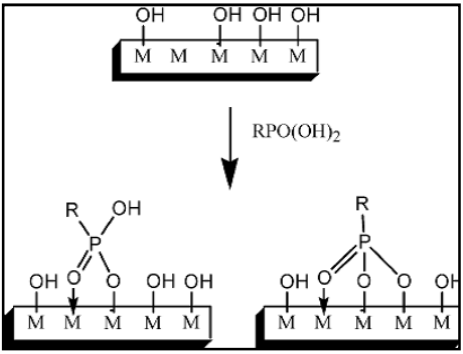

Figure 3.7. Schematic representation of the formation of the bidentate (on the left) and tridentate (on the right) binding species by coordination and condensation of a phosphonic acid to a metal oxide surface. The image is excerpted from [33].

As conclusion, we have seen that the functionalizing agent acidity may play an important role in the binding mode between the PAs and the titanium dioxide surface.

In Figure 3.8, the comparison among the ^{31}P MAS NMR spectra of the three different types of titanium dioxide (P25, anatase and rutile) modified with octylphosphonic acid is showed. All reactions were performed in room temperature condition.

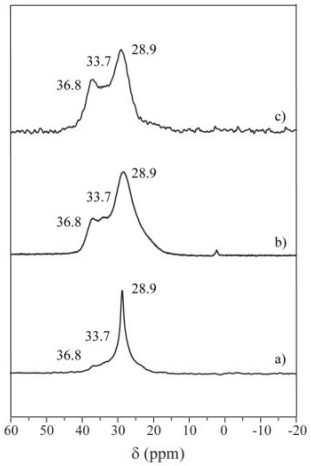

Figure 3.8. ^{31}P MAS NMR spectra of the different types of titanium dioxide modified with octylphosphonic acid at room temperature a) OPA@P25, b) OPA@anatase and c) OPA@rutile.

Even though each spectrum may be convoluted with three peaks, showing three maxima at around 36.8, 22.7 and 28.9 ppm, very different is the peaks width line and the peaks intensity that is quantitative, since ^{31}P NMR spectra were acquired with recycle delays five times T_1. The peak at about 28.9 ppm in the P25 spectrum is sharp and much more intense than other resonances, indicating that the P25 surface is quite homogeneous and the bidentate binding mode predominates on the others (Figure 3.9a). Anatase and rutile signals are instead much more broadened and other important peaks seems to occurs apart from that at 28.9 ppm, indicating the presence of other binding modes or distorted geometry. This result might be attributed to the heterogeneity of the anatase and rutile surface. In particular, anatase is partially coated by some

organic reaction residual, such as benzyl alcohol, that – even though it seems to be substituted by PAs during the reaction – its presence might modify the approach of the functionalizing agent to the metal oxide surface. On the other hand, rutile surface is partially coated with SiO_2, that does not bind with phosphonic acids, as we have already said. This situation might, for example, promotes the formation of the monodentate specie or distorted arrangements.

As conclusion, an important role is also played by the chemical properties of metal oxide surface.

The last variable is the temperature of reaction. Literature pointed out that under aggressive conditions (high pH, high temperatures, long reaction times) some dissolution of the TiO_2 matrix can occur, folroomed by the reprecipitation of metal phosphonate (see Figure 3.9).

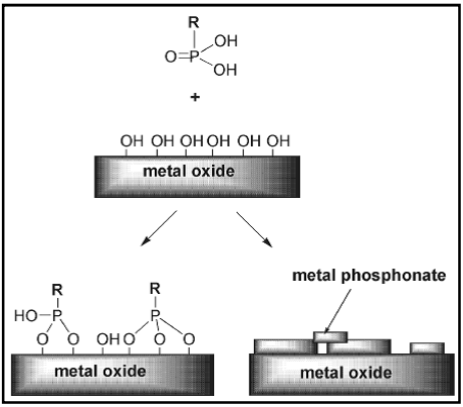

Figure 3.9. Schematic representation of the competition between the surface modification and dissolution-precipitation process in the reaction

between a metal oxide surface and a phosphonic acid. The image is excerpted from [34].

Figure 3.10 shows ^{31}P MAS NMR spectra of P25, anatase and rutile nanoparticles modified with octylphosphonic acid at high temperature conditions (100°C for 72 hours).

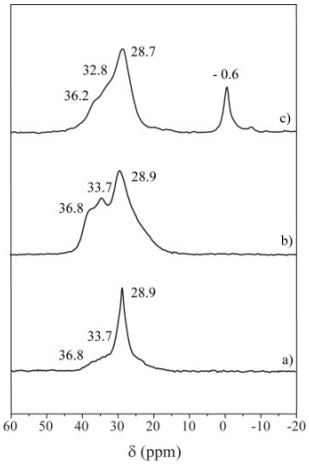

Figure 3.10. ^{31}P MAS NMR spectra of the different types of titanium dioxide modified with octylphosphonic acid at high temperature conditions a) OPA@P25, b) OPA@anatase and c) OPA@rutile.

Apart from the broad signal at room field, ^{31}P MAS spectrum of rutile nanoparticles modified by octylphosphonic acid at high temperature conditions (OPA@rutile) displays a narrow peak at about -0.6 (Figure 3.10c). This signal is attributed to a bulk titanium phosphonate as it is quite closed to the value - 4 ppm, reported for the layered phase of titanium phenylphosphonate [35]. In this case, the tail is a long aliphatic chain and, as consequence, we not expected the formation of a

layered phase, but the formation of a bulk phosphonate phase has been reported in literature with octadecylphosphonic acid as functionalizing agent [26]. The fact itself that there is no evidence of titanium phosphonate in the ^{31}P MAS spectra of OPA@rutile obtained at room temperature conditions (Figure 3.10c) confirms that aggressive conditions lead to a modification of the metal oxide surface. On the other hand, P25 and anatase spectra (Figure 3.10a and 3.10b) not show important differences compared to those obtained at room temperature. The high field peak not appears in their spectra, but the intensity ratio among the room field resonances: 36.8, 33.7 and 28.9 ppm are changed. In particular, anatase spectrum has the signal at 33.7 ppm more intense, while the main peak at 28.9 ppm of the P25 spectrum is broader. Probably, in the case of these particles more aggressive condition are required for the formation of the metal phosphonate phase. In particular, Gao et al. [26] revealed that the reaction between of P25 and the octadecylphosphonic acid may take at least a week in order to detect the signal of the bulk alkylphosphonate in the ^{13}P MAS NMR spectrum.

3.3.3 Colloidal Stability

The stability of the modified particles in methylmethacrylate (MMA) is studied by DLS. Colloidal dispersions are prepared by ultrasonication and measured after 3 days and 30 days in order to check the stability of nanoparticles in the monomer. Table 3 shows that the titania modified with phenyl phosphonic acid (PPA@TiO_2), independently by the type of the surface and

the conditions of the reaction, precipitates immediately in MMA, despite the hydrophobic character of the aromatic ring. On the other hand, octylphosphonic acid seems to be a good functionalizing agent to obtain titanium dioxide nanoparticles stable in MMA. In particular anatase and P25 modified at room temperature appear very stable in MMA. Surprisingly P25 clusters in MMA vary the size from several hundreds of nanometers in water to about 90 nm in MMA. The rutile nanoparticles modified by OPA (OPA@rutile) appear quite stable in MMA but after 30 days the major part is precipitated on the bottom of the flask. Table 3.3 summarize all these results.

Table 3.3. Hydrodynamic diameter of nanoparticles colloids in MMA after 3 days and 30 days from the preparation. Measurements has been performed by DLS.

Sample	Reaction Temp.	Hydrodynamic diameter [nm]	
		3 Days	30 Days
OPA@P25	RT	90 [40]	70 [30]
	HT	90 [40]	70 [30]
OPA@anatase	RT	100 [40]	80 [30]
	HT	460 [160]	180 [80]
OPA@rutile	RT	250 [100] *	200 [60] *
	HT	280 [100] *	110 [40] *
PPA@P25	RT	n.m. &	n.m. &
	HT	n.m. &	n.m. &
PPA@anatase	RT	500 [250]	n.m. &
	HT	n.m. & -	n.m. &
PPA@rutile	RT	n.m. &	n.m. &
	HT	n.m. &	n.m. &

[*] The numbers in the square brackets represent the standard deviation;
[&] "n.m." is used to signify that nanoparticles are not dispersible.

3.4 Summary

The surface modification of titanium dioxide nanoparticles in anatase, rutile and a mixture of the two phases, by octylphosphonic acid and phenylphosphonic acid was both performed at room and high temperature. FTIR and ^{31}P MAS NMR have alroomed to understand the nature the of bond established between titania and the modifying agents. In particular, the defects and heterogeneities of the metal oxide surface, the acidity of the functionalizing agent and the reaction conditions played an important role on the formation of different binding modes by coordination or condensation of phosphonic acids to the metal oxide surface. Also the formation of distorted geometries was used to explain the presence of the broadened ^{31}P MAS NMR signals. Thermogravimetry and phosphorous elemental analysis permitted to calculate the surface coverage up to 74% for anatase nanoparticles. In order to test the effectiveness of the titania surface modification, different dispersions of the treated nanoparticles in MMA have been prepared. DLS measurements of these colloidal solutions have alroomed to verify the stability of these nanoparticles in MMA in order to prepare TiO_2-PMMA nanocomposite. In all cases, independently by the type of the surface and the reaction conditions, phenylphosphonic acid has been not a good modifying agent

for the stabilization of the metal oxides in MMA. On the other hand, well dispersed nanoparticles clusters of about 90-100 nm in MMA has been obtained through the functionalization of P25 and anatase by octylphosphonic acid at room temperature. P25 nanoparticles were also stable in MMA after modification with OPA at high temperature conditions.

3.5 References

[1] Althues H, Henle J and Kaskel S 2007 *Chem. Soc. Rev.* **36** 1454

[2] Beecroft L L and Ober C K 1997 *Chem. Mater*. **9** 1302

[3] Demir M M, Koynov K, Akbey Ü, Bubeck C, Park I, Lieberwirth I and Wegner G 2007 *Macromolecules* **40** 1089

[4] Koziej D, Fischer F, Kränzlin N, Caseri W R and Niederberger M 2009 *Appl. Mater. Interfaces* **1** 1097

[5] Cinausero N, Azema N, Cochez M, Ferriol M, Essahli M, Ganachaud F and Lopez-Cuesta J-M 2008 *Polym. Adv. Technol.* **19** 701

[6] Goesmann H and Feldmann C 2010 *Angew. Chem. Int. Ed.* **49** 2

[7] Zhu J, Yang J, Bian Z-F, Ren J, Liu Y-M, Cao Y, Li H-X, He H-Y and Fan K-N 2007 *Appl. Catalysis B: Enviromental* **76** 82

[8] Chen X-Q and Shen W-H 2008 *Chem. Eng. Technol.* **31** 1277

[9] Caseri W R 2009 *Chem. Eng. Comm.* **196** 549

[10] Whetten R L and Price R C 2007 *Science* **318** 407

[11] Li Z, Gao J, Xing X, Wu S, Shuang S, Dong C, Paau M C and Choi M M F 2010 *J Phys. Chem. C* **114** 723
[12] Masala O and Seshadri R 2004 *Annu. Rev. Mater. Res.* **34** 41
[13] Neouze M-A and Schubert U 2008 *Monatsh Chem* **139** 183
[14] Luschtinetz R, Frenzel J, Milek T and Selfert G 2009 *J. Phys. Chem. C* **113** 5730
[15] Gao W, Dickinson L, Grozinger C, Morin F G and Reven L 1996 *Langmuir* **12** 6429
[16] Hotchkiss P J, Malicki M, Giordano A J, Armstrong N R and Marder S R 2011 *J. Mater. Chem.* **21** 3107
[17] Hotchkiss P J, Li H, Paramonov P B, Paniagua S A, Jones S C Malicki, Armstrong N R, Brédas J-L and Marder S R 2009 *Adv. Mater.* **21** 4496
[18] Niederberger M, Bartl M H and Stucky G D 2002 *Chem. Mate*r. **14** 4364
[19] Brunauer S, Emmett P H and Teller E 1938 *J. Am. Chem. Soc*. **60** 309
[20] Barret E P, Joyner L G and Halenda P P 1951 *J. Am. Chem. Soc*. **73** 373
[21] Ryu J and Choi W 2008 *Environ. Sci. Technol.* **42** 294
[22] Mueller R, Kammler H K, Wegner K and Pratsinis S E 2003 *Langmuir* **19** 160
[23] Carriére D, Moreau M, Barboux P, Boilot J P and Spalla O 2004 *Langmuir* **20** 3449
[24] Mutin P H, Guerrero G and Vioux A 2003 *C.R.Chimie* **6** 1153

[25] Guerrero G, Mutin P H and Vioux A 2001 *J.Mater.Chem.* **11** 3161
[26] Gao W, Dickinson L, Grozinger C, Morin F G and Reven L 1996 *Langmuir* **12** 6429
[27] Guerrero G, Mutin P H and Vioux A 2001 *Chem. Mater.* **13** 4367
[28] Luschtinetz R, Seifert G, Jaehne E and Adler H P 2007 *Macromol. Symp.* **254** 248
[29] Mohapatra S and Pramanick P 2009 *Colloids and Surfaces A: Physicochem. Eng. Aspects* **339** 35
[30] Demir M M, Castignolles P, Akbey Ü and Wegner G 2007 *Macromolecules* **40** 4190
[31] Mutin P M, Lafond V, Popa A F, Granier M, Markey L and Dereux A 2004 *Chem. Mater.* **16** 5670
[32] Pawsey S, McCormick M, De Paul S, Graf R, Lee Y S, Reven L and Spiess H W 2003 *J. Am. Chem. Soc.* **125** 4174
[33] Lafond V, Gervais C, Maquet J, Prochnow D, Babonneau F and Mutin P H 2003 *Chem. Mater.* **15** 4098
[34] Mutin P H, Guerrero G and Vioux A 2005 *J. Mater. Chem.* **15** 3761
[35] Anillo A A, Villa-Garcia M A, Llavona R, Suarez M and Rodriguez, J. **1999** *Mater. Res. Bull.* **34** 627

Chapter 4

Fabrication and Characterization of transparent TiO_2/PMMA nanocomposite sheets with Tunable Optical Properties

4.1 Introduction

Polymeric nanocomposites, namely polymer matrices containing nanometric particles, nowadays are extensively studied for the improved properties compared to the pure polymer [1]. The presence of a nanometric filler can enhance mechanical properties [2] thermal stability [3], and gas barrier properties [4]. In the last few years nanocomposites with optimized optical properties have also been described. The research has been focused mainly on the following goals: luminescence [5], change (increase) of the refractive index [6], UV absorption [7]. In these cases, the nanocomposite must be as transparent as possible to light in visible range. When a composite is constituted by a polymer matrix and nanofillers with different refractive index, light is scattered causing haze and low transparency depending on nanoparticles physical properties such as dimensions and refractive index. In particular, Rayleigh scattering applies when particles size is smaller with respect to wavelengths of light [8]. In most of the

published papers, the authors try to completely avoid the scattering of visible light, since they are mainly interested in having transparent materials in that region, but with high refractive index or UV or IR absorption. For this reason, starting from Rayleigh's Law, nanoparticles with diameters less than 50 nm are required (for spherical particles $2r < \lambda/10$).

However, in many applications a controlled scattering of light is beneficial; for example an optical diffuser spreads the incident light from sources over a wide angle to prevent light sources from being seen directly by viewers. Optical diffusers are used in lighting bodies, luminaries, illuminated signs, covers for automotive lights and decoration sheets [9]. Another important application are liquid crystal displays, where diffusing elements (plate and sheet) are used for uniform brightness.

Two distinct types of diffusers are recognized, namely, surface-relief and volumetric type. Surface-relief diffusers mainly depend on microstructures on the surface to scatter light, such as microlenses [10,11], pyramids [12], rough surface [13,14] and other microstructures. Volumetric diffusers mainly depend on transparent micro beads or fillers uniformly located inside the material [15]. The need of efficient diffusers becomes more relevant with the progressive replacement of conventional light bulbs with solid state light sources (LEDs) which are more efficient in terms of electricity to light conversion [16]. In fact, considering indoor illumination based on LED luminaries, critical issues are still present due to the directionality of light produced by the LED chip. Different approaches can be used to

overcome this limitation, the most popular is to build luminaries constituted by arrays of LEDs separated by lenses and mirrors or, more recently, to use suitable diffusing panels in which the LEDs are embedded. Such diffusers may be prepared by incorporation of micrometric fillers in transparent polymer matrix, but an optimal balance between light transmission and scattering is difficult to reach. A possible alternative is to use polymer nanocomposites containing particles with diameters comprised between 50 nm and 200 nm; in this case Rayleigh approximation applies. In this case, for a given spectral distribution, the amount of scattered light depends only on size distribution, volume concentration and refractive index of the nanoparticles. Diffusers with tailored properties can be synthesized according to the final application. One of the most appreciated polymers in the lighting industry is PMMA due to its transparency and good chemical and physical properties. Metal oxides, such as TiO_2, ZnO_2 and ZrO_2 are excellent candidates as diffusers because of their high refractive index, so that a limited amount of filler is needed. Since these oxides are hydrophilic, they tend to aggregate in hydrophobic environment, such as organic solvents and monomers, so that the modification of their surface is necessary. In this work, we studied some grafting agents in order to obtain stable titania colloids that can be used for the preparation of nanocomposites.

Bulk polymerization is the only synthetic method which leads to PMMA with excellent optical properties. It is a widely used industrial process, thus giving this method a very strong

potential in large scale production. Especially for thick sheets (1-2 cm), polymerization can last a few days [17]. In order to prepare these materials, stable dispersions of surface modified titania in MMA, precursor of the polymer, are required. Another approach for preparing nanocomposites is the casting from solvent, a process that consists in the dissolution of an already formed polymer in a suitable solvent and subsequent dispersion of nanoparticles in the solution, finally followed by evaporation of the solvent. In order to take advantage of this possibility we studied the stability of functionalized nanoparticles also in some solvents.

4.2 Experimental

4.2.1 Materials

Titanium(IV) oxide: rutile (CAS: 1317-80-2, Product Number Aldrich 637262), surface area 130-190 m^2/g, average diameter less than 100 nm.

Modifying agents: 1-Hexylamine (≥ 98.0%, Fluka), 1-Octylamine (99%, Aldrich) and Propionic Acid (99%, Aldrich), Octanoic Acid (≥ 99.0%, Sigma) were used without further purification. Solvents and other chemical reagents are also obtained as analytical grade and used without further purification.

Reagents for the fabrication of nanocomposites: the monomer MMA (99%, Aldrich), the first initiator 2,2′-Azobis(2-

methylpropionitrile) (98%, Aldrich) and the second initiator benzoyl peroxide (Fluka).

4.2.2 Functionalization of TiO_2 nanoparticles

4.2.2.1 Surface modification with carboxylic acid or alkyl amine.

1 g of TiO_2 in powder was directly added in excess amount of acid or amine (20 ml). After stirring for 24 h at room temperature, the formed precipitate was collected by centrifugation and washed 3 times with ethyl acetate. Finally the powder was dried at 313 K under mechanical vacuum overnight.

4.2.2.2 Surface modification with carboxylic acid and alkyl amine.

500 mg of TiO_2 obtained according to the previous recipe was dispersed in 30 ml of methanol. Excess amount of amine or acid (10 ml) is added to the colloidal solution of TiO_2 nanoparticles previously modified with acid or amine respectively. After stirring for 1 h at room temperature, the formed precipitate is collected by centrifugation and washed three times with ethyl acetate. Finally the powder is dried at 313 K under mechanical vacuum overnight.

4.2.3 Fabrication of Nanocomposite

The preparation of PMMA sheets was performed by bulk polymerization using the industrial cell casting process. The

polymerization is conducted in two steps. First the monomer and a small amount of the first initiator react in a beaker at 353 K where a prepolymerization took place up to monomer's boiling temperature is reached (363 K). At that point the prepolymer, called syrup, is quenched until the room temperature. Usually, in the prepolymerization step, only a modest monomer conversion values into the polymer are obtained (15-20%).

In the second step, the syrup is mixed with a dispersion of titanium dioxide nanoparticles in MMA (about 10% in weight of the syrup) and a second initiator dissolved in it. The obtained viscous liquid is degassed by mechanical vacuum and introduced into the casting mold where the polymerization reaction proceeds until most of the remaining monomer is consumed. The polymerization of the material contained between the glass plates is carried out by heating (323 K) the mold while the glass plates are clamped together. The clamps contain springs in order to accommodate the shrinkage of the polymer sheet during the polymerization process. Initially, the heating is provided by a bath of warm water in which the mold is inserted. Then, it is cured in an oven at 393 K. Cell cast polymerization is the only synthetic method which leads to PMMA with excellent optical properties (about 92-93% of transmittance in the visible range). Especially for thick sheets (1-2 cm), polymerization can last few days (3 for the polymerization and 1 for the curing); from this point of view it is important that the dispersion of titania would be stable in MMA.

4.2.4 Preparation of Colloidal Solutions

The colloidal solutions were prepared by ultrasonication for 5 minutes (21s pulse, 7s pause, 350 W) of the titanium dioxide powder in the monomer or in the solvent. Colloids were stored for 3 days in order to promote the complete wetting [18], and the separation of larger aggregates was performed through centrifugation at 6000 rpm for 1 minute. Dilutions of dispersions were prepared in order to characterize them by UV-Visible spectroscopy and Dynamic Light Scattering.

4.2.5 Characterization Tecniques

X-ray diffraction measurement was performed in order to examine the TiO_2 nanoparticle crystal structure. Powder X-ray diffraction pattern was obtained using a Bruker D8 Advance powder diffractometer, equipped with CuKα1 radiation (λ=1.5418Å) and secondary-beam monochromator. Nitrogen adsorption-desorption isotherms were measured at liquid nitrogen temperature using an ASAP 2010 analyzer (Micrometrics). The samples were outgassed for 12 h at 473 K. Nanoparticles' surface area was calculated using the Brunauer, Emmet, and Teller (BET model) [19]. Pore-size distributions were evaluated following the method developed by Barret, Joyner, and Halenda (BJH model). Nanoparticle' size and morphology were studied using transmission electron microscopy (TEM, JEOL JEM-1011) operated at 200 kV.

TiO_2 surface modification was studied with Attenuated Total Reflection (ATR) Fourier Transform Infrared (FTIR) and ^{13}C MAS NMR. ATR-FTIR spectra were recorded at room temperature from 4000 e 600 cm^{-1} with a spectral resolution of 4 cm^{-1} on a FTIR Spectrum 100 spectrometer (Perkin Elmer, USA). Each spectrum was averaged on 32 scans with 0.2 cm/s speed. ^{13}C MAS NMR spectra were recorded on a Avance 300 spectrometer (Bruker) (spinning rate 8 kHz) using a cross-polarization sequence with RAMP and TPPM decoupling; the contact time was 8 ms and a recycling delay of 10 s was used, 10000 scans were acquired. Thermogravimetry measurements were carried out with a TA Q500 analyzer (TA Instruments) in order to calculate the degree of surface coverage. The samples were heated to 1073 K at 10 K/min in air.

The size of the particles in dispersions was determined by Dynamic Light Scattering (DLS) using a 90Plus instrument (Brookhaven Instrumental Company) at 298 K equipped with a monochromatic light source working at 659 nm with a CCD detector at 90°. Transmission measurements of colloidal solution at different concentrations were performed at room temperature, using a Cary 50 UV-visible spectrophotometer. Collimates light from Tungsten Halogen sources (HL-2000, Ocean Optics) was used to evaluate transmission properties of PMMA/TIO_2 samples. The transmitted radiation was then collected by an integrating sphere and analyzed by a spectrometer (Ocean Optics ,USB 2000 UV-VIS).

4.3 Results and Discussions

4.3.1 Characterization of Pristine Rutile Nanoparticles

Powder XRD pattern of Sigma's titanium dioxide confirms that it was rutile with a surface area calculated by BET of 210 m^2/g. The (110) peak corresponds to a particle size of about 12 nm by Scherrer formula using 0.89 as shape factor. Even if this calculation is not accurate, the result is in a good agreement with the information showed by TEM image reported in Figure 4.1. In fact, TEM image shows lengthen nanoparticles of about 6 nm width and 12 nm length, aggregated in clusters with a hydrodynamic diameter over 100 nm.

Figure 4.1. TEM of TiO_2 rutile nanoparticles.

This data was confirmed by Dynamic Light Scattering, according to the colloids' size in water is measured about 115 nm.

The IR analysis of TiO_2 rutile reveals the presence of H_2O adsorbed on the surface. Minor signals, related to C-H species,

are also present, probably organic residues of the synthetic process. Moreover, a peak at 1100 cm^{-1} relative to the Si-O vibrational mode appears indicating that the nanoparticles' surface is partially coated with silicon dioxide. This operation is in general loaded in order to reduce the catalytic activity of titanium dioxide.

The TGA analysis of untreated particulate reveals several weight losses: below 393 K is the loss of the water physically absorbed on the sample [20], while between 393 K and 873 K we observe four losses at temperatures 459 K, 506 K, 577 K, and 648 K, associated to chemically bounded water (surface OH groups) and organics. Thermal treatment at 473 K for 24 hours and at 573 K for 3 hours caused the disappearance of the signals related to organic species in the IR spectrum estimated to be about 0.7% w/w using TGA. On the other hand, DLS measurements showed an increase of 16% of the particles average diameter.

Due to the large surface area of nanoparticles, the interface energy is an important contribution for the stabilization of colloids. From this point of view, in order to minimize the interface energy between nanoparticles and organic matrix (monomer such as MMA or solvents), some surface functionalizations have been tried. In this work, we focused on some amines and carboxylic acids

4.3.2 Chemical Characterization of Rutile Surface Modification

TiO_2 surface has several acid sites, which could be either Lewis acid sites (Ti^{4+}) or Brønsted acid sites (Ti-OH); so we have tried to exploit this diverse reactivity using carboxylic acids and amine groups [21]. In particular we used two acids: propionic acid (PA) and octanoic acid (OAc), and two amines: n-hexylamine (HA) and n-octylamine (OAm).

4.3.2.1 ATR-FTIR Results

In Figure 4.2 the IR spectra of TiO_2 particles' surface treated with propionic acid (PA@TiO_2) and octanoic acid (OAc@TiO_2) are reported together with the spectrum of the free propionic acid.

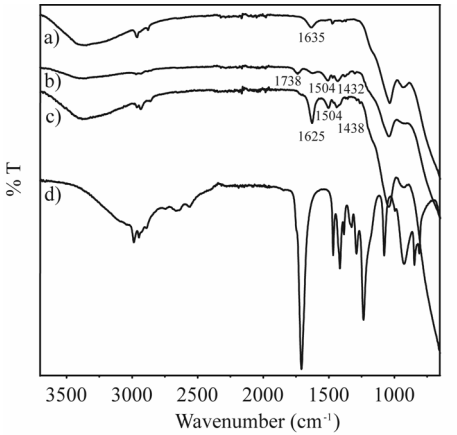

Figure 4.2. FT-IR spectra of a) pristine TiO_2, b) PA@TiO_2, c) OAc@TiO_2, d) propionic acid.

There is no evidence of the broad peak around 3300-2500 cm^{-1} typical of the vibrational modes of the OH-group, indicating that the head of the organic molecule is immobilized onto the surface. This interaction is confirmed by the disappearance of the vibrational mode of C=O group at 1707 cm^{-1}, characteristic of the free aliphatic acids, and the presence of the asymmetric and symmetric stretching bands of the deprotonated carboxyl moiety (COO^-), respectively at 1504 and 1434 cm^{-1} [22]. A minor two-modes vibrational band can be observed at 1738 cm^{-1} and 1722 cm^{-1} in the spectrum of TiO_2 treated with propionic acid, which can be attributed to the stretching of the C=O group of neutral acid molecules weakly interacting with titania surface [23]. The band at 1625 cm^{-1} in modified rutile and at 1635 cm^{-1} in pristine rutile spectra are attributed to adsorbed water.

In Figure 4.3 the IR spectra of TiO_2 treated with n-hexylamine and n-octylamine are reported together with the spectrum of the free n-hexylamine.

The persistence of vibrational modes at 2956, 2924 and 2855 cm^{-1} characteristic of the stretching of the methyl and methylene groups shows the integrity of the aliphatic chain of the organic molecule [25]. The bending vibrational mode of NH_2 moiety at 1585 cm^{-1} of the free hexylamine (Figure 4.3d) misses in the titania modified with amines spectra (Figure 4.3b and 4.3c). On the other hand, the presence of a new peak at 1526 cm^{-1} invokes the interaction between the Lewis acid sites of titanium (Ti^{4+}) and the amino group, forming a coordinative

bond Ti-NH_2^+. Also in this case, the peak at 1620 cm^{-1} is attributed to the OH bending mode of the water absorbed onto the titania surface.

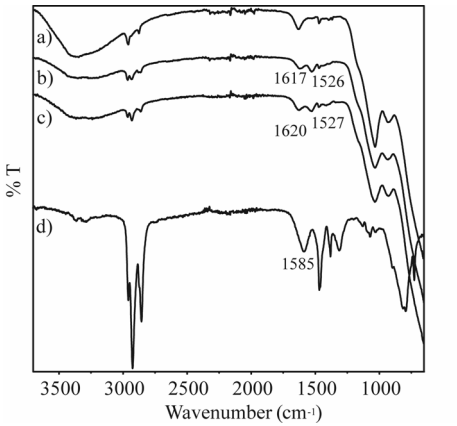

Figure 4.3. FTIR spectra of a) pristine TiO_2, b) HA@TiO_2, c) OAm@TiO_2, d) n-hexylamine.

Figure 4.4 shows IR spectra in the region between 1800 and 1200 cm^{-1} of the titania modified first with propionic acid then with n-hexylamine (HA/PA@TiO_2) and viceversa (PA/HA@TiO_2). The IR spectrum of the first sample (Figure 4.4c) shows that the carboxyl vibrational mode at 1738 cm^{-1} is absent, while the amine vibrational mode appears at 1526 cm^{-1}, as in the spectrum of HA@TiO_2 (Figure 4.4d). Instead, when propionic acid is added to the titania previously treated with n-hexylamine (Figure 4.4e) the vibrational modes typical of the acidic moiety are present: at 1738 cm^{-1} and 1432 cm^{-1} together with the signal at 1526 cm^{-1} typical of amine on the surface.

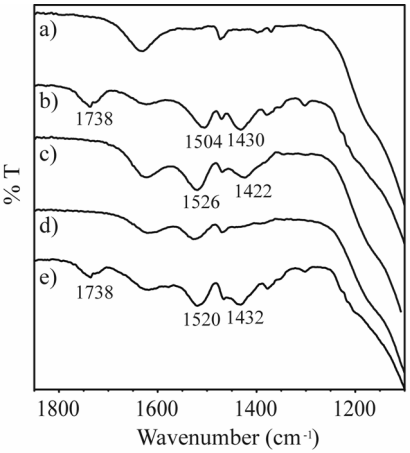

Figure 4.4. FTIR spectra between 1850-1100 cm^{-1} of a) TiO_2 nanoparticles, b) TiO_2 nanoparticles modified by propionic acid, c) TiO_2 nanoparticles modified by propionic acid and n-hexylamine (HA/PA@TiO_2), d) TiO_2 nanoparticles modified by n-hexylamine, e) TiO_2 nanoparticles modified by n-hexylamine and propionic acid (PA/HA@TiO_2).

4.3.2.2 TGA Results

The surface coverage of titania is determined from the difference between the mass loss of the pristine and treated rutile between 390 K and 873 K measured by TGA (Figure 4.5); in fact this temperature range allows us to neglect losses related to physically adsorbed water and the solvents used in the reactions.

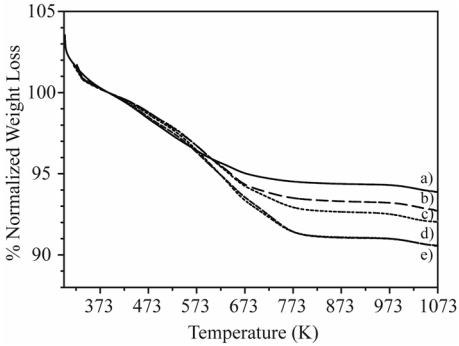

Figure 4.5. Samples' TGA curves: a) TiO_2 nanoparticles, b) TiO_2 nanoparticles modified by propionic acid, c) TiO_2 nanoparticles modified by propionic acid and n-hexylamine (HA/PA@TiO_2), d) TiO_2 nanoparticles modified by n-hexylamine, e) TiO_2 nanoparticles modified by n-hexylamine and propionic acid (PA/HA@TiO_2).

The calculation of the surface coverage is performed considering the molecular mass of the modifying agent (we was assumed that all the molecule detached from the surface at those temperatures), a titanium dioxide's surface area of 210 m^2/g, and a reactive cross-section of about 0.2 nm^2 both for acid [26] molecules and for amines [27].

Table 4.1 reports weight loss and the surface coverage for the acids and amines used. The highest coverage it is obtained using octylamine (24%) and the lowest using propionic acid (9%). When two modifying agents are used one after the other two different behaviors are evident. The addition of propionic acid to the sample of TiO_2 modified with hexylamine causes a decrease of the weight loss from 3.48% for HA@TiO_2 to 1.72% for PA/HA@TiO_2. Instead the addition of hexylamine to the sample of TiO_2 modified with propionic acid causes a

significant increase in the weight loss. Furthermore the strong similarity between TGA curves of titania functionalized with hexylamine (HA@TiO_2) and titania modified first with propionic acid and then with the amine (HA/PA@TiO_2) (Figure 4.5d and 4.5e) confirms the hypothesis supported by IR data that amine molecules shift the acid ones present on the titania surface.

Table 4.1. Weight losses and coverage for titania nanoparticles treated with acids and amine.

Sample	TGA Mass loss (%)	Molecule/nm^2	Coverage (%)
OAm@TiO_2	4.77	1.2	24
OAc@TiO_2	3.56	0.8	16
PA@TiO_2	1.03	0.4	9
HA/PA@TiO_2	3.38	n.d.*	n.d.*
HA@TiO_2	3.48	1.1	22
PA/HA@TiO_2	1.72	n.d.*	n.d.*

* We do not report the calculation of the number of acid and amine molecules on an area of 1 nm^2 and the surface coverage of HA/PA@TiO_2 and PA/HA@TiO_2 samples because we don't know the relative amount of these molecules on the titania surface.

4.3.2.3 CP MAS ^{13}C Results

Cross polarization (CP) exploits magnetization transfer from protons to carbon nuclei and it is more efficient for molecules with reduced mobility; furthermore recycle delay is determined by ^1H longitudinal relaxation times (T_1s) that are at least one order of magnitude shorter the ^{13}C ones. For titania functionalized with propionic acid and/or *n*-hexylamine, CP

MAS is a very valuable technique since highlights only bound species and neglects free molecules eventually present since they are in the liquid state. However ^{13}C MAS spectra of modified nanoparticles acquired without CP and short recycle delay (4 s) do not show evidence of mobile species. In Figure 4.6 ^{13}C CP MAS spectra, recorded at 8000 Hz spinning speed by applying 8 ms contact time with square ramp, of all samples are depicted. In Tables 4.2 and 4.3 ^{13}C chemical shifts (CSs) are reported for propionic acid and *n*-hexylamine carbons respectively together with some reference systems. The CSs of *n*-hexylamine molecules present on the titania surface are quite stable and they seem not affected by the preparation method with the only exception of the $CH_2\alpha$ carbon; in fact, each other type of carbon atom resonates practically at the same chemical shift in all the samples analyzed. For what concerns $CH_2\alpha$ carbon, in the case of HA/PA@TiO_2 the resonance is quite broad compared to HA@TiO_2 and PA/HA@TiO_2 samples.

This behavior is typical of a carbon directly bonded to a nitrogen in the special case of restricted mobility. The broadening of the resonance is due to the ^{13}C-^{14}N dipolar coupling strongly affected by the ^{14}N quadrupole interaction [28].

Analyzing in details ^{13}C chemical shift values, two carbons $CH_2\beta$ and $CH_2\delta$ are clearly outlying those of corresponding species for *n*-hexylamine in solution but are quite close to the values of *n*-hexylammomium cation. As an example in Table 4.2 CSs are reported for *n*-hexylammomium cation in a layered γ-titanium phosphate [29]. Quite striking is the case of

$CH_2\beta$ carbon which give rise to a strong and well resolved peak, its CS goes from 34.1 ppm for the neutral form to 31.0 ppm for the protonated ammonium salt; for the *n*-hexylamine bounded to the TiO_2 surface $CH_2\beta$ displays a CS ranging from 31.2 ppm to 31.5 ppm. Other methylenes are less sensitive to changes in electron density on amine's nitrogen. A chemical shift of 12.2 ppm for the terminal methyl is upfield compared either with neutral *n*-hexylamine or charged *n*-hexylammonium. This anomalous behavior can be explained considering that methyl carbons are only partially surrounded by organic molecules because they lie near an air interface in the dry state [30].

The NMR data provide a picture of *n*-hexylamine bound to the surface of titania via the formation of positive charged nitrogen, this interaction can be rather strong leading to reduced mobility of the head group as in the case of HA/PA@TiO_2.

The analysis of propionic acid signal reveals a more complex behavior. First, the preparation method strongly determines the amount of propionic acid bound to the titania nanoparticles. ^{13}C CP MAS spectrum of titania particles first treated with propionic acid and subsequently with *n*-hexylamine (HA/PA@TiO_2**)** does not show any evidence of propionic acid. This result clearly demonstrates that, at least in the condition used, on the rutile surface *n*-hexylamine is able to replace propionic acid differently with that reported by Nakayama et al. for anatase nanoparticles. On the other hand, ^{13}C chemical shifts of propionic acid adsorbed on titania nanoparticles do not

change if the nanoparticles are first treated with *n*-hexylamine (Table 4.3). The resonance of carboxyl group is considerably broad and presents maxima around 185-183 ppm. Since propionic acid in solution has the carboxylic resonance at 181.5 ppm and sodium propionate at 185.7, the adsorbed propionic acid covers all the range from the completely neutral form to fully depronated carboxylate.

However on the surface of titania more complex structures can be present, Nakayama et al. describe as possible two binding modes for carboxylic acids on the titania surface, the chelating and the bridging mode. These carboxylate geometries should give rise chemical shifts not easily predictable from solution data. To the best of our knowledge there are no works reporting the chemical shift of carboxylic acid binding titanium ions or titania surface with chelating or bridging geometry. However Ye et al. [31] report the chemical shift of chelating and bridging acetic acid in tetranuclear zinc-carboxylate complexes in the solid state. The authors state 1 ppm downfield shift with respect to acetic acid for the bridging mode and 5 ppm for the chelating mode. In the reasonable assumption that also in the case a titanium similar shifts occur, it is possible to conclude that on the surface of titania, propionic acid exhibits both binding modes, bridging and chelating, with a slight prevalence of the bridging mode. The unusual chemical shift values found for the methyl groups in PA@TiO_2 and PA/HA@TiO_2, 16.7 and 7.4 ppm, can be explained considering the different environments explored by the methyl groups in the solid state.

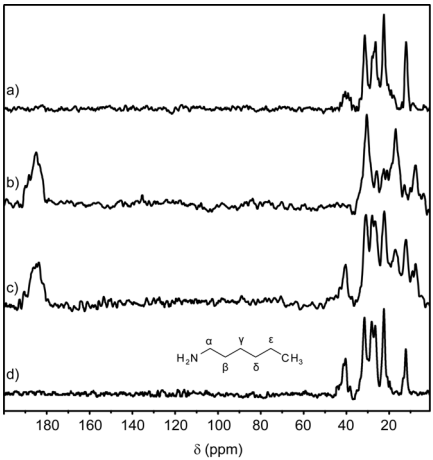

Figure 4.6. ^{13}C CP MAS NMR spectra: a) HA/PA@TiO_2, b) PA@TiO_2, c) PA/HA@TiO_2, d) HA@TiO_2.

Table 4.2. ^{13}C NMR Chemical Shifts of pure *n*-hexylamine and *n*-hexylamine capped TiO_2 nanoparticles.

	$CH_{2\alpha}$ δ(ppm)	$CH_{2\beta}$ δ(ppm)	$CH_{2\gamma}$ δ(ppm)	$CH_{2\delta}$ δ (ppm)	$CH_{2\varepsilon}$ δ(ppm)	CH_3 δ(ppm)
n-Hexylamine	42.7	34.1	27.1	32.3	23.1	14.2
n-Hexylammonium	39.6	31.0	26.0	26.7	21.1	13.4
HA@TiO_2	41.3-40.4	31.5	26.5	28.1	22.5	12.2
PA/HA@TiO_2	40.8	31.2	26.5	28.0	22.4	12.4
HA/PA@TiO_2	42.4-39.5	31.4	26.4	27.9	22.5	12.1

Table 4.3. ^{13}C NMR chemical Shifts of pure propionic acid, sodium propionate and propionic acid capped TiO_2 nanoparticles.

	Carboxyl δ (ppm)	CH_2 δ (ppm)	CH_3 δ (ppm)
Propionic Acid	181.5	27.6	8.9
Sodium Propionate	185.7	31.6	11.0
PA @TiO_2	184.9*	30.3	16.7 7.4
PA/HA@TiO_2	185.1-182.8	n.d.**	16.8 7.6

* Maximum intensity of carboxyl resonance; ** Signal not detectable since hidden by hexylamine ‘s peaks.

4.3.3 Characterization of Colloids

4.3.3.1 DLS Results

The stability of modified rutile in solvents with different polarity was studied by Dynamic Light Scattering. Table 4.4 reports the average diameter of rutile particles dispersed in acetone and MMA; there are not reported measurements relative to the dispersions in hexane and toluene since it was not possible to prepare stable colloids; particles precipitated in few hours since sonication.

The dispersion of titania modified with hexylamine (HA@TiO_2) is the most stable in MMA; and the mean diameter of particles is the same of pristine rutile in water (about 115 nm). The dispersion of titania modified with octylamine (OAm@TiO_2) is stable in MMA as HA@TiO_2 unless the mean diameter of particles is slightly larger (about 140 nm). The modification of rutile with carboxylic acids leads

to dispersions with a reduced stability in MMA; in fact the hydrodynamic diameter of PA@TiO_2 particles in MMA is 420 nm after 3 days and it decreases to 225 nm after 30 days. HA/PA@TiO_2 in MMA behaves similarly to HA@TiO_2 whereas PA/HA@TiO_2 resembles PA@TiO_2. From DLS measurements it seems that in the case of two modifying agents used one after the other, the most relevant is the one used in the final step.

Because of the higher stability of HA@TiO_2 in MMA we chose this colloidal dispersion for the polymerization in bulk of the nanocomposite.

In order to undestand the correct amount of nanoparticles to introduce in the syrup, scattering properties of HA@TiO_2 in MMA were studied before the fabrication of the sheet.

Table 4.4. Hydrodynamic diameter of colloids as measured with DLS at the reported time after colloid preparation

Solvent	Days	OAc@TiO_2	OAm@TiO_2	PA@TiO_2	HA/PA@TiO_2	HA@TiO_2PA/HA@TiO_2
Acetone	3	120 [40]*	135 [55]*	140 [50]*	140 [55]*	145 [55]*	140 [55]*
MMA	3	370 [130]*	140 [35]*	420 [200]*	160 [35]*	115 [55]*	425 [200]*
	15	310 [110]*	130 [50]*	290 [130]*	150 [40]*	115 [40]*	270 [120]*
	30	260 [110]*	125 [70]*	225 [20]*	145 [40]*	115 [40]	250 [80]*

* The numbers in the square brackets represent the standard deviation.

4.3.3.2. UV-Visible spectroscopy

In order to study the optical properties of the colloidal solution made up of the titanium dioxide modified with hexylamine ($HA@TiO_2$) in MMA, dispersions characterized by an increasing concentration of nanoparticles in the monomer were prepared and characterized with UV-visible spectroscopy. Figure 4.7 shows the transmittance spectra of colloidal solutions at different TiO_2 concentration in weight (from 0 ppm to about 1000 ppm) in a standard quartz cuvette.

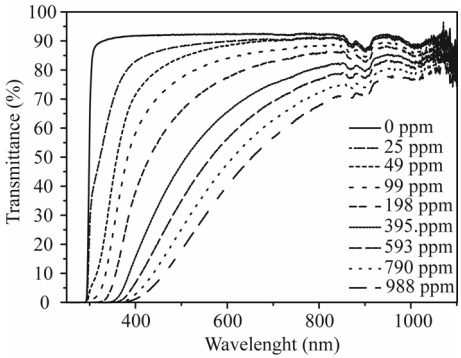

Figure 4.7. UV-visible spectroscopy of pure MMA (0 ppm) and of the colloidal solutions of $HA@TiO_2$ in MMA characterized by increasing concentrations (from 25 ppm to 988 ppm w/w).

The scattering coefficient α due to the TiO_2 in MMA solution reads as follows:

$$\alpha(\lambda, C_{w/w}) = \frac{1}{L}\ln\left(\frac{T_x(\lambda)}{T_x(\lambda, C_{w/w})}\right) \quad (1)$$

Where T_x is the measured transmittance of pristine MMA as a function of the wavelength λ, T_x is the same quantity for MMA charged with TiO_2 and L is the cuvette length (1 cm).
The log-log plot of α as a function of λ was performed. For these curves the dependence of α on $1/\lambda^4$ in 400-600 nm range was evident. In this wavelength region Rayleigh approximation is valid and α reads:

$$\alpha_{Rayleigh}(\lambda) = 32\pi^4 f_v \frac{r^3}{\lambda^4}\left(\frac{\varepsilon_{TiO2} - \varepsilon_{PMMA}}{\varepsilon_{TiO2} + 2\varepsilon_{PMMA}}\right)^2 = \kappa f_v \frac{r^3}{\lambda^4} \qquad (2)$$

Where r is the radius of spherical nanoparticles, f_v is TiO_2 concentration in volume, ε_{TiO2} and ε_{PMMA} are the relative electric permeability of the nanoparticles and the polymer respectively, assuming n_{PMMA}=1.49 and n_{TiO2}=2.61, κ=519. Fitting α/κ in the 400-600 nm range with a/λ^4 the coefficient $a=f_v r^3$ was obtained for all the TiO_2 known concentrations and hence the cube nanoparticle mean radius as the slope of *a* versus f_v.
By fitting the variable *a* versus the nanoparticles' fraction in volume f_v with a straight line, a nanoparticles' radius of about 45 nm was calculated by the slope of the fitting curve (see Figure 4.8). This value (about 90 nm of diameter) is in a good agreement with the nanoparticles' size measured by DLS (115 ± 55; see Table 4.4). In calculation densities of 0.94 g/cm^3 and 4.23 g/cm^3 for MMA and rutile TiO_2 respectively were assumed.

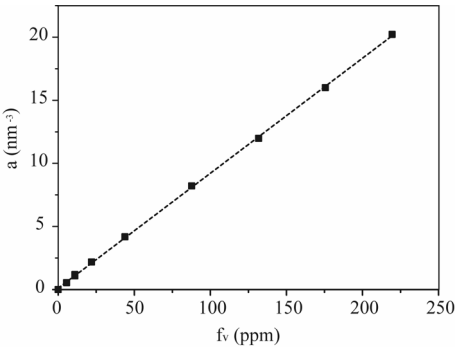

Figure 4.8. Fitting of the variable *a* versus the fraction of volume in ppm of the nanoparticles in the polymeric matrix. The curve that fits the points is a straight line whose slope is 92000 (nm^3).

4.3.4 Characterization of TiO_2-PMMA Nanocomposite sheets

Figure 4.9 shows a photo of a TiO_2 nanocomposite sheet charged with about 100 ppm of the sample HA@TiO_2. The sheet's size is about 20 cm of length and 20 cm of width and while the photo 4.9a shows its transparency, the Figure 4.9b reveals its diffusing properties using a white source. The sheet remember the blue sky, whose appearance is the result of the Rayleigh Scattering, like in this case.

In order to study the diffusing properties of the Rayleigh Scattering, measures in transmittance in the visible range were performed on a pure PMMA sheet, and two nanocomposite sheets characterized by 100 ppm and 200 ppm of nanoparticles in the polymeric matrix. Spectra were collected in three different points of the sheet's edge, in order to check the

distribution of the rutile particles in the bulk: 2.60 cm, 6.65 cm and 10.20 cm (Figure 4.10).

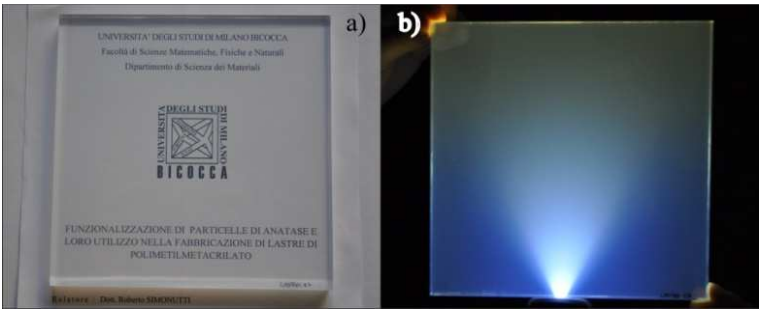

Figure 4.9. a) Images of one of the TiO_2/PMMA nanocomposite sheet. b) Diffusing properties of the nanocomposite when illuminated with a white light in the dark.

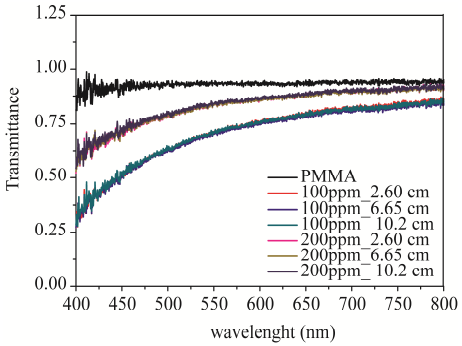

Figure 4.10. Measurements in transmittance of the PMMA sheet and two nanocomposite sheets characterized by the presence of 100 ppm and 200 ppm of nanopartcles in the bulk. Spectra was collected in three different position along the edge: 2.60 cm, 6.65 cm and 10.2 cm.

By the Figure 4.10 it is possible to verify the optical transparency of the pure PMMA sheet, that reflects about 4%

of the light for each face, as expected, while the nanocomposite sheets show an additional loss in transmittance which is wavelength dependent. Same transmission spectra analysis as for colloidal solution was carried out. Also in this case sample show a Rayleigh scattering between 400 and 600 nm; fitting of a parameter as a function of f_v gave a nanoparticles radius of about 50 nm, in good agreement with the result obtained for the sample in dispersion (see Figure 4.11). These results clearly show that no clusters appeared during the bulk polymerization of the monomer. In Figure 4.12, the nanocomposite TEM image confirms the presence of aggregates of about 100 nm as hydrodynamic diameter embedded by the polymeric matrix.

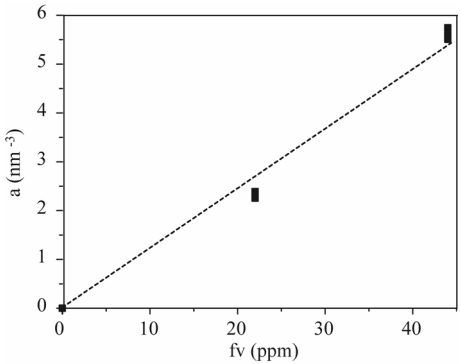

Figure 4.11. Fitting of the parameter *a* versus the fraction of volume (in ppm) of nanoparticles in the polymeric matrix. The fitting is linear and the slope of the straight curve is 12220 nm^3.

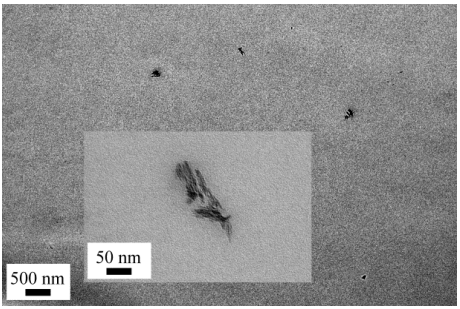

Figure 4.12. TEM images of the aggregates of rutile crystals dispersed in the polymeric matrix; by the magnification of one of the aggregates is possible to see that the size is about 100 nm. No agglomeration happened during the bulk polymerization.

4.4 Summary

In a first step was found that hexylamine is the best modifying agent among those tested with this rutile, in order to obtain stable dispersions of TiO_2 nanoparticles in MMA. The interaction seems to happen by protonation of the free amine for part of the Lewis acid sites present on the rutile's surface, according to ^{13}C CP MAS NMR and FTIR spectra. The nanoaparticles are anyway aggregates in clusters whose hydrodynamic size is about 100 nm in MMA. This is showed by TEM images and confirmed by DLS and UV-visible measurements. The optical properties of the dispersions and, in a second step, of the TiO_2-PMMA nanocomposite sheets were verified by UV-visible spectroscopy, confirming that titanium dioxide nanoparticles scatter according to the Rayleigh Law. The nanoparticles' size remains the same also after the bulk polymerization and no bigger agglomerates shape. From this

point of view, the bulk polymerization of nanocomposite sheets via cell-casting showed to be a good method in order to obtain this type of objects preserving a very high optical transparency.

4.5 References

[1] a) Alexandre M and Dubois P 2000 *Mat. Sci. Eng. R.* **28** 1; b) Balazs A C, Emrick T and Russell T P 2006 *Science* **314** 1107

[2] a) Usuki A, Kojima M, Okada A, Fukushima Y and Kamigaito O *J* 1993 *Mater. Res.* **8** 1179; b) Kojma Y *J* 1993 *Mater. Res*. **8** 1185

[3] Kiliaris P and Papaspyrides C D 2010 ***Progr. Polym. Sci.* 35 902**

[4] Osman M A, Mittal V, Morbidelli M and Suter U W 2003 *Macromolecules* **36** 9851

[5] a) Song H and Lee S. 2007 *Nanotechnology* **18** 055402; b) Neves M C, Martins M A, Soares-Santos P C R, Rauwel P, Ferreira R A S, Monteiro T, Carlos L D and Trindade T 2008 *Nanotechnology* **19** 155601

[6] Nussbaumer R J, Caseri W R, Smith P and Tervoot T 2003 *Macromol. Mat. Eng*. **288** 44

[7] Althues H, Potschke R, Kim G M and Kaskel S J 2009 *Nanosci. Nanotechnol.* **9** 2739

[8] Althues H, Henle J and Kaskel S 2007 *Chem. Soc. Rev.* **36** 1454

[9] Marek M and Steidl J 2006 *J. Mater. Sci.* **41** 3117

[10] Ruffieux T, Scharf I, Philipoussis H P, Herzig R, Voelkel K J and Weible 2008 *Opt. Express* **16** 19541

[11] Wu C Y, Chiang T H and Hsu C C 2008 *Opt. Express* **16** 19978
[12] Lin L, Shia T K and Chiu C J 2000 *J. Micromech. Microeng.* **10** 395
[13] Yeh S J 2006 *Opt. Commun.* **264** 1
[14] Ganzherli N M and Gulyaev S N 2007 *J. Opt. Technol.* **74** 56
[15] Kim G H 2005 *Eur. Polym. J.* **41** 1729
[16] a) Schubert E F and Kim J K 2005 *Science* **308** 1274; b) Kim J K and Schubert E F 2008 *Opt. Exp***. 16** 21835
[17] Rivera-Toledo M, Garcia-Crispin M E, Flores-Tlacuahuac A and Vilchis-Ramirez L 2006 *Ind. Eng. Chem. Res.* **45** 8539
[18] Mohapatra S and Pramanik P 2009 *Colloids and Surfaces A: Physicochem. Eng. Aspects* **339** 35
[19] Brunauer S and Emmett P H and Teller E *J* 1938 *Am. Chem. Soc*. **60** 309.
[20] Barret E P, Joyner L G and Halenda. P P 1951 *J. Am. Chem. Soc*. **73** 373
[21] Mueller R, Kammler H K, Wegner K and Pratsinis S E 2003 *Langmuir* **19** 160
[22] Nakayama N and Hayashi T 2008 *Colloids and Surfaces A: Physicochem. Eng. Aspects* **317** 543
[23] Ojamue L, Aulin C, Pedersen H and Käll P-O 2006 *J. Coll. Inter. Sci.* **296** 71
[24] Mudunkotuwa I A and Grassian V H 2010 *J. Am. Chem. Soc.* **132** 14986
[25] Li Z, Gao J, Xing X, Wu S, Shuang S, Dong C, Paau M C and Coi M M F 2010 *J. Phis. Chem. C* **114** 723

[26] Bickerstaffe A K, Cheah N P, Clarke S M, Parker J E, Perdigon A and Messe L 2006 *J. Phys. Chem. B* **100** 5570
[27] Boddenberg B and Eltzner K 1991 *Langmuir* **7** 1498
[28] a) Simonutti R, Comotti A, Bracco S and Sozzani P 2001 *Chem. Mater* **13** 771; b) Naito A, Ganapathy S and McDowell C A 1981 *J. Chem. Phys.* **74** 5393
[29] Mafra L, Almeida Paz F A, Rocha J, Espina A, Khainakov S A, Garcia J R and Fernandez C. 2005 *Chem. Mater.* **17** 6287
[30] Pursch M, Vanderhart D L, Sander L C, Gu X, Nguyen T, Wise S A and Gajewski D A 2000 *J. Am. Chem. Soc.* **122** 6997
[31] Ye B H, Li X Y, Williams I D and Chen X M 2002 *Inorg. Chem* **41** 6426

Chapter 5

Highly refractive poly 2-ethyl-2-oxazoline nanocomposite coatings loaded with TiO_2 nanoparticles with high optical quality

5.1 Introduction

Polymeric nanocomposites, namely polymer matrices containing nanometric particles, are extensively studied for the improved properties compared to the pure polymer [1, 2]. The presence of a nanometric filler can enhance mechanical properties [3, 4], thermal stability [5] and gas barrier properties [6]. In the last few years nanocomposites with optimized optical properties have also been described. The research has been focused mainly on the following goals: luminescence [7, 8], change (increase) of the refractive index (RI) [9], UV absorption [10]. In particular high RI polymer nanocomposites can be obtained by incorporation of inorganic building blocks with high RI (such as InP, PbS, TiO_2, ZrO_2, or ZnS) into organic matrices on the nanoscale. However it should be noted that although InP and PbS have high RI (>4.0 at 500 nm), they exhibit significant absorption coefficients in the visible region and cannot be used for applications where transparency in the visible is required. At present in fact, the most frequently

employed inorganic materials in the literature concerning high RI organic–inorganic nanocomposites are TiO_2 (n ≈ 2.6 at 500 nm in its rutile form) [11], ZrO_2 (n ≈ 2.2 at 589 nm) [12] andZnO (n = 2.0 at 550 nm) [13, 14]. The main reasons for which these high RI inorganic materials are used as nanoscale building blocks are that they can be obtained easily both in the laboratory and commercially, and they have good transparency in the visible and near-IR regions. In addition, some inorganic materials such as ZnO, TiO_2 (not as nanoparticles) are commonly used as UV-shielding pigments in sun-screen lotions, in polymeric materials and coatings. Negligible absorption in the visible region is a necessary but not sufficient condition for having optically transparent nanocomposites; in fact intense light scattering of inorganic domains, due to the large inorganic domain size and RI mismatch between the inorganic phase and the matrix, could determine an opaque appearance of the material. The amount of scattered light can be evaluated by using the Rayleigh scattering formula; as a rule of thumb scattering can be considered negligible when the average radius of the particles is less than 25-30 nm. Due to unique combination of optical and mechanical properties, these films have a wide range of applications in the optoelectronics and coating industries. Much effort is aimed at increasing the functional inorganic fraction, and several methods have been developed in order to avoid aggregation [15, 16] which usually has a negative impact on the properties of the composite.

Considering polymers used as embedding matrix for the inorganic nanoparticles, poly(meth)acrylates represent the most

studied class since they feature intrinsic high optical clarity, especially in the case of polymethymethacrylate [17-19], and the possibility to modulate the physico-chemical properties of the polymer by simply varying the nature of the side chains. Quite rarely water soluble polymers are used, although the hydrophilicity of the macromolecular chains can avoid aggregation of the nanoparticles, especially in the case of oxides that present hydrophilic surfaces. In fact one of the main efforts in the fabrication of nanocomposite is the surface modification of the nanoparticle in order to make it compatible with the polymer; in the case of hydrophilic polymers this is not necessary and the nanoparticle can be dispersed in water without any treatment. In the perspective of green chemistry, the fabrication of water soluble nanocomposites should be considered as a relevant target.

In this paper we report for the first time the preparation and optical characterization of nanocomposite films made of TiO_2 dispersed in the water soluble polymer poly 2-ethyl-2-oxazoline. This polymer was chosen because of its solubility in water, lack of toxicity and stability (the amide is tertiary and, as consequence, it is difficult to hydrolyze). It features several recognized applications as an adhesive and as a coating [20, 21]. Furthermore, polyoxazolines are an interesting class of polymers due to their ability to form functional materials and nanostructures with interesting applications as stimuli-responsive systems [22, 23]. Nanocomposite films characterized by three different concentrations of TiO_2 nanoparticles (20 nm average radius) in the polymeric matrix

(16%, 28% and 44% w/w) were obtained and refractive indices, UV absorption and transparency were tested using UV-visible spectroscopy. The nanocomposites surface was studied by AFM. The optical properties of the film were further investigated by specular gloss and distinctness-of-image (G_{Dol}) measurements.

5.2 Experimantal

5.2.1 Syntheses and characterization of TiO_2 nanoparticles

TiO_2 nanoparticles were synthesized according to method reported by Niederberger et al. [24], in which 4 ml of $TiCl_4$ (99.9%, Sigma Aldrich) are slowly added to 80 ml of anhydrous benzyl alcohol (≥99.0%, Sigma Aldrich) under stirring at room temperature. Benzyl alcohol was made anhydrous using $MgSO_4$ and by evaporation at 50°C under vacuum. Nanoparticles with the desired size were obtained using 80°C as reaction temperature and 24h as reaction time. The resulting white suspension was centrifuged and washed three times, twice with ethanol and once with THF. The nanoparticles were dried under environmental atmosphere at room temperature overnight and then ground into a powder.

X-ray diffraction measurement was performed in order to examine the TiO_2 nanoparticle crystal structure. The powder X-ray diffraction pattern was obtained using a Bruker D8 DISCOVER with GADDS microdiffractometer equipped with a Hi-Star area detector. Theta 1 (x-ray source) and Theta 2

(detector) starting angles were 17° and 17° with a frame width of 8. Runtime for each frame was 90 seconds. Beam conditions included Cu Kα radiation (λ = 1.54 Å) at 45 kV and 35 mA through a 500μm collimator in air.

Nanoparticle size and morphology were studied using transmission electron microscopy (TEM, JEOL JEM-1011) operated at 200 kV. The TEM sample was prepared by leaving 1-2 drops of the nanoparticle water dispersions onto lacey carbon copper grid.

In order to measure their surface area, nitrogen adsorption-desorption isotherms were measured at liquid nitrogen temperature using an ASAP 2010 analyzer (Micrometrics). The powder was outgassed for 12 h at 473 K. The surface area of the nanoparticles was calculated using the Brunauer, Emmet, and Teller model (BET model) [25]. ^{1}H Magic Angle Spinning NMR spectra were recorded on a Avance 300 spectrometer (Bruker) (standard spinning rate of 12 kHz) with a recycle delay of 4 s; 128 scans were acquired. Thermogravimetry measurements were carried out with a TA Q500 analyzer (TA Instruments), heating to 1073 K at 10 K/min in air.

5.2.2 Preparation and Characterization of nanocomposite films

Poly 2-ethyl-2-oxazoline (Aquazol 200®, Polymer Chemistry Innovation, M_w=200000) [20] film (A0) was prepared and used as reference. Solution of 5 wt % of the polymer in distillated water was cast on Milar® (Du Pont) sheets and microscope slides, and films were obtained by evaporation of the solvent at

room temperature and environmental pressure. Nanocomposite films were obtained by mixing the polymeric solution with the nanoparticle dispersions in water in different ratios. TiO_2 dispersions were prepared by adding the desired amount of dried nanoparticle powder to water and by ultra-sonicating the mixture (21s pulse, 7s pause, 350 W) for 15 minutes, in order to break bigger agglomerates. Films based on an increasing concentration of nanoparticles in the polymeric matrix: 16 wt %, 28 wt % and 44 wt %, called A16, A28, A44 respectively, were prepared by evaporation of the solvent at room temperature and environmental pressure. The colloid size in water dispersion was analyzed with a Zetasizer Nano Series (Nano-S) Dynamic Light Scattering (Malvern Instrument Ltd.) at room temperature using a λ=632.8 nm He-Ne laser.

Nanocomposite films were optically characterized with a Perkin Elmer Lambda 1050 spectrophotometer with air as reference spectrum. TEM images of the nanocomposite films were prepared as for the nanoparticles, but using the polymeric solution in water with dispersed nanoparticles, and waiting for evaporation of the solvent.

Atomic Force Microscopy (AFM) images were acquired with a Nanowizard II (JPK Instruments, Berlin) instrument. Measurements were performed in tapping mode in air using stiff silicon cantilevers (RTESPVeeco, resonant frequencies of ~300 kHz, and spring constant of ~40 N/m). Images were acquired at 1Hz scan rate and 512 x 512 pixel resolution. All data in this study were verified by sampling a wide range of areas over the sample surfaces. Water Contact Angle

measurements were performed with a PGX pocket goniometer (FIBRO systems) using 2 µL droplets, with 5 or 6 repetitions for each sample. Specular gloss measurements at 20°, 60° and 85° of the films were determined according to ASTM D523 using a micro-Tri-gloss apparatus [26]. Each result is an average of six measurements (repeated three times) acquired in different points. Relative error of these results is a maximum of 1%. In order to perform specular gloss measurements, films were cast on microscope slides with the uncoated side spray-painted black.

Distinctness-Of-Image gloss measurements were performed according to ASTM E430 using a Dorigon II abridged goniophotometer [27]. Each result is an average of six measurements. Relative error of these results is less than 1%. In order to perform these measurements the same samples used for measuring the specular gloss were used.

5.3 Results and Discussions

5.3.1 Characterization of nanoparticles and colloidal solutions

The powder XRD pattern of titanium dioxide synthesized by non-aqueous route is shown in Figure 5.1. The sample is highly crystalline anatase without indication of other titanium dioxide phases. The (101) peak corresponds to a particle size of 5.6 nm by Scherrer formula using 0.89 as shape factor.

The surface area of the titanium dioxide nanoparticles has been calculated by BET method which gives 249 m^2/g; using the relation for which the surface area (in m^2/g) = 6000/ [ρ (in g/m^3) *D* (in nm)], where ρ and *D* are the anatase density (3.9 m^2/g) and the diameter of nanoparticles [20] respectively, the nanoparticle size was calculated to be about 6.2 nm. Although particle size determined by the (101) peak broadening at half of maximum intensity is not very accurate, the result is in agreement with the BET measurements. TEM analysis presents a somewhat different landscape, also depicted in the inset of figure 5.1a, where TiO_2 nanoparticles appear as elongated objects with the longest axis around 40 nm. By more accurate investigation of images such as the one reported in figure 5.1, the objects show a finer structure, as they appear constituted by nanoparticles of about 5-6 nm with aspect ratio close to 1, although the actual shape cannot be attributed on the basis of the TEM images available.

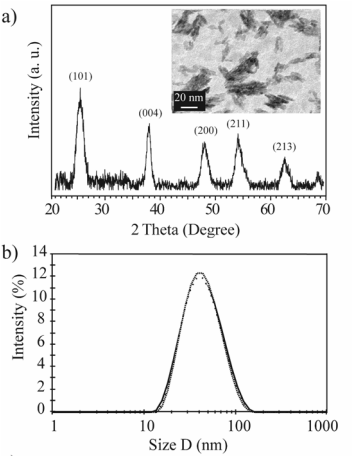

Figure 5.1. a) XRD pattern of synthesized TiO_2 nanoparticles and the corresponding TEM image. b) DLS measurement of particle size of the as synthesized TiO_2 dispersed in distilled water at room temperature, solid line corresponds to the fitting of experimental data by a Gaussian distribution.

The possibility to prepare a stable dispersion of titania nanoparticles in water is investigated by DLS. DLS measurements reveal that once dispersed in water, titania nanoparticles present an average diameter of 40±20 nm in reasonable agreement with TEM measurements (figure 5.1b).
Since benzyl alcohol has an active role in the synthesis of titania, as stated in several papers by the authors that proposed this synthetic route [28], the presence of benzyl alcohol residues on the titania surface has been evaluated by TGA and ^{1}H MAS NMR. Thermogravimetric trace shows an overall weight loss of about 14% from about 400 K to 900 K. The weight loss can be divided in two regions. The first one, from 400 K to 600 K, is characterized by a smooth decrease of the

sample weight with the increasing temperature, the second instead is quite abrupt and takes place in less than 50 K around 693 K (figure 5.2a). The first phenomenon is characteristic of a desorption process. In fact, physi-adsorbed molecules on a surface are released in a wide range of temperatures especially when the surface is highly defective as in nanoparticles. The second phenomenon can be related to the sintering of the nanoparticles once the organic molecules covering the surface are completely removed. The sintering process advances through the condensation of hydroxyl groups and elimination of water [29]. Taking into account the synthetic method used and that the boiling point of benzyl alcohol is about 478 K, the weight loss between 400 K to 600 K can be attributed prevalently to the desorption of benzyl alcohol from the titania surface [24].

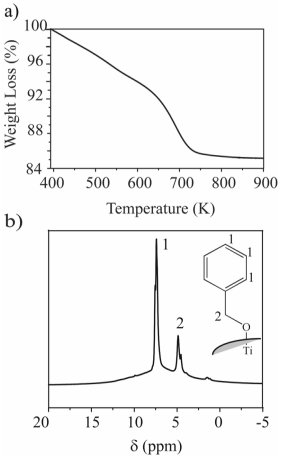

Figure 5.2. a) Thermogravimetric trace of TiO_2 nanoparticles. The curve is normalized at about 400 K in order to neglect weight losses due to physically adsorbed water. b)^{1}H MAS NMR of TiO_2 nanoparticles recorded at 300 MHz; in the inset a possible interaction between benzyl alcohol and titania is depicted.

^{1}H Magic Angle Spinning (MAS) NMR is a valuable tool for characterizing adsorbed molecules on solid surfaces [30]. Magic angle spinning is effective in reducing but not completely cancelling the proton-proton dipolar couplings. Therefore in a solid material residual dipolar couplings dominate the appearance of ^{1}H MAS NMR spectra. Molecules endowed with restricted mobility are characterized by strong dipolar couplings leading to broad spectra spanning tens of ppm, in which different chemical species cannot be recognized. Fast motions, instead, can average residual dipolar couplings to zero allowing the detection of well resolved spectra. In the case of TiO_2 nanoparticles two sharp resonances at 7.4 ppm and 4.9

ppm dominate the ^{1}H MAS NMR spectrum (figure 5.2b). Underneath these resonances a quite broad peak ranging from 15 to 0 ppm is also recognizable. The chemical shifts of the sharp peaks are quite close to those measured for benzyl alcohol in solution. This indicates that a relevant part of the benzyl groups anchored on the titania surface exhibit a liquid-like mobility. However, the occurrence of a broad peak points out to the presence of rigid protons having restricted mobility. They may be associated to hydrogen bonded OH groups of the titania, in agreement with the high temperature weight loss measured by TGA, or to some benzyl groups which are interacting more strongly with the anatase surface.

Overall, TGA and ^{1}H MAS NMR provide a picture of nanoparticles with an heterogeneous surface characterized by the presence of highly mobile organic molecules, hydrogen bonded OH groups and possibly organic molecules fixed on the surface. This heterogeneity explains the ability of the anatase nanoparticles to form stable dispersion in water.

Nanocomposites films are prepared by dissolving PEOX in water and subsequent addition of titania. The mixture is ultrasonicated in order to disrupt loose aggregates of titania nanoparticles, then the colloid is spread out on Mylar sheets, and finally evaporation of water leads to the formation of the nanocomposite. Films are transparent, do not present cracks and are easily removed from the supporting sheets.

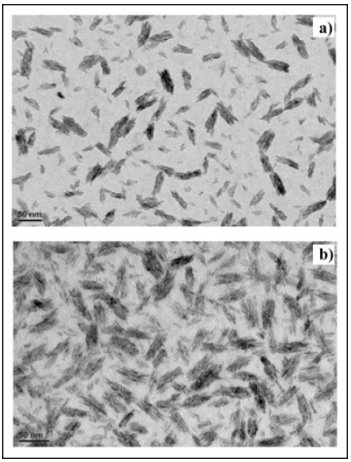

Figure 5.3. TEM images of titania PEOX nanocomposites films: a) A16 and b) A44. Bar scale: 50 nm

In figure 5.3, TEM micrographs of A16 and A44 nanocomposites are reported. The images confirm that the nanoparticles are well dispersed in the polymer matrix as aggregates of the primary crystallites; statistical analysis of the images provides average dimension of the aggregates comparable with the value measured in solution by DLS. Moreover, despite the small inter-aggregate distance due to high concentration anatase nanoparticles, the aggregates are homogenously distributed in the polymeric matrix. This result demonstrates that the fabrication procedure of the nanocomposite film does not induce further agglomeration of the aggregates.

AFM was used to examine the surface of the films. Figure 5.4 shows AFM “height trace” and “phase lag” images of the pristine polymer film and the nanocomposite films. The pure

polymer surface (figure 5.4a) appears to be smooth and characterized by an average peak-to-valley height of about 1 nm; the nanocomposite surface roughness increases with nanoparticles content as clearly shown from increased scale of the height surface profile (Figure 5.4d).

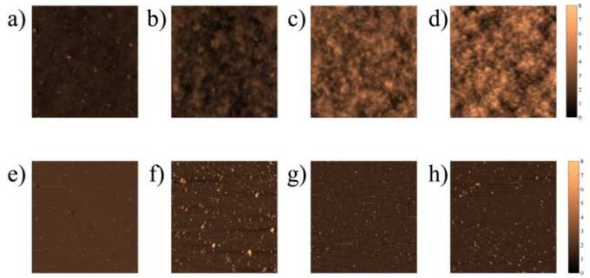

Figure. 5.4. AFM images of the samples in "height trace" mode: a) film A0; b) film A16; c) film A28, d) film A44, and "phase lag" mode: e) film A0; f) film A16; g) film A28; h) film A44. Images size is 2 μm x 2 μm. The colour scale bar corresponds to 8 nm for the images in "height trace" mode and 8° for the images in "phase lag".

In order to quantitatively characterize the surface alteration due to the presence of the nanoparticles we computed the bidimensional autocorrelation of the profile image and we extract the correlation length by fitting the obtained autocorrelation function of the image with a 2D gaussian profile. We chose to identify as correlation length the HWHM (Half Width – Half Maximum) of the function. Calculated values are reported in Table 5.1. It should be noted that in the A0 sample the correlation length is equal to the AFM tip radius which is the lower threshold of the sensitivity of the

instrument. On the contrary, the presence of nanoparticles results into a sizeable increase of the HWHM of the correlation function to a value which is comparable with the nanoparticles diameter.

Phase lag images (figure 5.4 e-h) show that most of the surface in all films presents similar dynamics of the vibrating AFM cantilever. In nanocomposites small spots of the phase-lag image show a large deviation from the average value. A significant change in the dynamics is expected when the tip interacts with different types of surfaces: the soft organic phase or the hard inorganic one. Therefore the presence of small spots showing large deviation of the phase-lag suggests that some nanoparticles protrude out of the polymer surface. Actually, the fact itself that the particles are not completely encased in the polymer is an indication of reduced compatibility.

Water Contact Angle (WCA) measurements also reveal a change in the nanocomposite surface with increasing TiO_2 content (figure 5.5). Table 5.1 reports average values and deviations for the studied systems. The water contact angle goes from an average value of 53° (figure 5.5a) for the pure polymer (A0) to more than 90° (figure 5.5d) for the most concentrated nanocomposite film (A44). This means there is an increase of the hydrophobic character of the material, which is associated to the particles protruding out of the surface.

Table 5.1. Correlation Length and WCA values of pure polymer and nanocomposite films .

Film	Correlation length (HWHM) (nm)	WCA (°)
A0	13	53 ± 3
A16	33	67 ± 5
A28	30	82 ± 3
A44	40	88 ± 4

The change of wetting behaviour can be attributed to the increased roughness of the nanocomposite and to the presence of benzyl groups on the titania surface. It is well established that the wettability of a solid surface is governed both by surface geometrical microstructures and by the chemical composition, as pointed out in the case of nanograss and similar systems [31, 32, 33].

The observed reduced compatibility of the titania nanoparticles on the nanocomposite surface is in apparent contrast to the good stability of their dispersion in the polymeric matrix. However, we must consider that both PEOX and the titania surface present a complex structure which may be responsible for the observed behaviour of the nanocomposite. In particular, as detected by ^{1}H MAS NMR, titania nanoparticles are partially covered by hydrophobic moieties like phenyl rings which tend to repel each other, possibly contributing to stabilize their dispersion both in water and in PEOX.

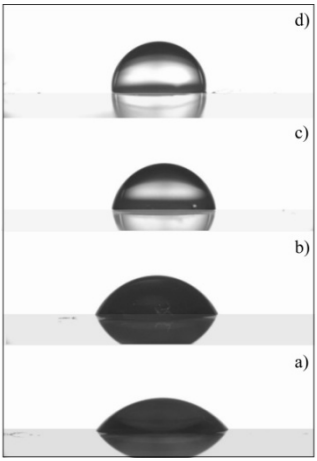

Figure 5. Water contact angle measurements of the pristine polymer: a) A0; and of the nanocomposite films: b) A16; c) A28; d) A44.

Presence of both an hydrophobic main chain and polar side chains in PEOX results into a peculiar balance between solubility in water and polar organic solvents [34] mediated by hydrogen bonds with carbonyl groups of the side chain, and aggregation through collapse of the main chain above a lower critical solution temperature (LCST). While hydrogen bonds between PEOX and residual hydroxyls on the titania surface might help to stabilize the dispersion of nanoparticles in PEOX, as in the case of fumed silica [36], phenyl rings covering the titania surface possibly provide the additional stabilizing interactions, like CH-π, with the hydrophobic main chain of PEOX [35], which determines precipitation of a well

dispersed nanocomposite as water evaporates during the formation of the film. However, at the final stage of solvent evaporation, when a solid-air interface forms, PEOX aggregation is possibly stronger, thus it is not anymore able to wet the nanoparticles surfaces, which remain exposed to air.
As a first conclusion, we obtained materials whose surface properties, such as the roughness and hydrophobicity, can be tuned by the synthesis method of nanoparticles and, as consequence, by the nanoparticles content in the polymeric matrix. In particular, obtaining hydrophobic films by working in a hydrophilic environment is interesting per se.

5.3.2 Optical Characterization of nanocomposite films

Both pure poly(2-ethyl-2-oxazoline) (A0) and nanocomposite films fabricated with increasing concentrations of nanoparticles are optically transparent for the most part. Their UV-visible spectra are reported in Figure 5.6. Below 400 nm it is possible to observe the pronounced nanocomposite absorption edge, linked to the nanoparticle band gap. Therefore, unlike the pristine polymer, the nanocomposite films provide complete UV filtering up to the proximity of the visible.
Because of the high concentration of the nanoparticles in the polymeric matrix, the refractive index of the nanocomposites is expected to be larger than the value for the pure polymer. The effective nanocomposite refractive index is predicted by the following equation [15]:

$$n_{comp} = f_v n_p + f_m n_m \quad (2)$$

where n_{comp}, n_p and n_m are the refractive indices of the nanocomposite, nanoparticles and polymeric matrix respectively; f_v and $f_m = 1 - f_v$ are the *volume* fractions of the nanoparticles and the polymeric matrix. In order to estimate nanocomposite refractive indices, 1.52 (λ = 589 nm) and 2.49 (λ = 589 nm) were used as refractive indices of the polymeric matrix [20] and of the anatase nanoparticles [37] respectively, and densities of 1.14 g/cm^3 [20] and 3.9 g/cm^3 [24] were used in order to calculate the volume fraction from the weight fraction of the nanoparticles in the nanocomposite. The film characterized by about 28% w/w of nanoparticles in the polymeric matrix (A28) should have a refractive index of about 1.62 theoretically, up to about 1.70 for the film filled with 44% w/w of nanoparticles (A44).

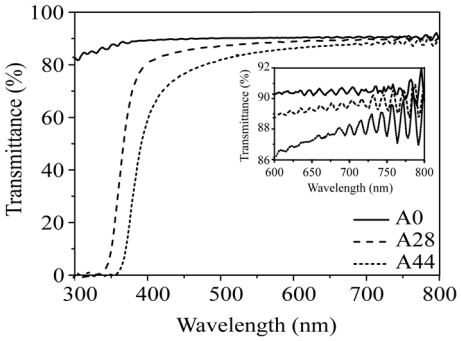

Figure 5.6. UV-visible spectra of the pure polymer (A0) and nanocomposite films characterized by 28% w/w and 44% w/w of nanoparticles in the polymeric matrix (A28 and A44 respectively). In the

inset the near IR spectra in the region comprised between 600-800 nm is shown.

The inset of figure 5.6 shows the near IR portion of the spectra of the samples at an enlarged scale. Assuming that surface and bulk scattering are negligible at long wavelengths, the average transmittance in this range is given by $T_0=(1-R)^2$, with $R=\left(n_{comp}-1\right)^2/\left(n_{comp}+1\right)^2$ the interface reflectance. With these assumptions, the 91.5% transmittance of the A0 film at 694 nm correspond to n_{comp}=1.52, matching literature data. Good agreement with the index predicted by equation (2) is also found for nanocomposites: indeed the 89.8% transmittance at 694 nm for the film A28 corresponds to a refractive index of 1.60, while the 88.4% of transmittance for A44 corresponds to a refractive index of 1.65. All measured values are slightly lower compared to the expected values calculated using equation (2). A reason for this minor deviation could be linked to an overestimation of the particles refractive index because of the small size of the crystallites. Moreover, as discussed above, a fraction of water and benzyl alcohol molecules are present on the surface of the nanoparticles. Thus, the effective index of the nanoparticles is possibly lower compared to the refractive index of pure anatase. Finally, the conformation of the polymer chains in close proximity to the nanoparticles surface is possibly modified by the different environment. This may lead to a lower density of the polymer, which becomes significant for the large volume fractions of nanoparticles present in our samples [38, 39].

The film thicknesses L were calculated by measuring the wavelength separation between adjacent transmission peaks $\Delta\lambda$ in the region of interference, using the Fabry-Pérot law [40], according to:

$$\Delta\lambda = \frac{\lambda^2}{Ln_{comp}} \tag{3}$$

where λ is the central wavelength of the nearest transmission peaks (in this case 694 nm), and n_{comp} is the film refractive index calculated above from reflectance measurements. Considering the periodicity of the interference fringes of 14 nm, a thickness of about 11 μm was obtained for all samples.

The weak change of transmittance in the visible range is not due to the TiO_2 band gap, thus Rayleigh Scattering can be hypothesized. Below the near IR range, and into the visible region, the slopes of the nanocomposite transmission spectra $T(\lambda)$ between 400 nm and 650 nm were evaluated using the Rayleigh law [41], which applies well for spherical scatterers having diameters below $\lambda/10$:

$$T(\lambda) = T_0 e^{-\left[\frac{32\pi^4 r^3}{\lambda^4} f_v \left(\frac{n_p{}^2 - n_m{}^2}{n_p{}^2 + 2n_m{}^2}\right)^2 L\right]} \tag{4}$$

where r is the radius of the nanoparticles, L is the thickness of the film, λ is the wavelength, and n_p , n_m and f_v have been

introduced above and are the refractive indices of the nanoparticles, of the polymeric matrix, and the volume fraction of the nanoparticles in the nanocomposite respectively. Figure 5.7 shows the logarithm of the bulk absorbance $\alpha(\lambda)L = -ln(T(\lambda)/T_{A0}(\lambda))$ versus the logarithm of the wavelength λ, along with a linear fitting with slope -4. The good fit with such a slope shows that the transmittance losses are indeed can be attributed to Rayleigh scattering in the region between 400 and 650 nm. Using n_m = 1.52, n_p = 2.49, the thicknesses measured from the near IR transmission as explained above, and the measured concentrations f_v, the expected radius of the nanoparticles could be extracted from the intercepts in figure 5.7 to be around 25 nm, in good agreement with DLS measurements and TEM micrographs, confirming that no agglomeration in occurs during the formation of the film.

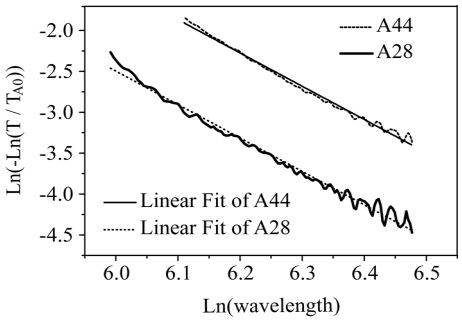

Figure 5.7. Film absorbance logarithms (A28 and A44), normalized to the pristine polymer absorbance, versus the wavelength logarithm in the visible range. The curves were fitted with two straight lines with slope -4, distinctive of Rayleigh scattering also shown in the figure.

In conclusion, UV-visible spectroscopy shows that the nanocomposite films are essentially transparent, with a weak bulk scattering mainly linked to the high concentration of the nanoparticles in the films. Moreover, the measurements showed that the films absorb the UV radiation up to the proximity of the visible and have refractive indices higher than the pure polymer growing with the concentration of the nanoparticles in the polymeric matrix.

The optical quality of the films was assessed through optical measurements of reflectivity and surface scattering. Measurements of specular gloss $G_s(\Theta)$ at 20°, 60° and 85° and distinctness of image gloss (G_{DOI}) were performed allowing an assessment of the impact of surface scattering on the visual appearance of the film. Specular gloss is a measurement of the ratio of the luminous flux reflected from the sample at an angle Θ, relative to the luminous flux reflected from a standard smooth glass surface with a refractive index of 1.567. Increase in the bulk RI will increase specular gloss but surface roughness reduces the specular gloss through diffusion. An estimate of the RMS surface roughness σ can be obtained by fitting the measured specular gloss using the Fresnel equation $G_s(\Theta,n_{comp})$ [40] times a term that accounts for the loss from scattering, in this case from the total integrated scattering model [42]:

$$G_s(\Theta) = G_s(\Theta, n_{comp}) \exp\left[-\left(\frac{4\pi\sigma \cos\Theta}{\lambda} \right)^2 \right] \qquad (5)$$

where n_{comp} is the sample RI obtained by the UV-Visible measurements described above, and σ is the RMS surface roughness.

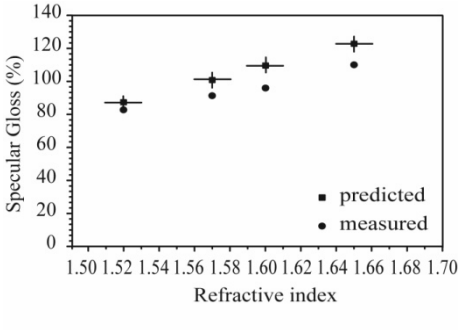

Figure 5.8. Measured (dots) specular gloss values $G_s(\Theta)$, and predicted (squares) values $G_s(\Theta, n_{sam})$ versus film refractive indices at Θ=20° incident angle.

Figure 5.8 shows the predicted gloss $G_s(\Theta, n_{scomp})$, assuming no loss from surface scattering, and the measured specular gloss $G_s(\Theta)$ at 20° and at a wavelength λ of 550 nm versus the measured refractive indices of the samples. The x-error bars represent a relative error below 1% on the measured refractive indices of films, resulting into about 3% of relative error on the predicted gloss. Films of pristine polymer and with the lowest concentration of nanoparticles in the polymeric matrix (A16) seem to produce quite a smooth surface on the polished glass,

while some relevant deviations from the values expected for a perfectly smooth surface appear for the more concentrated nanocomposites A28 and A44. The mismatch is attributed to the increased surface roughness, which is evaluated from Equation (5), and summarized in Table 5.2.

Table 5.2. Films RMS roughness σ obtained from the specular gloss measured and predicted values using Equation (5) for small incident angles (Θ = 20°), and at λ = 550 nm, and distinctness of image measurements

Film	TiO_2 (% w/w)	R.I.	σ (nm)	G_{DoI}
A0	0	1.52	11±3	98.5 ± 0.5
A16	16	1.57	15±2	98.0 ± 0.5
A28	28	1.60	17±2	95 ± 1
A44	44	1.65	16±2	96 ± 1

We remark that σ grows with the nanoparticles concentration in the nanocomposite, in agreement with the AFM height image results presented above.

In the perspective of using this material as a protective coating, we evaluate distinctness-of-image (G_{DoI}) gloss which evaluates the effectiveness of the coating in preserving the information of an image covered by the film. This measurement compares the amount of scattered light at ±0.3° from the specular angle Θ = 30°, $I_{30°\pm0.3°}$, to light reflected in the specular direction, $I_{30°}$, according to the formula $G_{DoI} = 100\ (I_{30°}-I_{30°\pm0.3°})/I_{30°}$. Therefore, a value of 100% indicates that no light is diffused off-axis, while lower values indicate that a fraction of light is scattered slightly off-axis, blurring image formation in a far

optical system such as the eye. Such an off-axis scattering is mainly related to surface roughness [43], as the contribution of Rayleigh bulk scattering is instead quite diffuse in angle, and is therefore negligible into the very low aperture used in G_{DoI} measurements (below 0.3°). Results for G_{DoI} are also shown in Table 2. G_{DoI} is always very close to 100 %, i.e. the fraction of light diffused slightly off-axis is relatively small for all samples. Indeed, also specular gloss measurements point out to a relatively weak total surface scattering. The slight decrease of G_{DoI} with increasing nanoparticles content indicates an increase in surface roughness, also in agreement with specular gloss measurements. However, we remark that the RMS surface roughness is only slightly larger in A28 and A44 compared to A16, an increase which is not sufficient to explain the more significant reduction of G_{DoI}. Here, a change in the structure of surface roughness over length scales much beyond those considered in AFM measurements is probably involved. Detailed investigation of these aspects of the nanocomposite surface will be the subject of further study. The chapter 5 describes a continuation of this work.

5.4 Summary

In summary, the surface and optical properties of poly(2-ethyl-2-oxazoline) were modified by the introduction of TiO_2 nanoparticles in the polymer. TEM images showed that nanoparticles are clustered in elongated aggregates of about 40 nm confirming the DLS measurements of the aqueous dispersion, and that they are homogeneously distributed in the

polymeric matrix. On the other hand, regardless of the TiO_2 content, AFM images showed that some nanoparticles protruded out of the films surface, modifying the hydrophilic behavior of the pristine polyoxazoline. In particular, a growth of the material's contact angle with water up to more than 90° has been observed. This phenomenon has been attributed to the partial coverage of the TiO_2 surface with the benzyl alcohol originating from the nanoparticles synthesis. Moreover, films were characterized by an increase of the surface roughness with the nanoparticles concentration in the polymeric matrix, according to AFM height trace and specular gloss measurements. From this point of view, nanocomposite films were characterized by tunable surface properties, such as roughness and hydrophobicity.

Optical properties were also investigated and refractive index and UV filtering can be tailored by the increasing concentration of nanoparticles in the polymeric matrix. In particular, films characterized by high refractive index up to about 1.65 and UV absorption up to the proximity of the visible range were obtained. Moreover, nanocomposite films were optically transparent, albeit showing weak bulk scattering that may result into a slight coloring of the film (having an impact when used as a functional coating), and weak surface scattering resulting into a slight reduction of gloss. Thus, several optical properties of these nanocomposites, and their visual appearance when used as coatings, may be tailored by varying the concentration and nature of the nanoparticles in the polymeric matrix. The good chemical and physical properties of these

materials could allow their application in the paint and coating industry and in the field of conservation of cultural heritage.

5.5 References

[1] Alexandre M and Dubois P 2000 *Mat. Sci. Eng. R.* **28** 1

[2] Balazs A C, Emrick T and Russell T P 2006 *Science* **314** 1107

[3] Usuki A, Kojima Y, Kawasumi M, Okada A, Fukushima Y, Kurauchi T and Kamigaito O 1993 *J. Mater. Res.* **8** 1179

[4] Kojima Y, Usuki A, Kawasumi M, Okada A, Fukushima Y, Kurauchi T and Kamigaito O 1993 *J. Mater. Res.* **8** 1185

[5] Kiliaris P and Papaspyrides C D 2010 *Progr. Polym. Sci.* **35** 902

[6] Osman M A, Mittal V, Morbidelli M, Suter U W 2003 *Macromolecules* 36 9851

[7] Song H and Lee S 2007 *Nanotechnology* **18** 55402

[8] Neves M C, Martins M A, Soares-Santos P C R, Rauwel P, Ferreira R A S, Monteiro T, Carlos L D and Trindade T 2008 *Nanotechnology* **19,** 15560

[9] Nussbaumer R J, Caseri W R, Smith P and Tervoort T 2003 *Macromol. Mat. Eng*. **288** 44

[10] Althues H, Potschke R, Kim G M and Kaskel S 2009 *J. Nanosci. Nanotechnol.* **9** 2739

[11] Handbook of Optical Constants of Solids 1985 ed. E. D. Palik, Academic Press, Orlando

[12] French R H, Glass S J, Ohuchi F S, Xu Y-N and Ching W Y 1994 *Phys. Rev. B: Condens. Matter* **49** 5133

[13] Tsuzuki T 2008 *Macromol. Mater. Eng.* **293** 109

[14] Demir M M, Memesa M, Castignolles P and Wegner G. 2006 *Macromol. Rapid Commun.* **27** 763
[15] Althues H, Henle J and Kaskel S 2007 *Chem. Soc. Rev.* **36** 1454
[16] Goesmann H and Feldmann C 2010 *Angew. Chem. Int. Ed.* **49** 1362
[17] Koziej D, Fischer F, Kränzlin, Caseri W, and Niederberger M 2009 *App. Mater Interfaces* **1** 1097
[18] Lin C, Berry M T, Anderson R, Smith S and May P S 2009 *Chem. Mate*r. **21** 3406
[19] Demir, M M, Koynov K, Akbey U, Bubeck C, Park I, Lieberwirth I and Wegner G 2007 *Macromolecules* **40** 1089
[20] Chui T T, Thill B and Fairchock W J 1986 Water Soluble Polymers *Advances in Chemistry Series* vol. 213, ed. J. E. Glass (Washington DC, American Chemical Society) 426
[21] Wolbers R C, McGinn M and D. Duerbeck 1998 Proceedings of the symposium organized by the Wooden Artifacts Group of AIC, 1994, Williamsburg, eds. V. Dorge and F. C. Howlett. (Los Angeles, Getty Conservation Institute) 514
[22] Hoogenboom R and Schlaad H 2011 *Polymers* **3** 467
[23] Adams N and Schubert U 2007 *Adv. Drug Deliv. Rev.* **59** 1504
[24] Niederberger M, Bartl M H and Stucky G D 2002 *Chem. Mate*r. **14** 4364
[25] Brunauer S, Emmett P H and Teller E 1938 *J. Am. Chem. Soc.* **60** 309

[26] ASTM Standard Test Method for Specular Gloss D523-89 2000 (Philadelphia)
[27] ASTM Standard Test Method for Measurement of Gloss of High-Gloss Surfaces by Goniophotometry E430-97, 2000 (Philadelphia)
[28] Niederberger M, Bartl M H and Stucky G D 2002 *J. Am. Chem. Soc*. **124** 13642
[29] Mueller R, Kammler H K, Wegner K and Pratsinis S E 2003 *Langmuir* **19** 160
[30] Brindle R, Pursch M and Albert K 1996 *Solid State Nucl. Magn. Reson.* **266** 251
[31] Dorrer C and Rühe J 2008 *Adv. Mater*. **20** 159
[32] Pareo P, De Gregorio G, Manca M, Pianesi M S, De Marco L, Cavallaro F, Mari M, Pappada S, Ciccarella G and Gigli G. 2011 *J. Colloid Interface Sci.* **363** 668
[33] Caputo G, Cortese B, Nobile C, Salerno M, Cingolani R, Gigli G, Cozzoli P D and Athanassiou A 2009 *Adv. Funct. Mater*. **19** 1149
[34] Chen F P, Ames A E and Taylor L D 1990 *Macromolecules* **23** 4688
[35] Sozzani P, Comotti A, Bracco S and Simonutti R 2004. *Chem. Comm.* 768
[36] Chen C H, Wilson J E, Davis R M, Chen W and Riffle J S 1994 *Macromolecules* **27** 6376
[37] Lu C and Yang B 2009 *J. Mater. Chem.* **19** 2884
[38] Mont F W, Kim J K, Schubert M F, Schubert E F and Siegel R W 2008 *J. Appl. Phys.* **103** 083120

[39] Nussbaumer R J, Caseri W R, Smith P and Tervoort T 2003 *Macromol. Mater. Eng.* **288** 44
[40] Nassau K 2001 The Physics and Chemistry of Color, ed. Wiley Series in Pure and Applied Optics (New York) 231
[41] Caseri W 2009 *Chem. Eng. Comm.* **196** 549
[42] Bennett H E 1963 *J. Opt. Soc. Am.* **53** 1389
[43] Delaney J K, de la Rie E R, Charron E, Elias M, Sung L-P and Morales K M 2008 *Stud. Conserv.* **53** 170

Chapter 6

Optical Effect of Nanocomposite Films on Matte Painted Surfaces

6.1 Introduction

Painted layers are usually the characterizing element of paintings; the picture and the picture's subjects hold the artwork's meaning. From this point of view, the appearance of the painting is very important. Traditionally, a varnish is used in order to homogenize the light reflection of the paintings' surface, and makes colors darker and more saturated, with a consequent increasing of gloss. As well as at the end of conservation treatments, with a lot of materials added on the paintings' surface, varnish is applied in order to hide optical imperfections under an homogenous and glossy layer. This is why the study of how different varnishes modify paintings appearance is a topic of interest in the field of conservation science. According to these researches, the modification of surface roughness is the main reason for resultant changes in the reflecting light of different coatings, whose refractive indices are included between about 1.47 and 1.52 [1, 2]. These optical changes are connected to different smoothing behavior that are dependent by materials' chemistry [3].

At the same time, paintings made with watercolors or tempera, and a lot of contemporary works of art, require other attentions.

The addition of a new material on their surfaces may change their characteristic matte appearance: the difficulty of intervention on such surfaces can result in conservation problems.

This paper describes the potentialities of nanocomposites films as consolidants and coatings for matte painted surfaces. Nanocomposites were fabricated loading a poly 2-ethyl-2-oxazoline with titanium dioxide nanoparticles, in order to obtain optically transparent UV filter and highly refractive coatings. The poly 2-ethyl-oxazoline was chosen as the polymeric matrix because of recognized properties such as good adhesive force, pigments' binder and coating capabilities [4-6], light stability [7], water solubility and lack of toxicity [8]. All these qualities made these materials matter of scientist interest [9, 10] and known in the conservation field [11, 12]. Titanium dioxide was used because of its high refractive index (2.5-2.9 depending on the crystalline phase) and the UV absorption, linked to the semiconductive electronic properties (indirect band gap of 3.2 eV) [13]. By charging the polymeric matrix with an increasing concentration of nanoparticles, nanocomposites' bulk refractive indices can be tuned without changing the organic phase's processability.

The major requirement for transparent nanocomposites is the nanoparticles' size: it must be less than 40 nm (for spherical nanoparticles $2r \leq \lambda/10$) in order to minimize the light scattering described by the Rayleigh Law [14]. This is one of the main drawbacks of working with nanoparticles, as they tend to aggregate irreversibly because of the high surface area.

Therefore, the development of methods for minimizing nanoparticles' aggregation is a topic of great interest in the scientific field [15-16].

In chapter 5, films characterized by an increased concentration of nanoparticles in the polymeric matrix, were prepared and investigated using UV-visible spectroscopy, Atomic Force Microscopy, specular gloss and distinctness-of-image gloss (DOI) measurements. Even if nanocomposites' films were optically transparent, they had a little percentage of loss in the transmitting light, because of the Rayleigh scattering, depending by nanoparticles' high refractive index and their high concentration inside the polymeric matrix. At the same time, an increase in the surface roughness of the films with the addiction of the nanoparticles to the nanocomposites was recorded by AFM, and confirmed by specular gloss measurements. On the other hand, distinctness-of-image gloss results revealed that the surface's scattering contribution seemed tiny.

In the course of this research, nanocomposite films made up with the poly 2-ethyl-2-oxazoline and silicon dioxide nanoparticles were prepared and compared to nanocomposite films charged with titanium dioxide. The aim of this work was comparing the optical properties of the highly refractive films filled with titanium dioxide, and the optical properties of nanocomposites charged with silicon dioxide, whose refractive index is similar to the polymeric matrix's one.

In the research described here, the two sets of nanocomposite films (charged with titanium dioxide and with silicon dioxide

nanoparticles), were prepared in three different concentrations inside the polymeric matrix (16%, 28% and 44% w/w); they were then investigated with UV-visible spectroscopy, specular gloss and distinctness-of-image gloss measurements.
In order to verify the nanocomposites' optical properties in practice, they were cast on a matte acrylic black painted surface and characterized by Reflectance Spectroscopy.

6.2 Experimental

6.2.1 Preparation and Characterization of Nanocomposite Films

Pure Aquazol 200® (Polymer Chemistry Innovation, M_w=200000) films (A0) were prepared from a solution of 5% w/w of the polymer in distilled water and cast on a quartz plate and microscope slides; thin films were obtained by evaporation of the solvent at room temperature.
Nanocomposite films loaded with nanoparticles were obtained by mixing the polymeric solution of Aquazol in water with the dispersions of nanoparticles in water in different ratio. Films characterized by an increasing concentration of nanoparticles in the polymeric matrix (16% w/w, 28% w/w and 44% w/w) were prepared by evaporation of the solvent. Titanium dioxide nanoparticles were synthesized using Niederberger et al. recipe [17]; the method for obtaining the water nanoparticles' dispersion was already explained in the previous chapter. Nanocomposite films filled with silicon dioxide, the brand dispersion LUDOX 40TM® (Sigma Aldrich), was opportunely

diluted and added to the polymeric solution in water. We chose this commercial product because the nanoparticles' diameter is about 40 nm, the same of the titanium dioxide nanoparticles measured by Dynamic Light Scattering in water (40 ± 20 nm).
Finally, seven films were prepared: A0 (the pristine polymer), A16, A28, A44 (characterized by an increasing concentration of titanium dioxide nanoparticles in the polymeric matrix (16%, 28% and 44% w/w respectively)), and S16, S28, S44 (filled with silicon dioxide nanoparticles at the same concentrations of A16, A28 and A44).
Films cast on quartz plates were characterized with a Cary Varian 300 spectrometer, using a clean quartz plate as reference. The films' thickness was calculated by the Scanning Electron Microscopy (Hitachi S3400-N) images, achieved using backscattered electron detector (BSE). Information were obtained using digital calipers, which are part of the onboard imaging processing software included in the SEM software package. Sample fragments were mounted on conductive carbon tape and coated with a Au/Pd film of about 120 angstroms of thickness. Films' specular glosses at 20°, 60° and 85° were determined according to ASTM D523 using a micro-Tri-gloss apparatus [18]. Every result is an average of three sets of measurements taken in different positions, and each one is an average of six measurements. Relative error of these results is a maximum of 1%. In order to perform specular gloss measurements, films were cast on microscope slides with the uncoated sides spray-painted in black. Distinctness-Of-Image gloss measurements were performed according to ASTM E430

using a Dorigon II abridged goniophotometer [19]. Every result is an average of six measurements. Relative error of these results is less than 1%. In order to perform these measurements the same samples used for measuring the specular gloss were employed.

6.2.2 Preparation and Characterization of Black Painted Model

The painting model was obtained by casting an acrylic black color (Windsor and Newton® tube) on a pre-prepared canvas. When the painted layer was dry, it was coated with the nanocomposites films (A16, A28, A44, S16, S28, S44) and the pure polymer (A0). Every sample was characterized by the 5% w/w of polymer in water dispersion and every box was treated with the same amount in weight of material.

A fiber-optic spectroradiometer, FS3 (ASD Inc, Boulder, CO) was used to obtain FORS (Fibers Optics Reflactance Spectroscopy) spectra at various sites. The spectrometer operates from 350 nm to 2500 nm with a spectral sampling of 1.4 nm from 350 to 1000 nm and 2 nm from 1000 to 2500 nm. The spectral resolution at 700 nm is 3 nm, and at 1400 and 2100 nm it's 10 nm. The light source of a leaf probe head (ASD Inc) was used at a distance of 10 cm in order to illuminate the painting (4000 lux),; and the fiber was placed ~1 cm from the object, giving a ~3 mm spot size to the painting. The samples were illuminated at 45 degrees and the light

collected normal to the sample. Typically 64 spectra are averaged and total acquisition time is 7 s per point.

Through the integration of the reflectance spectra in the visible range (380-720 nm) the determination of the samples' colors was performed. Colors were reported in the CIE-L*a*b* color space, where CIE is the *Commission International de L'Eclairage*, the main international organization concerning color and color measurement, while L*, a* and b* are the colorimetric coordinates plotted at right angles one to the other in order to form a three dimensional coordinate system. Equal distances in the space represent approximately equal color differences. Value L* represents Lightness, value a* represents the Redness/Greenness axis, and value b* represents the yellowness/blueness axis [20]. Calculations were performed using the CIE Standard Illumination D65, based on actual spectral measurements of daylight, that represents a color temperature of 6504 K. This is the most widely used color temperature in the industry of graphic arts and in the field of cultural heritage, where it's employed to see color changes on works of art [21, 22]. The color differences are generally calculated as the square root of the combined squares of the chromaticity differences and is defined as Delta Error (ΔE):

$$\Delta E = \sqrt{(a^*)^2 + (b^*)^2 + (L^*)^2} \quad (1)$$

ΔE has to be higher than 1.0 so that the changes of colors are perceptible by the human eyes [20].

6.3 Results and Discussions

6.3.1 Optical Measurements of nanocomposites films

UV-visible measurements of the films show their different optical behavior (Figure 6. 6.1). The poly-oxazoline (Film A0) absorbs completely the incident light up to about 225 nm and, the addiction of the SiO_2 nanoparticles (Film S28), doesn't change the absorption properties of the polymer in practice. This is connected to the insulator character of silica (energy bandgap of 8.9 eV). On the other hand, films loaded with TiO_2 show a strong adsorption up to the proximity of the visible range, because of the semiconduttive electronic properties of anatase (indirect energy gap of 3.2 eV). In particular, they absorb up to about 300 nm, suppressing completely the UV-B radiation, and their absorption increases with the concentration of the nanoparticles in the polymeric matrix according to the Bouguer-Lambert-Beer Law (see Figure 6. 6.1 magnification).
Furthermore, even if all the films are transparent in the visible range (while, at the same range, the curves of the pristine polymer and those of the nanocomposite charged with silicon dioxide are flat), titanium dioxide nanocomposites show a weak loss in transmittance, such as already showed in chapter 5. In order to verify the nature of the loss of transmittance of the films charged with TiO_2, the logarithm of the absorbance versus the logarithm of the wavelength was fitted with a straight line. The slope of the curve was about -4, demonstrating that films scatter according to the Rayleigh Law. Films' thickness was an order of size less than the samples

described in chapter 5 according to SEM images. Through the measure of the intercept, a ray of the particles of about 20 nm was calculated, in good agreement with the result obtained with the other films filled with TiO_2 (see chapter 5).

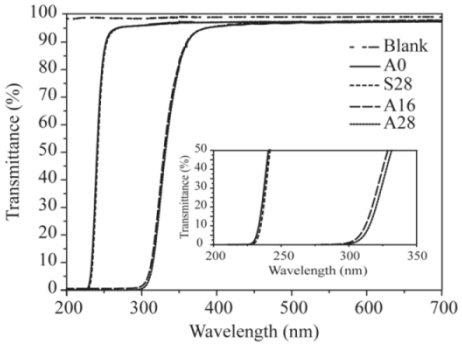

Figure 6.1. Spectra UV-visible of the pristine polymer (A0), the film filled with the average concentration of SiO_2 nanoparticles (S28), and the films characterized by 16% w/w and 28% w/w of TiO_2 in the polymeric matrix (respectively A16, A28). Blank is the reference, that is the quartz plate, the same material on which films were cast.

In order to compare the reflectivity properties of the nanocomposite films filled with silicon dioxide and titanium dioxide, measurements of the specular gloss at 20°, 60° and 85°, and distinctness-of –image gloss (G_{DoI}) were performed.
Figure 6.2 shows the specular gloss data at 20° for the pristine polymer film, and the films characterized by the increasing concentration of TiO_2 and SiO_2 nanoparticles. The measured data (black symbols) are compared with the predicted results obtained using the Fresnel equation (white symbols). As the poly-oxazoline and SiO_2 colloidal solution have similar RI

(respectively 1.52 at 589 nm [8] and 1.46 in the visible range [23]), the predicted values of specular gloss are similar for the pristine polymer and the nanocomposites filled with SiO_2. A small deviation between the measured values and those we expected, was revealed for the samples characterized by the highest concentration of the SiO_2 nanoparticles in the polymeric matrix.

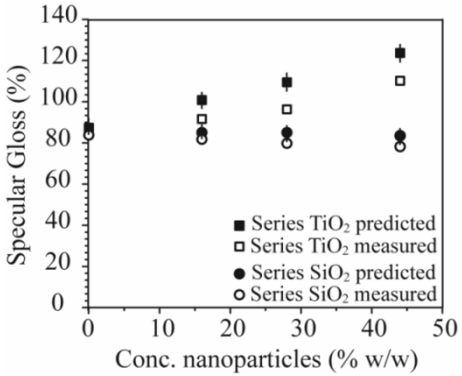

Figure 6. 2. Comparison between the specular gloss measured (white symbols) and predicted values (black symbols) of the pristine polymer (0% w/w of nanoparticles), TiO_2 (squares) and SiO_2 (circles) sets. Data are reported versus the concentration of the nanoparticles in the polymeric matrix.

The specular gloss data relative to the pristine polymer and the titanium dioxide series are the same reported in the Figure 6. 5.6 of chapter 5; the only difference is that, in this case, data are depicted versus the concentration in weight of the nanoparticles in the polymeric matrix instead of the films' refractive index. The films filled with the higher concentrations

of titanium dioxide in the polymeric matrix show the major deviation between the measured and expected values. The y-error bars are linked to the propagation of the uncertainty on films' refractive index, as already explained in the previous chapter. Relative error is always less than 3%. An estimate of the RMS surface roughness σ was extracted from the expected gloss as calculated with the Fresnel formula [24] using the Total Integrated Scattering formula (equation 4 of chapter 5) [25]. A summary of the results is reported in table 6.1.

Table 6.1. RMS Roughness of films σ obtained from the specular gloss using equation 4 of chapter 5 for small incident angles (Θ = 20°).

Film	TiO_2 conc. (w/w)	R.I.	σ(nm)[1]
A0	0	1.52	11±3
S16	16	1.51	8±4
S28	28	1.50	9±4
S44	44	1.50	11±4
A16	16	1.57	15±2
A28	28	1.60	17±2
A44	44	1.65	16±2

[1] λ=550 nm.

Table 6.1 shows that the presence of the silicon dioxide nanoparticles in the polymeric matrix leads to a small reduction of the surface roughness, in comparison with the pristine polymer film; in particular, the smoothest coating is the one

with the lowest concentration of SiO_2 nanoparticles in the polymeric matrix. On the other hand, a modest growth of the surface roughness with the increasing concentration of TiO_2 nanoparticles in the polymeric matrix is observed. Further studies will be performed in order to understand interactions between the polymeric chains and the nanoparticles (SiO_2 and TiO_2) that lead to these different surface properties. As to this, an important role is played by the chemistry of the nanoparticles' surface.

In order to verify the role of the surface roughness on the films' reflectivity properties, distinctness-of-image gloss measurements were performed. Figure 6.3 shows the measured G_{DOI} values of the pristine polymer film (white square), and the nanocomposite films. SiO_2 and TiO_2 sets (respectively the white circles and the black squares) are showed versus the percentage in weight of nanoparticles in the polymeric matrix.

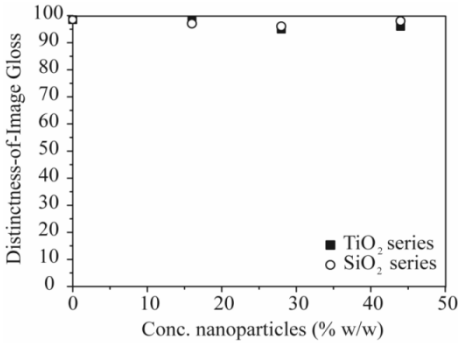

Figure 6.3. Distinctness-of-image gloss measurements of the pristine polymer film (white square), and the nanocomposite films filled with SiO_2 nanoparticles (white circle) and TiO_2 nanoparticles (black square). Data are

reported versus the concentration in weight of nanoparticles in the polymeric matrix.

Distinctness-of-image gloss measurements are approximately the same for all samples and they are very close to the pristine polymer results, with no influence of the type of particles and their concentration in the polymeric matrix. This could be a demonstration that the roughness surface plays a small role in the scattering properties of films and, as a consequence, in their appearance. In order to verify the results obtained with the optical characterization of films, samples were cast on a matte acrylic black surface as coatings, and characterized using Reflectance Spectroscopy. Then, the spectra in reflectance of the reference (the pristine paint), and the coatings were used to describe the paint's changes of color with the colorimetric coordinates L*a*b* and ΔE.

6.3.2 Optical Measurements of coatings on the Black Painted Model

In order to test the optical properties of the nanocomposite films characterized in the previous section, the dispersions of the nanoparticles in the aqueous polymeric solution were cast on a black painted surface. Films were obtained by evaporation of the solvent. As described in literature [26], the gloss behaviour of paints is a function of the pigment volume concentration (PCV) in the binder; it was found that the maximum gloss is achieved when the minimum amount of

binder gets to cover all the particles without air voids. Therefore, over a critical PVC value, the formation of air voids leads to an increase of the surface roughness and, consequently, a strong reduction of the paint's refractive index. Because of the surface scattering and the low refractive index, closer to the air one (about 1.0), painted surfaces generally appear matte and bleached. The application of a smoother coating reducing surface scattering and characterized by a higher refractive index (generally about 1.5) on the paint's surface makes it appear more saturated and darker [27, 28]. This is the typical effect obtained by varnishes in the field of paintings conservation and, in general, by most of coatings used in the paint industry. Anyway, "anti-reflecting" coatings are searched in many situations and for different reasons [28]. Even in the conservation field, the maintenance of the characteristic matte appearance is necessary for some kind of artworks (i.e. watercolor and tempera paints, some contemporary works of art, paper and stone artefact). The penalty is the loss of the social, cultural and economical artworks' value.

According to the theory, covering our black painted model with one of the films described, should obtain a glosser surface because of the increase of mismatch between the refractive indices of the paint and the air. This effect should be more evident for nanocomposite films filled with TiO_2. On the other hand, AFM images and the specular gloss measurements revealed a growth of the RMS surface roughness with the

increasing concentration of TiO_2 nanoparticles in the polymeric matrix.

Figure 6.4 shows the appearance of the painted layer before (box Ref) and after the application of the pristine polymer (box A0), the film filled with the average concentration of silicon dioxide (box S28), and the films characterized by the presence of titanium dioxide in the polymeric matrix with increasing concentrations (respectively box A16, A28, A44).

With the optical inspection, it is possible to see the glossy appearance of the coating made of the pure poly-oxazoline and the polymer filled with SiO_2; instead, coatings characterized by the presence of the embedded TiO_2 appear more matte and haze with the increase of the concentration of nanoparticles in the polymeric matrix.

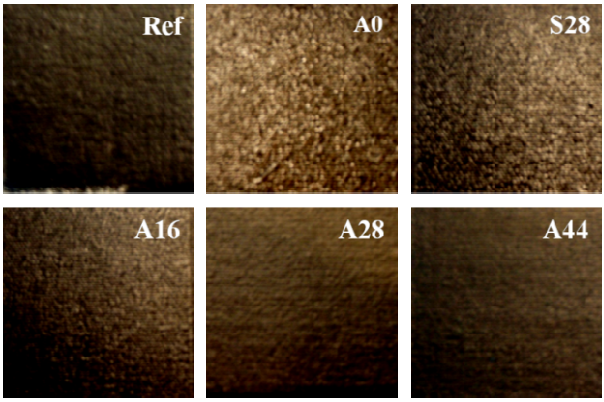

Figure 6.4. Images of the black painted surface before (Ref) and after the application of the coating: pristine poly-oxazoline (Film A0); nanocomposite with the 28% w/w of SiO_2 in the polymeric matrix (Film S28); nanocomposite with the 16% w/w of TiO_2 in the polymeric matrix

(Film A16); nanocomposite with the 28% w/w of TiO_2 in the polymeric matrix (Film A28); nanocomposite with the 44% w/w of TiO_2 in the polymeric matrix (Film A44).

The optical effect is exactly the opposite of the one expected because of the increasing refractive indices of the films.

The optical characterization of uncoated and coated surfaces was performed using the Reflectance Spectroscopy with Fiber Optics (FORS) placed at 45° by the source (see Figure 6.5)

Figure 6.5. FORS setup used to collect the spectra in reflectance of the uncoated and coated black paint.

The spectra in reflectance of samples are in good agreement with the visual inspection (Figure 6.6): the coating of the pristine polymer and films made up with the silicon dioxide nanoparticles are too dark and bright. In particular they appear darker with the decrease of the nanoparticles in the polymeric matrix and, in general, brighter than the pristine polymer; this might be connected to the decrease of the surface scattering because of the reduced RMS surface roughness (see Table 6.1).

On the other side, the set of films filled with TiO_2 nanoparticles shows the opposite optical behavior of those charged with silicon dioxide: they appear more matte and haze with the increase of nanoparticles' concentration in the polymeric matrix. In particular, the spectrum of the sample characterized by the average concentration of TiO_2 nanoparticles is the best match for the reference's spectrum from the reflectivity point of view.

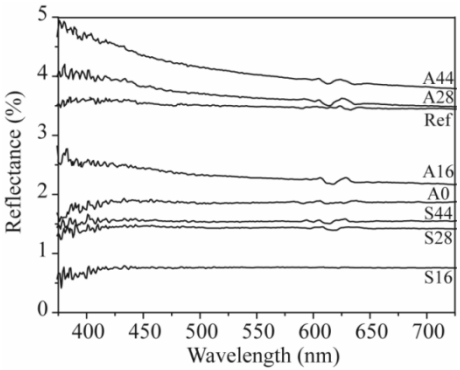

Figure 6.6. FORS spectra of the uncoated and coated black paint.

Furthermore, a feature of the films charged with titanium dioxide nanoparticles is a growth of the curve of reflectance in the visible range before the nanoparticles' UV absorption; it is the only difference between the reference and the sample A28 spectra. It is probably related to the Rayleigh Scattering.

In order to have a better understanding of the color changes induced by the presence of coatings on the painted surface, the conversion of the reflectance spectra in the colorimetric

coordinates L*, a* and b* was performed. Table 6.2 shows the results obtained using the CIE Standard Illuminant D65, whose spectrum is representative of the daylight condition. ΔE values were also calculated using as reference the pristine black painted surface in order to verify whether the color changes were effectively perceptible by human eyes.

Table 6.2. Colorimetric coordinates L* a* b* of the black paint (Ref.) and of the surface coated with the pristine polymer (A0), and the sets of films filled with SiO_2 (S16, S28 and S44) and TiO_2 (A16, A28 and A44). ΔE values are also reported. In bold font the only result less than 1.0 is reported, as it indicates that the change of color is imperceptible for human eyes.

	Ref.	**A0**	**S16**	**S28**	**S44**	**A16**	**A28**	**A44**
L*	21.80	14.80	7.10	12.20	12.90	17.10	22.40	23.80
a*	0.02	0.2	-0.02	0.07	0.12	0.1	0.1	0.09
b*	-0.33	-0.25	-0.01	-0.28	-0.12	-1.18	-1.17	-1.77
ΔE	0	4.8	9.7	6.4	6.1	2	**0.9**	3.4

As it can be seen at the last line of table 6.2, the only ΔE value less than 1.0 is the one of the box coated with the film of poly-oxazoline charged with the average concentration of TiO_2 in the polymeric matrix (Film A28). The difference of color between the other coatings and the reference is higher than 1.0, but it is mainly related to the coordinate L*, that is too low. This indicates an important decrease of the surface lightness. In fact, the paint appearance is too dark and saturated. On the other hand, the colorimetric coordinates a* and b* for film A28 show the major changes; in particular, the first one heads for

the red (higher value), while the second one heads for the blue (lower value). It is a typical characteristic of the Rayleigh Scattering that, with the surface scattering, can contribute for the diffusing properties of the TiO_2-nanocomposite films. Probably the film with the major concentration of titanium dioxide scatters too much and appears lighter than the reference.

6.4 Summary

The verification of the optical properties of nanocomposite films charged with titanium dioxide nanoparticles was carried out comparing them with the nanocomposite films loaded with silicon dioxide nanoparticles. Both sets of films showed an increase of the surface roughness with the increasing concentration of nanoparticles in the polymeric matrix; the coatings filled with SiO_2 always appear smoother than the pristine polymer film and the set of films charged with TiO_2. Distinctness–of-image gloss measurements showed that the contribution of the surface scattering on the films' reflective properties was very small. Anyway, only TiO_2 nanocomposite films showed additionally bulk scattering, because of the high refractive index. The reflective properties of these films were better understood by casting them on an acrylic black paint, whose pristine appearance was matte. Coatings made of the pure polymer and charged with SiO_2 nanoparticles appeared optically darker and more saturated than the pristine painted surface, data confirmed by the films' reflectance spectra. With the increasing concentration of nanoparticles in the polymeric matrix, instead, coatings filled with TiO_2 nanoparticles changed over from too dark to too light films. From this point of view, the average concentrated film was the best optical match for

the paint; the reasons of this optical behaviour were the surface and bulk scattering, both contributing to the final optical result. In any(?) case, apart from the simplified model used in this work, it is possible to tune the reflective properties of the TiO_2 nanocomposite films with the concentration of nanoparticles in the polymeric matrix. These optical properties could have interesting applications in the paint and coating industry, and in the field of conservation of cultural heritage in which matte surfaces and supports has to be coated preserving the pristine appearance.

6.5 References

[1] Elias M, de la Rie R E, Delaney J K, Charron E and Morales K M 2006 *Opt. Commun.* **266** 586

[2] Delaney J K, de la Rie E R, Charron E, Elias M, Sung L-P and Morales K M 2008 *Stud. Conserv.* **53** 170

[3] de la Rie E R, Delaney J K, Morales K M, C A Maines and Sung L-P 2010 *Stud. Conserv.* **55** 134

[4] Warchol J F, Walton C D 1998 US 97-795911

[5] Brinkhuis R H G 2003 WO 2002-EP13898, 2003

[6] Ma S-H, Rodriguez-Parada J N 1998 US 97-963839

[7] Wolbers R C, McGinn M and Duerbeck D Proceedings of the symposium organized by the Wooden Artifacts Group of AIC, 1994, Williamsburg, eds. V. Dorge and F. C. Howlett. Los Angeles: Getty Conservation Institute (1998) 514-527.

[8] Chui T T, Thill B and Fairchock W J 1986 Water Soluble Polymers *Advances in Chemistry Series* vol. 213, ed. J. E. Glass (Washington DC, American Chemical Society) 426

[9] Hoogenboom R and Schlaad H 2011 *Polymers* **3** 467

[10] Adams N and Schubert U 2007 *Adv. Drug Deliv. Rev.* **59** 1504

[11] Arslanoglu J 2003 *WAAC Newsletter* **25** 12
[12] Arslanoglu J 2004 *WAAC Newsletter* **26** 10
[13] Koziej D, Fischer F, Kranzlin N, Caseri W R and Niederberger M 2009 *Appl. Mater. Int.* **1** 1097
[14] Caseri W 2009 *Chem. Eng. Comm.* **196** 549
[15] Althues H, Henle J and Kaskel S 2007 *Chem. Soc. Rev*. **36** 1454
[16] Goesmann H and Feldmann C 2010 *Angew. Chem. Int. Ed.* **49** 1362
[17] Niederberger M, Bartl M H and Stucky G D 2002 *Chem. Mater*. **14** 4364
[18] ASTM Standard Test Method for Specular Gloss D523-89 2000 (Philadelphia)
[19] ASTM Standard Test Method for Measurement of Gloss of High-Gloss Surfaces by Goniophotometry E430-97, 2000 (Philadelphia)
[20] Nassau K 2001 The Physics and Chemistry of Color, ed. Wiley Series in Pure and Applied Optics (New York) 231
[21] Bacci M, Picollo M, Porcinai S and Radicati B 2000 *Thermochimica Acta* **365** 25
[22] Bacci M, Casini A, Cucci C, Picollo M, Radicati B and Vervat M 2003 *Journal of Cultural Heritage* **4** 329
[23] Duckin A S and Goetz P J 2010 Characterization of Liquids, Nano- and Microparticulates, and Porous Bodies using Ultrasound, ed Elsavier (Oxford) 346
[24] Meeten G H 1986 Optical Properties of Polymers, ed. Elsevier Applied Science (London) 326
[25] Bennett H E 1963 *J. Opt. Soc. Am.* **53** 1389

[26] Elton N J and Legrix A 2008 Surfoptic Applications Note n° 8 (AN8)
[27] Amra C 1993 *Appl. Opt.* **32** 5481
[28] Giovannini H and Amra C 1997 *Appl. Opt.* **36** 5574

Chapter 7

Light Stability of the poly 2-ethyl-2-oxazoline nanocomposite coatings loaded with TiO_2 nanoparticles

7.1 Introduction

In the previous chapters, the potentialities of the TiO_2-poly 2-ethyl-2-oxazoline nanocomposite as coating for painted surfaces were studied and valued. In particular, the introduction of titanium dioxide nanoparticles (anatase phase prepared by non-aqueous route) in the polymeric matrix permitted to obtain films highly transparent with tunable refractive index and UV absorption up to the proximity of the visible light. Great applications in the field of cultural heritage was pointed out like consolidants and protectives for substrates whose appearance should not to change, such as for example contemporary works of art, objects in metal, paints on wall and paper, paintings made of tempera and watercolours. Distinctness-of-image gloss measurements showed, in fact, that the presence of the films did not inhibit the visibility of the underlying image, even if the surface roughness and a weak bulk scattering increase with the TiO_2 content. The hydrophobic behavior of the final film point up also interesting application in the paint and coating industry. On the other

hand, the water solubility of this material makes itself an environmentally friendly product, interesting as biomaterial for packaging industry and biomedical applications.

Apart from the material optical properties, another thing that should be considered is the photo-catalytic activity of titanium dioxide [1], that can induce the degradation of the polymeric matrix used for the nanocomposite preparation. This titanium dioxide property can be considered a drawback in the case in which the durability of the material is an important requirement, but - in recent years - several efforts has been performed in order to catalyze the decomposition of various organic chemicals, such as aldehydes, and polymers. The activated decomposition by titanium dioxide of polyolefins [2-4], polystirene [5], and some biodegradable polymers, such as polylactide [6], pointed out the attention of the scientific literature. These researches joins in the necessity of a "green chemistry", involved also on the development of processes to reduce or to eliminate the use and generation of hazardous substances. Moreover studies of mechanism of degradation of polymers were investigated catalyzing the aging process with TiO_2, such as Lemaire et al. [7] with polyundecanamide.

The photocatalysis reaction is well known to active oxygen species, e.g. O_2^- and peroxides radicals, from water and oxigen, by redox reactions (see paragraph 2.3.2.2), under UV conditions. These active oxygen species lead to a degradation reaction by attacking polymer chains and accelerating chain cleavage.

From this point of view, after the fabrication of TiO_2-PEOX nanocomposites, characterized by a good dispersion of the inorganic phase in the polymeric matrix, the material photo-degradation under visible light was studied. The nanocomposite degradation was followed on time by FT-IR. The radical species generated during the polymer degradation were studied by Electron Paramagnetic Resonance (EPR).

7.2 Experimental

Nanocomposite films of poly(2-ethyl-2-oxazoline) (PEOX) filled with 16%, 28% and 44% in weight of TiO_2 (see paragraph 5.2.2 for the preparation) were cast on microscope slides and exposed to long-wavelength radiation ($\lambda > 420$ nm) in a xenon arc Weather-ometer (Atlas). The Weather-ometer irradiance was set to 0.9 W/m^2 at 420 nm using a xenon arc lamp (6500 Watt) with an inner soda lime and outer borosilicate filter giving a spectral power distribution that approximates daylight through window glass. The temperature and humidity was maintained at 25^oC and 38 ± 6% RH. In order to avoid the reflection of the light, a black cardboard was set on the back of the samples.

Micro-ATR FTIR was performed with a Si crystal μATR (Thermo) with an infinity reflachromat 15X objective and a Nexus 670 bench. Transmission micro-FTIR measurements were characterized by same samples in an effort to differentiate changes in bulk from eventual oxidation on the surface. FTIR spectra were collected at 256 scans with a resolution of 8 cm^{-1}

for μATR measurements and 32 scans with a resolution of 4 cm^{-1} for data collected in transmission mode. FTIR spectra were collecting on time until to the complete degradation of the samples.

The electron paramagnetic resonance (EPR) investigation was performed by a Bruker EMX spectrometer working at the X-band frequency and equipped with an Oxford cryostat working in the range of temperature 4–298 K.

The powder sample - non aqueous anatase (see paragraph 5.2.1 for the synthesis) – and the powder embedded in the polymer matrix scratched from the glass slide - were contained within quartz glass tubes connected both to a high vacuum pumping system and to a controlled gas feed (O_2).

Spectra were recorded in vacuum conditions (10^{-5}mbar) at 130 K, before and after 40 min of UV-irradiation at the same temperature inside the EPR cavity. The experimental procedure guaranteed low recombination rate for the photogenerated species. No significant differences resulted between the spectra recorded just before and 20 min after switching off the UV irradiation, except a small decrease of the signal intensity.

Modulation frequency was 100 kHz, modulation amplitude 2–5 gauss, and microwave power 10 mW. Irradiation was performed by Vis 150W Xe lamp (Oriel) with the output radiation focused on the samples in the cavity by an optical fiber (50 cm length, 0.8 cm diameter).

The g values were calculated by standardization with α,α'-diphenyl-β–picryl hydrazyl (DPPH). Care was taken in order to

always keep the most sensitive part of the EPR cavity (1 cm length) filled.

7.3 Results and Discussion

7.3.1 IR Results

In Figure 7.1 the IR spectra of the pristine polymer and of the films characterized by an increasing concentration of titanium dioxide are reported. Apart from the peaks relative to the polymer - the vibration of the tertiary amide carbonyl at 1630 cm^{-1}, the stretching and bending of the methyl and methylene groups around 1950-1850 cm^{-1} and in the finger print region respectively - it is possible to observe the absorption of TiO_2 over 750 cm^{-1} that increases with TiO_2 content in the polymeric matrix.

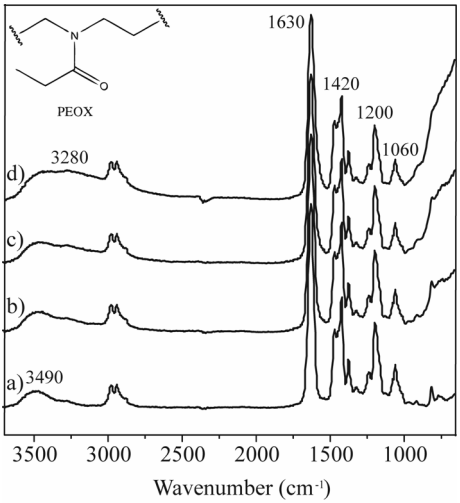

Figure 7.1. FT-IR spectra of films before aging: a) A0; b) A16; c) A28; d) A44

Moreover a broad band at 3280 cm^{-1} overlapped with the band at 3490 cm^{-1}, attributed to the physi-adsorbed water, growths with the concentration of TiO_2, attributed to the vibrational mode of acid hydroxyls present on the anatase surface.

In Figure 7.2 and 7.3 the IR spectra of the samples A0, the pristine polymer, and A44, the sample characterized by the 44% of titanium dioxide in the polymeric matrix, are reported after different time of irradiation. Other samples spectra are not reported, but it was verified that the photodegradation rate of nanocomposites is controlled by TiO_2 nanoparticles content.

The polyoxazolines, as already reported in literature [8], are a very stable material, and after 1517 h, corresponding to about 20 years of natural aging in indoor condition, the PEOX IR

spectrum does not show evident changes (see the spectrum f reported in figure 7.2).

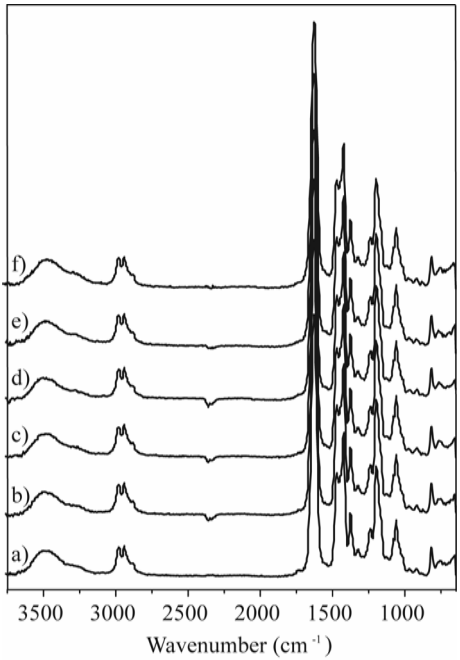

Figure 7.2. Poly 2-ethyl-oxazoline (A0) spectrum after a) 0h; b) 90h; c) 180h; d) 311h; e) 655h and f) 1517h of aging.

On the other hand, in the IR spectrum of the sample A44 collected after different times of irradiation, important changes appear after only 6 hours. Figure 7.3b shows a new band at 1730 cm^{-1} that increases on time. Moreover, after 24 hours (see figure 7.3c) a shoulder of the amide carbonyl band appears at 1670 cm^{-1}, while the main peak at 1630 cm^{-1} decreases. In the spectrum of the sample after 48 hours of aging, the new peak is

more intense than the pristine. After 180 hours (see figure 7.3f), the peak of the tertiary amide carbonyl disappears completely. In the same time, the intensity of the peaks at 1420 cm^{-1} and 1200 cm^{-1} decrease, while the bands at 1341 and 1375 cm^{-1} growth on time and a new peak at 1170 cm^{-1} appears.

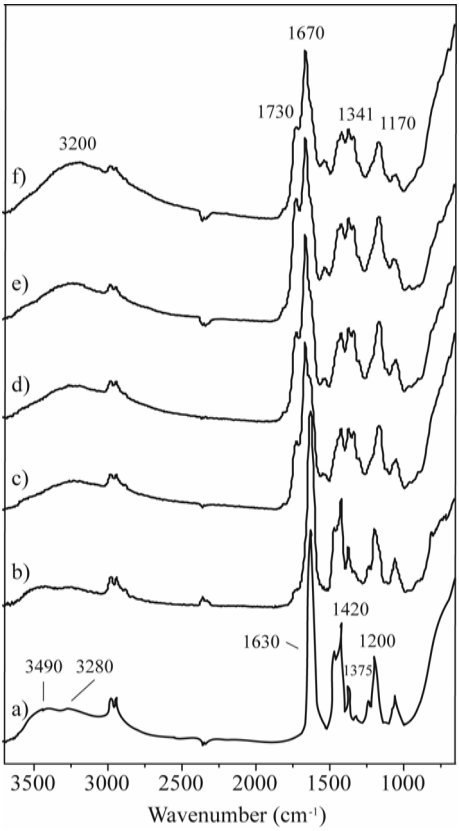

Figure 7.3. FT-IR spectrum of the most concentrated nanocomposite A44 after a) 0h b) 6h; c) 24h; d) 48h e) 90h ;f) 180h of aging. The spectrum of

the nanocomposite after 311h is not reported since the material is completed destroyed and no IR bands appear.

So, the bands at 1730 and 1670 cm^{-1} increase until the complete polymer degradation, observed after 311 hours of irradiation (the spectrum is not reported here because is a sort of flat line). These peaks have been attributed to the carbonyl of a carboxylic acid and a free secondary amide respectively.
Moreover the appearance of a broad band at about 3200 cm^{-1} confirms the formation of acid hydroxyls.
These information permitted to develop a mechanism of poly (2-ethyl-2-polyoxazoline) degradation.

7.3.2 Mechanism of polymer degradation

The mechanism of TiO_2-photocatalyzed degradation of poly (2-ethyl-2-oxazoline) is showed in Scheme 7.1. The excitation of titanium dioxide with the visible light in presence of oxygen leads to the formation of reactive species such as $OH\cdot$, $OH_2\cdot$, $O\cdot$. A conventional radical mechanism promotes the hydroper-oxidation of the α carbon to the nitrogen. No experimental results favor the break between the nitrogen and the carbonyl and, in general, stronger condition of aging such as UV-B light ($\lambda < 300$ nm) are required [11]. Moreover, the attack on other carbons could not be completed ruled out. In the scheme 1, apart from the peroxy radicals, other intermediate products are described, such as the alkyl and the alkoxy radicals, but the final result is the decomposition of the polymer in a free

secondary amide and a carboxylic acid, as experimental data showed.

Scheme 1. Predicted mechanism for polyoxazoline degradation

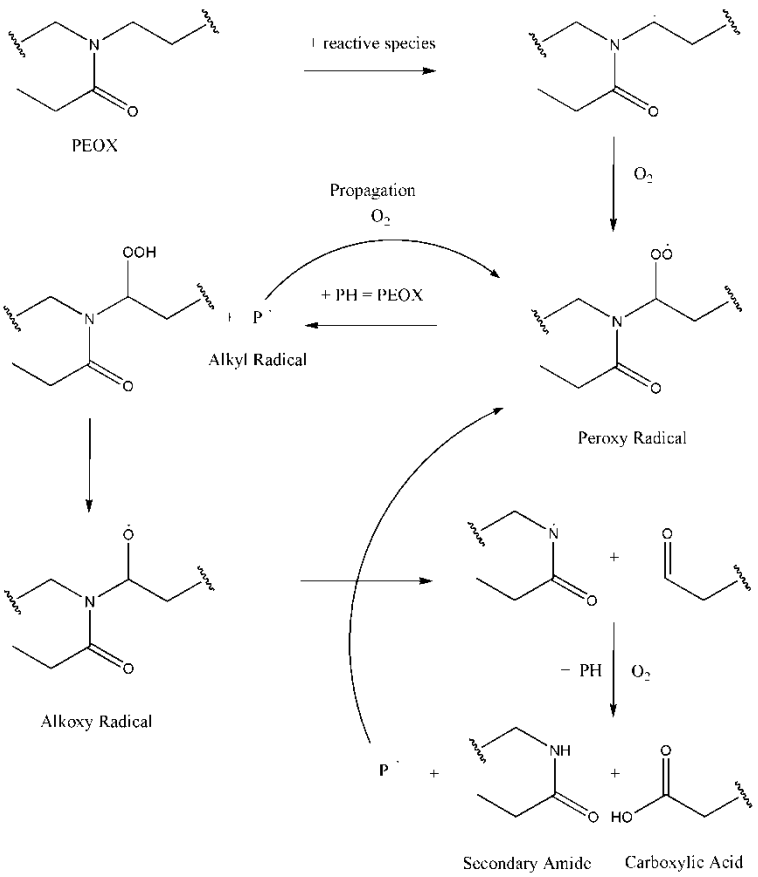

7.3.3 EPR Results

After irradiation in vacuum, an intense and broad feature associated to different Ti^{3+} species arises in the spectrum of anatase powder (Figure 7.4a). The spectrum is complex, due to the superimposition of three different resonances: the narrow signal at $g_{A\perp} = 1.985$ corresponds to the perpendicular g-tensor component of anatase Ti^{3+} bulk centers ($g_{A\parallel}$ is not detectable due to overlap with the other lines); the other two signals are assigned to electrons become trapped on two distinct surface trapping sites ($g_B = 1.934$, and weaker at $g_C = 1.954$). We propose that these two species are originated by two different coordination environments of anatase surface Ti^{4+} due to surface binding of residual benzyl alcohol molecules (see figure 5.2 explained in paragraph 5.3.1). Generally, Ti^{3+} in titania are found in a tetragonally distorted octahedral crystal field (Scheme 7.2, structure "A"). Therefore, the g-factor of the EPR signal will depend on the extent of tetragonal distortion. In the present case, we suggest that when two benzyl alcohol molecules are coordinated to the Ti center (Scheme 7.2, structure "B"), the crystal field does not become significantly distorted and a small shift from the g-factor of Ti(III) surface centers (g = 1.924) is observed (g_B). When three OH groups are replaced with benzyl alcohol terminations (Scheme 7.2, structure "C"), the crystal field becomes more tetragonally distorted due to the larger extent of covalent bonding and the shift of the g-value (g_C) becomes higher [9]. Finally, weak

signals associated with surface trapped holes in titania (O^- species) are also detectable.

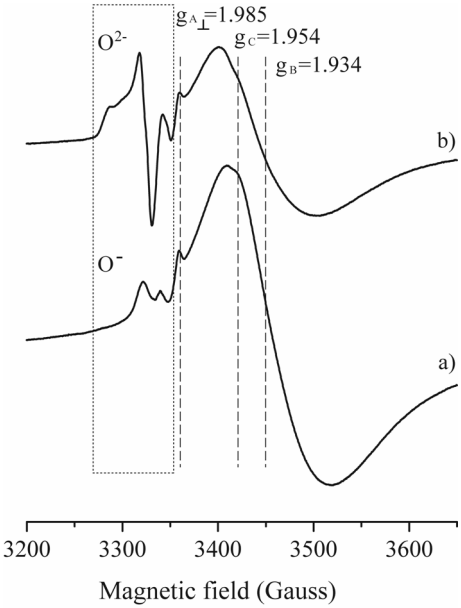

Figure 7.4. EPR spectra at 130 K of TiO_2 after a) Vis irradiation in vacuum ($p < 10^{-5}$ mbar) or b) in the presence of $p(O_2)$ = 10 mbar.

Scheme 7.2. Predicted structure of surface Ti atoms uncoordinated and coordinated with benzyl alcohol.

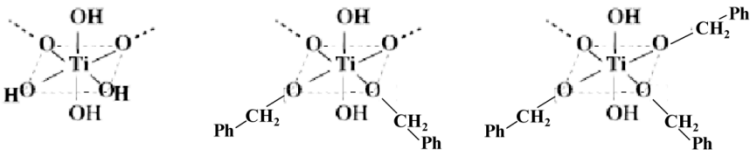

A B C

After irradiation under O_2 (10 mbar) the resonances associated to the surface electron trapping sites show a significant decrease probably due to their photoxidation, while the signal intensity of bulk Ti^{3+} centres remains more-less constant. Moreover, new intense signals attributable to Ti^{4+}- O_2^- species (g_1= 2.0290 g_2 = 2.0086, g_3= 1.9930) become evident (figure. 7.4b).

Concerning the anatase powder embedded in the polymer matrix, after visible irradiation in vacuum (figure 7.5a), EPR spectrum shows resonance lines attributable to a radical specie associated with the polymer matrix; this could confirm the alkyl radical specie described in the scheme 7.1. The resonance lines attributed to Ti^{3+} surface trapping sites significantly decrease (figure 7.5a) and the g-values undergo a small shift, while the features associated to Ti^{3+} bulk species become more evident and also the parallel component is detectable ($g_{\parallel A}$ = 1.956).

Irradiation under oxygen leads to the increase of the radical amount associated to the polymer matrix (figure 7.5b). The Ti^{3+} amount remains instead more-less constant. These results suggest that in the polymeric nanocomposite the photogenerated holes are trapped by the polymeric matrix which better stabilizes radicals, while the electrons are involved in reduction of Ti^{4+} to Ti^{3+} centres [10].

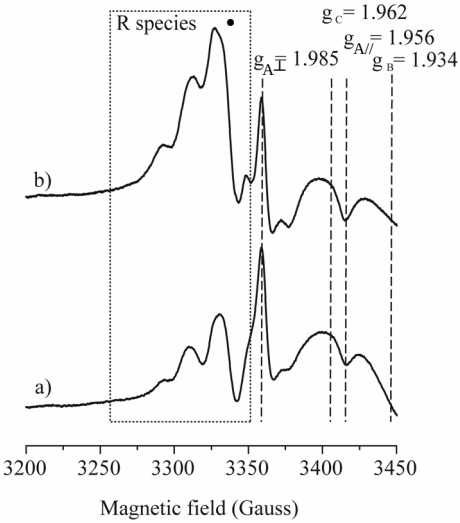

Figure 7.5. EPR spectra at 130 K of polymeric nanocomposite after a) Vis irradiation in vacuum ($p < 10^{-5}$ mbar) or b) in the presence of $p(O_2)$ = 10 mbar.

The formation of Ti^{3+} species is macroscopically confirmed by blue coloration of nanocomposite films after irradiation with the xenon lamp. The blue coloration faded away after about 12 hours since the samples were removed from the weather-ometer and preserved in atmospheric oxygen and other oxidizing agents. Under these conditions, in fact, Ti(III) is oxidized again in the more stable Ti(IV) (see figure 7.6). Moreover the induced degradation of the polymeric matrix is manifested by the intense yellowing of the films. Photo 7.6b shows the films appearance after 90 hours of light aging of the samples in the weather-ometer.

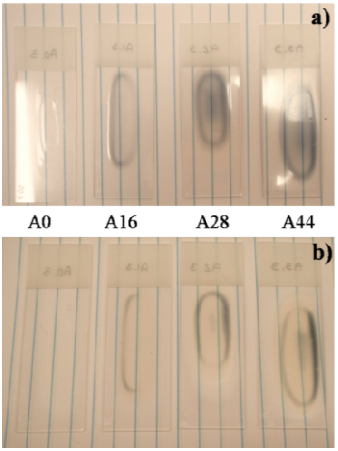

Figure 7.6. Images of the pristine polymer and nanocomposites films after 6 hours (a) and 90 hours (b) of light aging. Samples were removed from weather-ometer and photos performed just after some hours of atmospheric conditions.

7.4 Summary

In this chapter the visible light stability of the TiO_2-PEOX nanocomposites was verified. We found that titanium dioxide, in the anatase phase, obtained by the non-aqueous synthesis, induced a rapid depolymerization of the polymeric matrix in simple condition of visible light. The mechanism of polymer degradation was studied by FTIR, while the species involved in this process were studied using EPR.

On the basis of the results obtained by EPR spectroscopy, we have demonstrated the existence of two surface Ti(III) centers on TiO_2 particles having different extents of tetragonal distortion of the octahedral crystal field. The reason of these

heterogeneities was attributed to the presence of the benzyl alcohol on the anatase surface as synthesis residual. Illumination of the TiO_2 nanocomposite results in the formation of trapped electrons (Ti(III) centers) and trapped holes. In particular, photoproduced holes are stabilized by the polymer, generating radicals, which in turn react with O_2 to form peroxy radicals. The process contributes to keep the electrons, located on Ti^{3+} centers, separated from the holes and fixed on the polymer, favoring the photocatalytic efficacy.

7.5 References

[1] Szczepankiewicz S H, Colussi A J and Hoffmann M R 2000 *J. Phys. Chem. B* **104** 9842

[2] Ohtani B, Azuma S, Nishimoto S and Kagiya T. 1992 *Polym Degrad Stab.* **35** 53

[3] Zan L, Fa W and Wang S. 2006 *Environ. Sci. Technol.* **40** 1681

[4] Ohtani B, Azuma S, Nishimoto S and Kagiya T. 1989 *Polym. Degrad. Stab.* **23** 271

[5] Kim S H, Kwak S-Y and Suzuki T. 2006 *Polymer* **47** 3005

[6] Nakayama N and Hayashi T 2007 *Polym. Degrad. Stab.* **92** 1255

[7] Tang L, Sallet D and Jacques Lemaire 1982 *Macromolecules* **15** 1437

[8] Wolbers R C, McGinn M and D. Duerbeck 1998 Proceedings of the symposium organized by the Wooden Artifacts Group of AIC, 1994, Williamsburg, eds. V. Dorge

and F. C. Howlett. (Los Angeles, Getty Conservation Institute) 514
[9] Rajh T, Ostafin A E, Micic O I, Tiede D M and Thurnauer M C 1996 *J. Phys. Chem.* **100** 4538
[10] D'Arienzo M, Crippa M, Essawy A A, Scotti R, Wahba L and Morazzoni F 2010 *J. Phys. Chem. C* **114** 15755

Chapter 8
General Conclusions and Recommendations

As conclusion, we developed a good strategy in order to obtain transparent TiO_2-PMMA sheets with tunable diffusing properties.
The objective of the first step was to turn the hydrophilic character of the TiO_2 surface into hydrophobic, in order to improve the nanoparticles dispersion in MMA.
The surface modification of anatase nanoparticles with an aliphatic phosphonic acid, and of rutile nanoparticles with an aliphatic amine permitted to obtain stable colloids in MMA. Then, the bulk polymerization of the monomer filled with the nanoparticles was led, obtaining optically transparent sheets.
Appropriate fine tuning of a spectrometer permitted to measure the optical properties of these objects, whose size is at least 20cm x 20cm.

In parallel, transparent TiO_2-PEOX nanocomposite films were fabricated: anatase nanoparticles synthetized by non-aqueous route were dispersed in water and mixed with the aqueous polymeric solution. Optically transparent and highly refractive films were obtained by evaporation of the water. TEM images showed a good dispersion of the nanoparticles in the polymeric

matrix, even if the high content of TiO_2 (up to 44% w/w). Moreover, the organic residual on the TiO_2 surface induced an hydrophobic character of the most concentrated nanocomposite film.

Thanks to their improved optical and surface properties these nanocomposite films could be used in the coating industry and particular application was thought in the conservation of cultural heritage.

We also make recommendation that further research remain to be carried out to explain the role played by benzyl alcohol on the surface and catalytic properties of the anatase nanoparticles used in this work.

Moreover, other ceramic nanopowders, such as ZnO and ZrO, characterized by UV absorption, transparence in the visible range and high refractive index, but – on the other hand – reduced catalytic activity, will be interesting to investigated.

The next step in the project for lighting application is the introduction of phosphors or chromophores in the TiO_2-PMMA nanocomposite sheets in order to perform the conversion of the blue in a warm white light.